Wettability of Tight and Shale Gas Reservoirs

by

Qing Lan

A thesis submitted in partial fulfillment of the requirements for the degree of

Master of Science

in
Petroleum Engineering

Department of Civil and Environmental Engineering
University of Alberta

Abstract

Abundant hydrocarbon resources in low-permeability formations are now accessible due to technological advances in multi-lateral horizontal drilling and multi-stage hydraulic fracturing operations. The recovery of hydrocarbons is enhanced by the creation of extensive fracture networks. Fluid invasion into the rock matrix has been identified as a possible mechanism that could enhance hydrocarbon recovery, however, low levels of fracturing fluid are recovered after fracturing operations. Therefore, studying the mechanism of spontaneous liquid imbibition into reservoir rocks is essential for understanding (1) rock wetting affinity, (2) enhanced hydrocarbon recovery, and (3) the fate of non-recoverable fracturing fluid.

The primary aim of this study is to investigate the wettability characteristics of shales and tight rocks by conducting a series of comparative and systematic imbibition experiments. Using multiple samples, we study functional dependence on petrophysical properties, petrographic properties, rock fabric, depositional lamination, and gamma ray response. Moreover, we investigate the relationship between water loss and rocks' petrophysical properties, and the correlation between water loss and soaking time (i.e., well shut-in time). Finally, we present a simple method for estimating the degree of water loss at the field level.

The results of spontaneous imbibition experiments show that the imbibition rate of water is significantly more than that of oil for shale samples drilled from the Horn River (HR) Basin. This observation is in contrast to the measured contact angle. We also measured and compared spontaneous imbibition of oil and water into crushed

packs of similar HR samples. Interestingly, in contrast to the intact samples, the crushed samples consistently imbibed more oil than water. Therefore, clay swelling, micro-fracture induction, depositional lamination and osmotic potential are collectively responsible for excess water uptake. In similar comparative imbibition experiments of several binary samples collected from cores drilled in the Montney (MT) tight gas play, samples did not show any visible physical alteration. Both the measured contact angle and imbibition data indicate that MT tight sandstone is strongly oil wet. The comparative study suggests that the connected pore network of HR samples is strongly hydrophilic due to the presence of clay minerals and precipitated salt crystals coating the rock grains, while the well-connected pore networks of the MT samples are dominantly hydrophobic and very likely to be coated with pyrobitumen.

AKNOWLEDGEMENTS

It is with tremendous gratitude that I acknowledge the support and help of my supervisor Dr. Hassan Dehghanpour for his valuable guidance, support and encouragement through the learning process of this master thesis. He has always been accessible and willing to help me with my research. His kindness and encouragement will be engraved on my mind.

Furthermore, I would like to express my deepest gratitude to my family. I am indebted to my parents for their unconditional love, care and support that enlightened my path and give me the strength to pace towards my achievements.

I am grateful to people who helped me. Special thanks to Kaiqi for his unflagging support, understanding and encouragement throughout the entire process of studying.

I gratefully acknowledge National Science and Engineering Research Council of Canada (NSERC) for providing funding for this research. I acknowledge BC Oil and Gas Commissions and Encana Corporation for providing samples and petrophysical data. I also acknowledge James Wood, Hamed Sanei and Robert Hawkes for their useful discussion and guidance. I am also thankful to Engineering Technologist Todd Kinnee for his help and assistance in conducting laboratory experiments.

TABLE OF CONTENTS

LIST OF FIGURES

LIST OF TABLES

CHAPTER 1

INTRODUCTION

1.1 Overview and Background

In response to increasing global energy requirements, the development of unconventional resources has become a major priority for the oil and gas industry. As a result, North American formations containing shale gas (and oil) and tight gas have become tremendously important. A significant characteristic of these unconventional resources is very to extremely low permeability, which makes commercial production of hydrocarbons quite difficult. Thus, new geological, geographical and reservoir-simulation techniques are required not only enhance our understanding of unconventional reservoirs, but also address economic, environmental and sustainability concerns associated with the exploitation of unconventional resources.

Stimulation of natural gas production from tight reservoirs is based on the ability to create fracture networks that greatly expand contact with shale matrix. Fracturing stimulations of shale (and tight) reservoirs have been developed to address fracture-creation challenges and enable exploitation of abundant resources in unconventional reservoirs. As we are witnessing, the recovery of reservoir hydrocarbons has been enhanced by fracture networks produced by multistage hydraulic fracturing coupled with horizontal well drilling technology.

The hydraulic fracturing process, developed on a commercial scale in 1949, has been successfully employed to increase production in many formations that could not otherwise have been developed from an economic standpoint (Coulter 1976). Hydraulic fracturing exposes an extensive surface area of a reservoir to fracturing fluids. While the reaction between fracturing fluids and reservoir rocks is one possible mechanism for optimizing hydrocarbon recovery, pronounced interaction may also be associated with clay swelling, water adsorption, spontaneous imbibition, etc.

In reactive shales, clay swelling and water adsorption result in wellbore instability, which has been studied extensively in the drilling engineering context (Osisanya et al. 1994; Osisanya 1995; Chenevert 1970). Swelling of reactive shale depends on the type and concentration of both aqueous phase ions and rock clay minerals. However, liquid intake of organic shales must be further investigated in the context of reservoir engineering.

Spontaneous imbibition can be described as the suction of a fluid into a porous medium by capillary attraction. This process has been identified as a mechanism for fracturing fluid loss and reservoir damage as fracturing fluid is imbibed into a reservoir rock matrix. On the other hand, spontaneous imbibition of fracturing fluid in a fractured organic reservoir is one possible mechanism for enhanced oil recovery. Capillary suction allows the fracturing fluid to flow from fractures to oil-saturated matrix blocks which causes the oil to be displaced from the matrix into the fractures (Nurkamelia et al. 2004). This oil then is displaced by oncoming fracturing fluid through the fracture system to the production wells. Furthermore, this imbibition process is a reliable and reproducible way to quantitatively determine reservoir rock wettability.

Wettability (wetting affinity) of reservoir rock is a crucial parameter that depends on rock mineralogy and and organics, the hydrophobic and hydrophilic nature of rock components. The estimation of reservoir wettability and its effect on reservoir fluid flow, hydrocarbon recovery and fluid distribution has been widely studied and remains a challenging problem (Mohammadlou et al. 2012). Wettability is a complicated petrophysical property that influences the particular behaviors and characteristics of a reservoir. Therefore, it is usually estimated based on laboratory measurements.

A great deal of research work has been performed in recent decades to understand the imbibition process in rocks with low permeability (Schembre et al. 1998; Takahashi et al. 2010; Wang et al. 2011). For example, the use of spontaneous imbibition to

duplicate processes happening in fractured shale reservoirs has been studied both experimentally and theoretically (Akin et al. 2000; Roychaudhury et al. 2011; Dutta et al. 2012). Moreover, the reservoir engineering literature is extensive and mainly focused on enhancing our understanding of shale and tight formations. However, the complex physical and petrophysical properties of unconventional reservoir rocks and the effects of these properties on the spontaneous imbibition process must be further investigated by simulating fluid-rock performance.

1.2 Statement of the Problem

As a consequence of significant hydrocarbon recovery breakthroughs, reservoirs with matrix permeability as low as millidarcies in conventional reservoirs, microdarcies in tight gas reservoirs and nanodarcies in shale gas reservoirs are now accessible (Kundert et al. 2009; Arogundade et al. 2012). Hydraulic fracturing is one breakthrough that has unlocked oil and gas resources from unconventional reservoirs. The key objective of multistage hydraulic fracturing in low permeability reservoirs is to create extensive interface on the rock matrix, which enhances the hydrocarbon production rate (Novlesky et al. 2005). However, recent studies and field data demonstrate that significant amounts of injected fracturing fluid are retained in fractured reservoirs, partly due to spontaneous imbibition in the rock matrix and seepage into secondary fractures of rock matrix (Fan et al. 2010; Soeder 2011).

The imbibition of fracturing fluids into shale pores leads to fluid loss and reservoir damage (Khansari 2011; Lan et al. 2014). Fluid interaction with shale, however, is more complicated than with other types of rocks. For example, shale clay minerals may swell and adsorb a considerable amount of water. Mineral dissolution and electrostatic charges also occur frequently during imbibition. Due to these interactions between fracturing fluid and shale, data from several field studies have confirmed that only a small fraction of injected fluid can be recovered after hydraulic fracturing; it

has been found that only 25% fluid can be recovered after nearly 40 days of flowback operations (Kaiyrzhan 2013).

Moreover, measuring and modeling petrophysical properties in low-permeability formations, which is required for reserve estimation and reservoir engineering calculations, remains challenging. In particular, characterizing the wetting affinity of tight rocks is challenging due to their complex pore structures, which can be in either hydrophobic organic materials or hydrophilic inorganic materials.

Questions such as how much fracturing fluid permeates the rock matrix and how much is retained in fractures remain unanswered. These are key questions for field engineers, since the selection of fracturing and treatment fluid closely corresponds to the wetting affinity of a reservoir. Measuring reservoir wettability remains a primary challenge, particularly for unconventional formations. Comparing laboratory test results with actual field data would improve our understanding of water loss during and after hydraulic fracturing operations, and help us better understand how wetting affinity affects reservoir engineering.

1.3 Objectives of the Research

Objectives of this study include:

1. Characterize petrophysical properties of (1) shale core samples collected from the Horn River Basin, and (2) tight sandstone core samples collected from the Montney formation.
2. Investigate (1) imbibing fluid properties and (2) core sample properties, and the corresponding influences on spontaneous imbibition rates; and (3) core sample wetting affinity characteristics based on spontaneous imbibition data.
3. Measure and model wettability of the rock samples, and investigate their functional dependence on other petrophysical properties, petrographic properties, rock fabric, and mineralogy.

4. Use (1) the dimensionless time upscaling theory to estimate the degree of reservoir gas recovery (or the volume of fracturing fluid imbibed into the unconventional rock matrix) during the shut in period after the hydraulic fracturing operation, and (2) mathematical models to characterize challenging sample parameters such as permeability and pore size diameter.

1.4 Methodology of the Research

We use the following methodology to accomplish the thesis study objectives:

1. Determine the petrophysical properties of unconventional rocks by directly measuring their porosities and contact angles (for wettability analysis) and analyzing well log data.
2. Conduct spontaneous imbibition experiments, and measure spontaneously imbibed liquid mass (and volume). Analyze the various imbibition rates based on different liquid types (aqueous or oleic phase), various aqueous phase salt concentrations, diverse sample properties, etc.
3. Analyze the results of spontaneous imbibition experiments by plotting imbibition data against dimensionless time. Qualitatively study the wettability of samples after removing effects for other factors such as sample size, various fluid viscosities, boundary conditions, etc.
4. Interpret and model imbibition data to obtain wettability indices and investigate functional dependence on other parameters. Use mathematic models to estimate permeability and pore size of Montney samples.
5. Estimate the volume of fracturing fluid imbibed into the unconventional rock matrix at the field scale during the soaking time. Calculate a simple estimate of the fracturing fluid loss rate using an analytic procedure.

1.5 Structure of the Thesis

In **Chapter 1**, I present a brief overview and background of the current state of energy resources, advanced technology in unconventional reservoirs and interactions between fracturing fluid and rock matrices during and after hydraulic fracturing. I introduce some existing associated problems, and discuss the objectives and methodology of the thesis study.

In **Chapter 2**, I review the literature related to the importance of unconventional resources. I introduce the main technology with respect to spontaneous imbibition in tight porous media. Moreover, I provide a detailed overview of the characteristics of Horn River shale and Montney tight sandstone.

In **Chapter 3,** I present petrophysical properties of core samples selected from the Horn River Basin, including porosity, results of XRD and TOC measurements, and interpret well logs from two selected wells drilled in the Horn River Basin.

In **Chapter 4**, I compare the imbibition rates of brines of various salinities and two oil liquids in similar shale samples.

In **Chapter 5**, I present an analytical scaling of spontaneous imbibition in Horn River Basin shales. I plot the imbibition data of each formation versus dimensionless time in order to ensure consistent comparisons.

In **Chapter 6**, I investigate the properties of core samples selected from the Montney formation, including results of XRD and TOC measurement, and interpret well logs from selected well drilled in Montney formation.

In **Chapter 7**, I measure and compare spontaneous imbibition of oil and brine into fresh (uncleaned) binary core plugs selected from different depths of one vertical well

drilled in the Montney formation. I analyze imbibition data in order to obtain corresponding effective porosity and wetting affinity of rocks.

In **Chapter 8**, I interpret measured spontaneous imbibition data to estimate challenging petrophysical properties (such as permeability and porosity) of Montney samples using models.

In **Chapter 9**, I examine factors affecting the wettability of unconventional rocks by conducting comparative imbibition experiments on several binary core plugs from the Montney tight gas formation and the Horn River Basin.

In **Chapter 10**, I examine the relationship between water loss and petrophysical properties in Horn River shale and Montney tight rock. I also present a simple model for scaling lab data in order to predict field characteristics and water loss during soaking time (well shut-in time).

In **Chapter 11**, I summarize important findings of the thesis and provide recommendations for future research.

CHAPTER 2

LITERATURE REVIEW

2.1 Overview of Unconventional Resources

In recent years, resources recoverable from reservoirs of difficult nature have come to be called "Unconventional Resources". In addition to fractured reservoirs, unconventional plays include tight gas, shale gas (and oil), oil sand and coal-bed methane (CBM) (Haskett et al. 2005). Growing shortages of the available conventional hydrocarbons amount has aggravated the importance of unconventional hydrocarbon resources in recent years. The demand for oil and natural gas will continue to increase for the foreseeable future and the gap between demand and supply should rely on unconventional resource to fill (Rajnauth 2012).

Unconventional oil and gas resources are presenting a significant potential for meeting world's increasing energy demand. Proven shale gas reservoir, for example, are estimated over 6622 trillion cubic feet which is 40% of world's technically recoverable gas reserves (Niag, 2012). Moreover, the Horn River shale gas basin has been estimated to hold more than 500 trillion cube feet by the Canadian Society of Unconventional Gas (Pond et al. 2010). It is defined as the third largest natural gas accumulation in North America (Pond et al. 2010).

Currently, there are 28 North American shale basins with 56 identified shale plays (EIA report, 2011). Figure 2.1 shows location of the major commercial unconventional plays including Horn River, Montney, Barnett, Horton Bluff, and Eagle Ford etc.

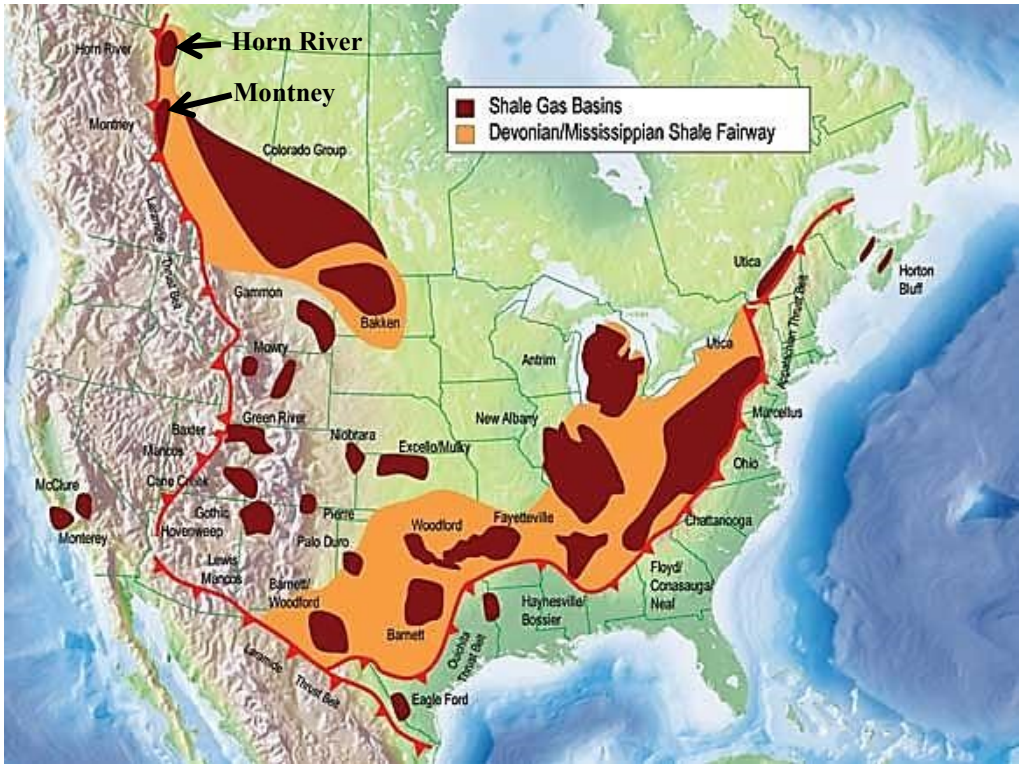

Figure 2.1 Shale gas plays of North America (Source: National Energy Board Report, 2009).

Shale gas is natural gas that is found trapped with shale formations. Tight gas is natural gas produced from reservoir rocks with such low permeability. Although shales have low permeability and low effective porosity, shale gas is usually considered separate from tight gas, which is contained most commonly in sandstone, but sometimes in limestone. Horn River Basin shale and Montney formation tight sandstone are the unconventional reservoir rocks for our study in this thesis.

2.1.1 Overview of Horn River Basin Shale

The Horn River Basin is a Middle to Upper Devonian aged shale basin located in Northeast British Columbia. It is one shale gas play in Canada and similar, in many aspects, to the Barnett shale in the Fort Worth Basin of Taxes (Pond et al. 2010). The main target zone of Northern British Columbia is the Horn River formation, which is composed of four members (Figure 2.2): the Fort Simpson member, the Muskwa member, the Otter Park member and the Evie member. Except for Fort Simpson

member is clay-rich formation, the other three members are dominantly composed of organic and silica-rich shale (National Energy Board, 2011).

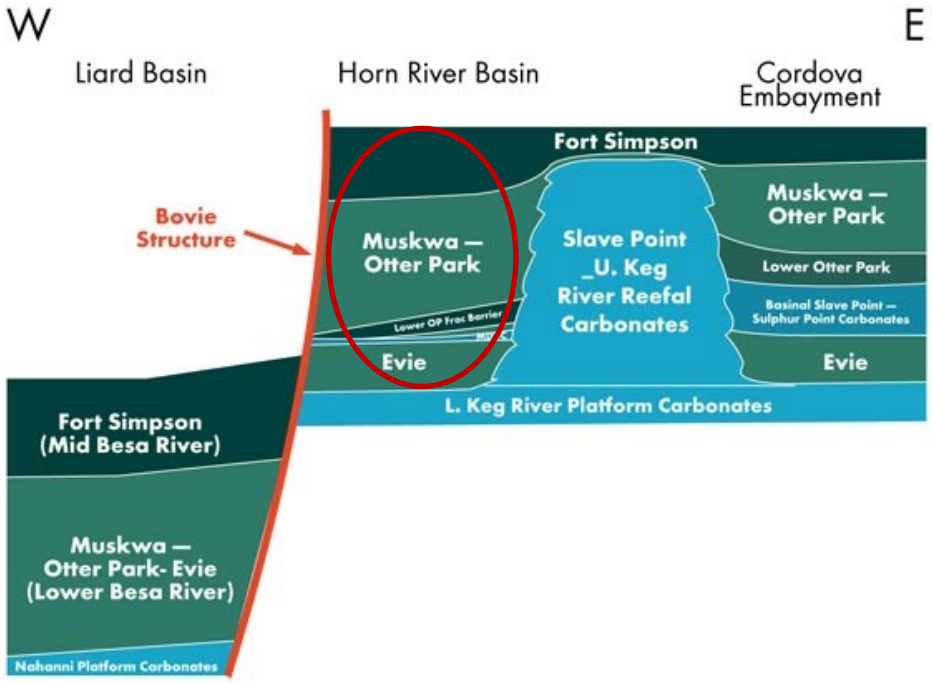

Figure 2.2 Depositional cross-section of the Horn River basin (Source: National Energy Board, 2011)

The compositions of Horn River Basin are listed as following:

1) Fort Simpson member (the top part) is the organic-lean shale, which is clay rich, with very high concentrations of illite, kaolinite, and chlorite (Khan et al. 2011). This member is weak, frangible shale and of high quartzitic content (Stewart et al. 2000)
2) Muskwa member (the upper part) is the organic-rich black bituminous shale, which contain high radioactivity on Gamma Ray logs (Griffin 1965) and high concentration of pyrite, siliciclastic (Neito et al. 2009).
3) Otter Park member (the middle part) is gas-saturated organic shale that reaches a maximum thickness of more than 270 m in the southeast corner of the Horn River

Basin (Johnson et al. 2011). Moreover, this member includes siliceous black interbeds (National Energy Board, 2011).

4) Evie member (the bottom part) is organic-rich. This formation contains variable calcareous and siliceous shale with very high radioactivity on Gamma Ray logs and high concentration of pyrite and calcite (Johnson et al. 2011).

2.1.2 Overview of Montney Tight Sandstone

The Montney resource play straddles across the Canadian provinces of British Columbia and Alberta (Figure 2.3). It is considered by many researchers to be one of the largest natural gas resource plays in North American (Wilson et al. 2011). The Montney sand is a Triassic-age siliclastic reservoir. It is a tight, low permeability siltstone reservoir (Song et al. 2012). This formation is divided into Upper Montney and Lower Montney, and is generally composed of both siltstone and dark gray shales. The Upper Montney is characterized by light brown siltstones interlaminated with fine grained sands, while the Lower Montney is a dark grey, dolomitic siltstone with interbedded shales (Glass et al., 1997).

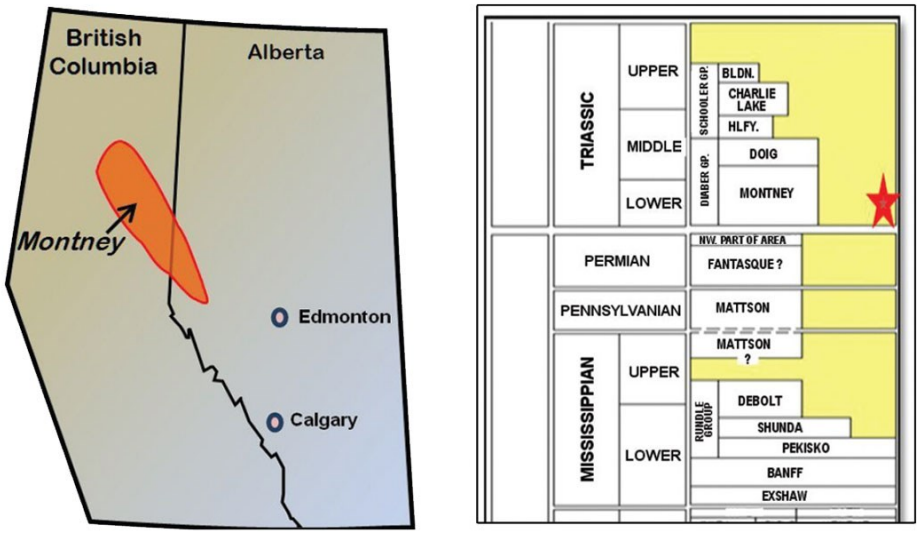

Figure 2.3 Location and depositional stratigraphy of Montney formation (Star part is Montney formation, Source: Neito. J., 2013)

The Montney gas reservoir presents an exciting potential and is very likely to become a critically important component of future gas supply in Canada. This reservoir spans approximately 2961 km2 and has 449 trillion cube feet recoverable and marketable natural gas (National Energy Board, 2013).The Montney play is a complex geological sequence that varies from conventional gas (or oil) along the eastern edge of the basin, to a combination of tight gas and gas shale play in the center, and further to the classical black massive gas shale along the western edge (Keneti et al. 2011).

2.2 Horizontal Drilling and Multi-stage Hydraulic Fracturing Technique

Shale gas production in the United States grew at an average of 48 percent (annual rate) over the 2006 to 2010 period (Gruensprcht 2011). Recent advance in horizontal drilling and multistage hydraulic fracturing have shifted the industry focus toward hydrocarbon recovery from organic shales. Multi-stage fracturing and horizontal well techniques have revolutionized the development of many tight reservoirs around the world. The technologies enable many tight reservoirs economic production from low-permeability areas of reservoirs that were previously uneconomic to develop with vertical wells (Klein et al. 2012). In other words, advances in horizontal drilling and multi-stage hydraulic fracturing technologies were two primary keys to unlock shale and tight resources.

The horizontal well with the advantages of large drainage area has been used to enhance the resource recovery. These mentioned advantages promote the multi-stage horizontal fracturing replace vertical fracturing in drilling engineering. For example, due to the horizontal drilling and multi-stage hydraulic fracturing technologies, the exploited production amount of Barnett shale reservoir (US) rapidly increased from 2003 to 2007 (Browning et al. 2013). Moreover, during the hydraulic-fracturing process, a viscous fluid is pumped down the well under high pressure to create induced fractures (Shah 1993). After this stage, another viscous fluid containing proppant is pumped to maintain the fracture and cracks (created by the previous clean

viscous-fluid stage) open after pumping stops. Then the fracturing fluids gain more chance to communicate with rock matrix by the induced fractures and result in the enhanced resource recovery. The schematic of horizontal well and multi-stage hydraulic fracturing is shown in Figure 2.4.

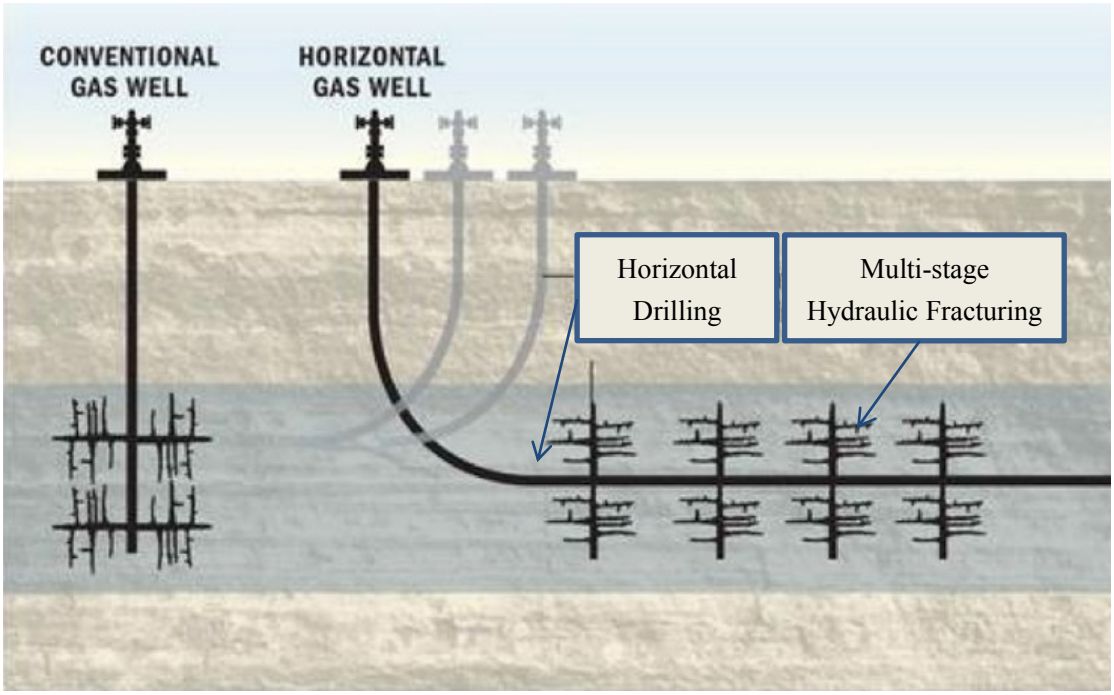

Figure 2.4 Schematics of horizontal well and multi-stage hydraulic fracturing (Source: Clover Global Solution).

2.3 Spontaneous Imbibition Mechanism

Imbibition is an immiscible displacement process, whereby a non-wetting fluid within a porous medium is spontaneously expelled by wetting fluid that surrounds the medium and is sucked into the medium by capillary pressure (Schembre et al. 1998). Spontaneous imbibition of the aqueous phase in fractured reservoir has been studied as a possible mechanism for enhanced oil recovery (Morrow et al. 1994). Extensive experimental and mathematical investigations have been conducted for relating the imbibition rate and total gas recovery to the capillary and gravity forces and the geometrical parameters (Zhang et al. 1996, Ma et al. 1999). The imbibition rate is

primarily related to the rock permeability, pore structure, wetting affinity characteristic and fracturing fluid (or treatment fluid) viscosity, density, and interfacial tension between resident phase and imbibing phase. Moreover, spontaneous imbibition is also the vital mechanism for the reservoir damage and fracturing fluid loss. Therefore, it is important to characterize the fluid flow during hydraulic fracturing to estimate the relationship between gas production rate and fracturing fluid loss rate (Zhao, 2009).

Within this thesis, imbibition experiments were performed on tight rocks: Horn River shale and Montney tight sandstone. Our samples were exposed to various fluids to mimic the invasion characteristics of the fracturing fluid from the main hydraulic fracture through the micro-fracture network into tight rock matrix. On the basis of spontaneous imbibition experiments, fundamental studies of fluids imbibition in relevant tight rocks are necessary to improve the understanding of physical mechanisms that control fluids transport and subsequent gas recovery.

2.4 Wettability (Wetting Affinity) Mechanism

The affinity of a reservoir rock on a particular fluid is defined as Wettability, which depends on various factors such as rock mineralogy and the properties of the materials coating the rock surface (Anderson 1986; Rao et al 1994; Hamon 2000; Alotaibi al 2010; Mohammadlou et al. 2012). Characterizing the wettability of reservoir rocks is important for 1) selecting fracturing and treatment fluids, 2) investigating residual phase saturation, and its pore-scale topology, 3) investigating the occurrence water blockage at fracture face, and 4) selecting relevant capillary pressure and relative permeability models for reservoir engineering calculations.

2.5 Research Gap

Various techniques such as modified Amott test, the U.S. Bureau of Mines (USBM) tests, contact angle measurement and spontaneous imbibition (Anderson 1986; Olafuyi et al 2007; Odusina et al. 2011) have been used to characterize wettability of

reservoir rocks (Morrow et al. 1994; Zhou et al 2000; Mohanty et al 2013). However, conventional methods such as modified Amott and USBM can hardly be applied for measuring wettability of tight rocks primarily due to their extremely low permeability and mixed-wet characteristics (Sulucarnain et al 2012; Mirzaei-Paiaman et al 2013). Thus, it is more practical to characterize wettability of tight rocks by conducting and analyzing spontaneous imbibition experiments. (Ma et al. 1999; Zhang et al. 1996; Takahashi et al. 2010).

CHAPTER 3

CHARACTERISTICS OF ORGANIC HORN RIVER SHALE

The gas transport in low permeability shales has already been well-detailed recently. However, the liquid transport in gas shales, which is critical for designing the fracturing and treatment fluids, needs further investigation. This chapter aims to review the shale properties measured in the laboratory and downhole by the x-ray diffraction, contact angle measurement and logging tools. In the previous paper (Dehghanpour et al. 2012) they selected five shale samples with different properties from the cores of two wells drilled in the Horn River Basin.

3.1 Origin and Geology

The Horn River Basin is located along the northern border between British Columbia and the North West Territories, approximately 750 miles northwest of Edmonton, Alberta (Reynolds et al. 2010). This basin produces from the Middle to Late Devonian aged shale basin which is comprised by (Figure 2.2): 1) Fort Simpson member, 2) Muskwa member, 3) Otter Park member, and 4) Evie member.

3.2 Shale Samples Properties

This section shows the physical and petrophysical properties of Horn River Basin shales. Rock properties have been obtained primarily through log measurement and X-ray diffraction. Table 3.1 and 3.2 summarize the specific rock properties as obtained from those measurements.

Table 3.1 Properties of the five samples selected from Horn River Basin

Label	depth (m)	GR (API)	$Ø_N$	$Ø_D$	$Ø_{core}$	R (Ω m)	TOC (wt.%)
FS	1755	138	0.3	-0.015	0.06	3.9	1.73
UM	1771	188	0.25	0.06	0.05	7	2.25
LM	1792	243	0.152	0.152	0.21	15	3.91
UOP	2632	131	0.108	0.108	0.15	60	3.01
LOP	2640	162	0.135	0.135	0.07	35	3.01

"The neutron porosity ($Ø_N$) and density porosity ($Ø_D$) of samples UOP and LOP are determined in limestone units and those of FS, UM and LM are determined in sandstone units. GR and R represent natural gamma radiation and resistivity of the rock measured by the downhole logging tools. The percentage of total organic carbon (TOC) is estimated from the GR values. The core porosity ($Ø_{core}$) is determined by eq. 3.1."

Table 3.2 Mineral Concentration (wt. %) of the five shale samples determined by XRD

Label	Calcite (wt.%)	Quartz (wt.%)	Dolomite (wt.%)	Chlorite (wt.%)	Illite (wt.%)	Plagioclase (wt.%)	Pyrite (wt.%)	matrix density
FS	0.5	29	2.7	6.5	55.4	4.1	1.7	2.747
UM	0	36.7	5.2	4.4	48.3	3.6	1.7	2.744
LM	0.9	45	1.9	0	43	5.2	4.0	2.79
UOP	4.4	60.8	2.6	0	25.7	3.7	2.8	2.748
LOP	12.9	43.6	2.2	0	33.8	4.4	3.2	2.772

3.2.1 Wire Line Log Interpretation

We select three formation members of Horn River Basin (Fort Simpson, Muskwa and Otter Park), and run a series of tests to characterize these formations properties. In particular, the three formation members are divided into five parts: 1) Fort Simpson (FS), 2) Upper Muskwa (UM), 3) Lower Muskwa (LM), 4) Upper Otter Park (UOP), and 5) Lower Otter Park (LOP). Samples FS, UM and LM were selected from one well, and the other two samples (UOP and LOP) were selected from another different well.

The reproduced logs of these two wells are shown in Figure 3.1 and Figure 3.2. The huge separation between the neutron porosity and density porosity displayed in Figure 3.1 (b) indicate that Fort Simpson formation is a non-organic shale. The middle

formation (Muskwa) is a gas-saturated organic shale that is indicated by the increasing trend of density porosity and the decreasing trend of neutron porosity observed in Figure 3.1 (b). The bottom formation (Otter Park) is a gas-saturated organic shale that is indicated by the overlap of density porosity and neutron porosity as observed in Figure 3.2. Table 3.1 summaries the porosity and other properties of the five samples measured by the logging tools. The natural gamma radiation, GR, of the five samples is relatively high, which indicates the presence of clay minerals composed of the radioactive elements. However, the average GR response of Fort Simpson formation with a higher clay concentration is lower than that of Muskwa and Otter Park formations. This indicates the presence of organic material with a possibly high uranium concentration in Muskwa and Otter Park formations. The neutron porosity of Fort Simpson samples is much higher than its density porosity, which is a typical response in water-saturated shales. The neutron porosity and density porosity values of samples LM, UOP and LOP are relatively close together. This indicates the simultaneous presence of gas and clay minerals. The resistivity of FS is relatively lower than that of other samples, which is expected because the presence of hydrocarbon increases the resistivity value.

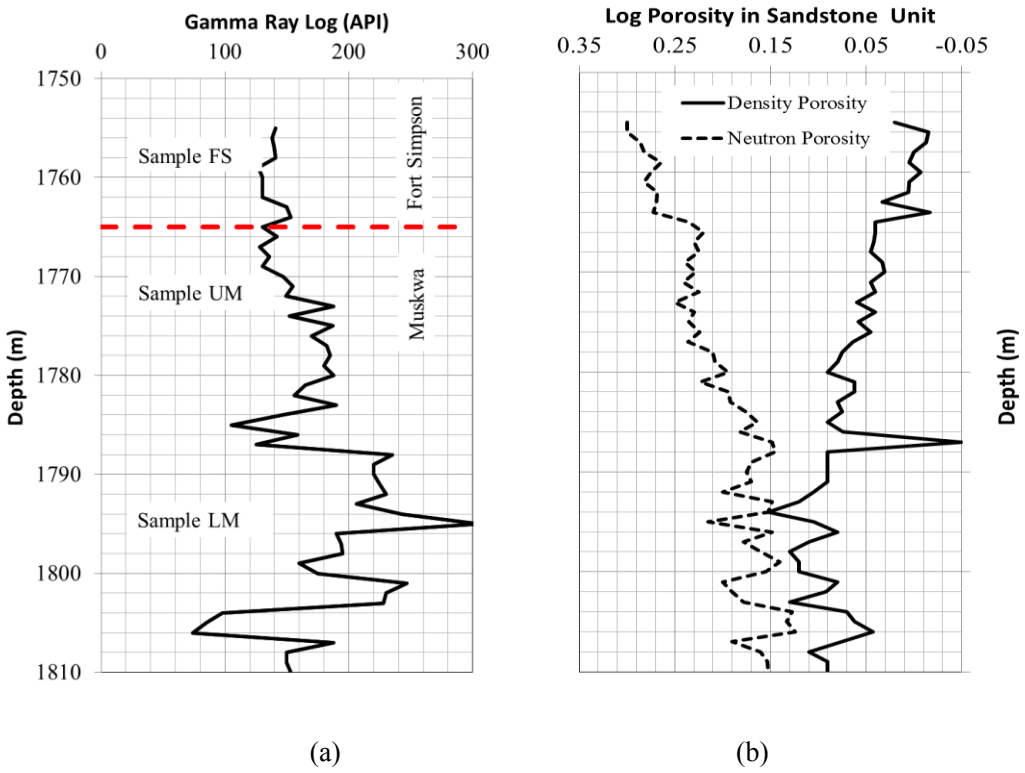

(a) (b)

Figure 3.1 Properties of Fort Simpson and Muskwa formation measured by logging tools and the location of the samples selected for the imbibition tests. (a) Gamma Ray log, (b) Density porosity and Neutron porosity logs (Dehghanpour et al. 2012)

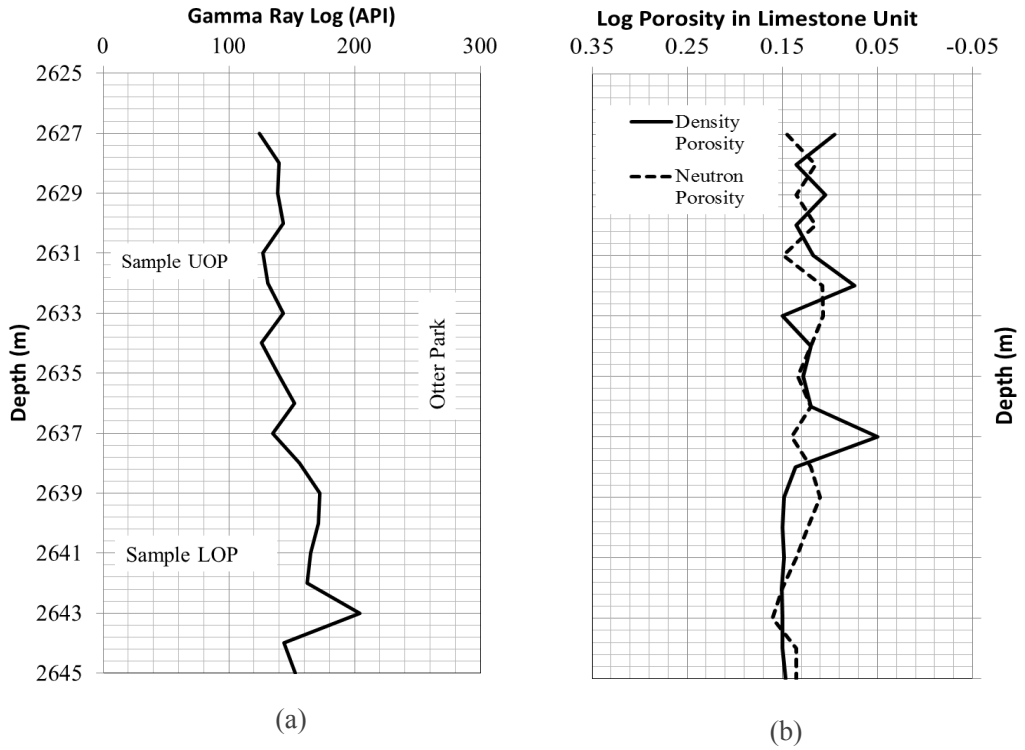

(a) (b)

Figure 3.2 Properties of Otter Park formation measured by logging tools and the approximate location of the sample selected for the imbibition tests. (a) Gamma Ray log, (b) Density porosity and Neutron porosity logs (Dehghanpour et al. 2012).

3.2.2 XRD Analysis

Table 3.2 presents the concentration of the different minerals constitution of the five shale samples determined by the XRD technique. The dominate clay mineral is illite, and the dominate non-clay mineral is quartz. For our test samples, in general, with the increase of the depth, the quartz concentration increases and the illite concentration decreases. Sample FS has the minimum quartz concentration and the maximum illite concentration. Moreover, the calcite concentration of our measured samples FS, M1 and M2 is negligible, while its concentration in samples OP1 and OP2 is noticeable.

3.2.3 Porosity Determination

The density and neutron porosity values of Figure 3.1 are determined in freshwater-filled sandstone unites, and those of Figure 3.2 are determined in freshwater-filled limestone units. Therefore, determining the true in situ porosity requires the true rock matrix density and the true in situ fluid density such as formation water and gas. In general, the neutron log overestimates the shale porosity because of the pressure of hydroxyl groups in the clay minerals, and the density log underestimates the porosity when gas is present in the rock pore space. Figure 3.1 shows that by moving form a non-organic shale toward a gas-saturated organic shale, the separation between the neutron and density porosity logs decreases. The two logs of this well completely overlap in Otter Park formation, as shown in Figure 3.2.

Density porosity is very sensitive to the matrix density used in the density porosity equation. Therefore, we use the XRD results presented in Table 3.2 to correct density porosity for the matrix density. Figure 3.2 (b) shows that the lithology correction increases the density porosity values. We found that the size of crushed shale samples

should be small enough to obtain meaningful porosity values by the helium porosimeter. This can be explained by pore accessibility which can also result in the dependence of mercury injection capillary pressure (MICP) profiles on the sample size. In the next step, we use the matrix density determined by XRD to determine the sample porosity by a simple weight balance equation:

$$\emptyset = \frac{v_b - \frac{m_{ma}}{\rho_{ma}}}{v_b} \qquad (3.1)$$

Here, v_b is the bulk volume of the shale sample. m_{ma} and ρ_{ma} are the total mass and matrix density of the shale samples, respectively. We use the porosity and the lab porosity determined by eq. 3.1 to normalize the liquid volume imbibed in each shale sample. However, this is not the effective shale porosity because it also includes the disconnected pores.

3.3 Liquid-Rock Surface Properties

Kerosene and water are used as the oleic and aqueous phase, respectively.

(a)

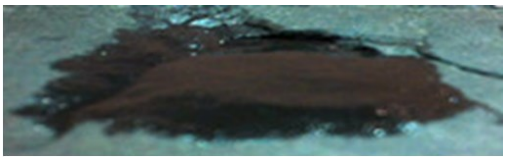

(b)

(c)

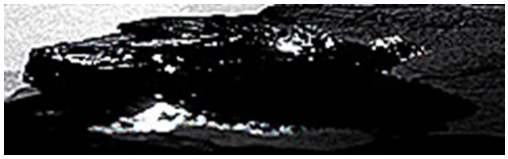

(d)

(e)

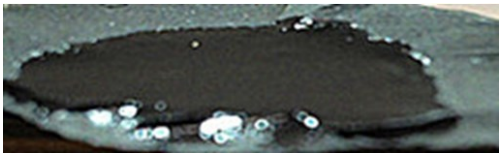

(f)

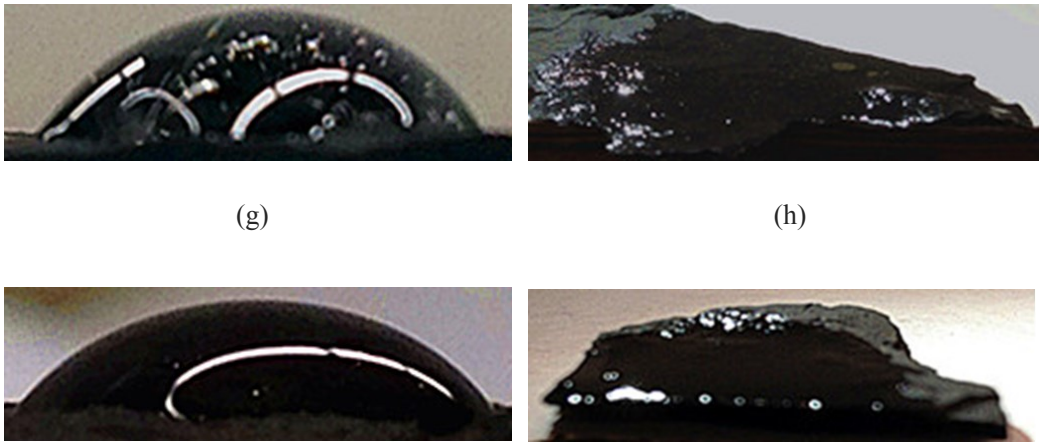

(g) (h)

(i) (j)

Figure 3.5 Pictures of water and oil droplets equilibrated on the surface of the five shale samples. The first and second columns show the water and oil droplets, respectively. The five rows relate to samples FS, UM, LM, UOP and LOP from the top to the bottom (Dehghanpour et al. 2012).

They measured the equilibrium contact angle to compare the interface properties for shale / oil and shale / water. Figure 3.5 compares the water and oil droplets on the clean surface of the five shale samples. Oil completely wets all of the samples, which is quantified by a zero contact angle. Water partially wets all of the samples. The approximately measured water contact angles, under room temperature and atmosphere pressure, are listed in Table 3.3. The water contact angle increases by increasing the depth, which can be explained by the increase of the organic material concentration. Table 3.3 also listed the ratio between the water and oil capillary pressure based on the Young Laplace equation. The ratio decreases from 2.14 for sample FS to 1.54 for sample OP2.

Table 3.3 Approximate values of water and oil contact angles (θ_w and θ_o) and the ratio between water and oil capillary pressures based on the Young-laplace equalition.

parameter	FS	UM	LM	UOP	LOP
θ_w (deg)	27	38	45	46	50
θ_o (deg)	0	0	0	0	0
$(\sigma_{wa}\cos(\theta_w))/(\sigma_{oa}\cos(\theta_o))$	2.14	1.89	1.7	1.67	1.54
"The water and kerosene surface tension (σ_{wa} and σ_{oa}) are assumed to by 72 and 30 dyn/cm, respectively."					

CHAPTER 4

SPONTANEOUS IMBIBITION OF BRINE AND OIL IN HORN RIVER GAS SHALES: EFFECT OF WATER ADSORPTION AND RESULTING MICROFRACTURES

In Chapter 3 we discussed the physical and petrophysical properties of dry shale samples from Horn River Basin. This chapter will compare the spontaneous imbibition rate of brine of various salinities and two oil samples in the similar shale samples. The rest of this chapter is divided into two sections: (1) the materials and methodology used for each set of imbibition experiments, (2) various plots of normalized imbibed mass versus time.

We measured the spontaneous imbibition of deionized (DI) water, potassium chloride (KCl) solution of various concentrations, and oil (kerosene and iso-octane) in shale samples from Fort Simpson (FS), Muskwa (M), and Otter Park (OP) formations of Horn River Basin.

4.1 Material Properties

The experimental materials include shale rock samples and fluids used for imbibition tests.

4.1.1 Shale Samples

A total of 54 shale samples were selected from the cores of two wells drilled in the Horn River Basin. The samples are classified into five sections of Fort Simpson (FS), Upper Muskwa (UM), Lower Muskwa (LM), Upper Otter Park (UOP), and Lower Otter Park (LOP). The average depth, core porosity, and total organic carbon (TOC) content of the five sections are listed in Table 4.1. The average concentration of

different minerals determined by x-ray diffraction (XRD) analysis is given in Table 4.2. The petrophysical properties of the five sections have been detailed in Chapter 3.

Table 4.1 Average values of depth, core porosity, and TOC of the five shale sections used in this study.

Label	Formation	Depth (m)	Øcore (%)	TOC (wt. %)
FS	Fort Simpson	1755	6.5	1.73
UM	Upper Muskwa	1771	8.4	2.25
LM	Lower Muskwa	1792	7.1	3.91
UOP	Upper Otter Park	2632	8.7	3.01
LOP	Lower Otter Park	2640	8.7	3.01

Table 4.2 Average mineral concentration (wt. %) of the five shale sections determined by x-ray diffraction.

Label	Calcite (wt.%)	Quartz (wt.%)	Dolomite (wt.%)	Chlorite (wt.%)	Illite (wt.%)	Plagioclase (wt.%)	Pyrite (wt.%)	matrix density
FS	0.5	29	2.7	6.5	55.4	4.1	1.7	2.747
UM	0	36.7	5.2	4.4	48.3	3.6	1.7	2.744
LM	0.9	45	1.9	0	43	5.2	4.0	2.79
UOP	4.4	60.8	2.6	0	25.7	3.7	2.8	2.748
LOP	12.9	43.6	2.2	0	33.8	4.4	3.2	2.772

4.1.2 Imbibing Fluids

Kerosene, iso-octane, DI water, and KCl solutions of various concentrations were used for the imbibition tests. Density, viscosity, and surface tension of fluids are listed in Table 4.3.

Table 4.3 Properties of different fluids used for imbibition experiments at 20^{o}C

Fluid	Density (g/cm^3)	Viscosity (cp)	Surface tension (dyn/cm)
Kerosene	0.81	1.32	28
Iso-octane	0.69	0.5	18.8
DI water	1	0.9	72
2wt. % KCl	1	0.89	72.7
4wt. % KCl	1.02	0.89	73.3
6wt. % KCl	1.03	0.89	73.9

4. 2 Boundary Conditions and Imbibition Types

Spontaneous imbibition is the process which occurs mainly due to the capillary suction forces, developed as a result of solid-fluid interaction. On the basis of the flow direction within porous medium, spontaneous imbibition can be classified into two following types: co-current spontaneous imbibition and counter-current spontaneous imbibition.

During this experiment, the spontaneous imbibition type is primary counter-current imbibition. In counter-current imbibition the imbibing fluid and the fluid being displaced flow in the opposite direction. While conducting imbibition experiments, certain boundary conditions: 1) all face open (AFO), 2) one end open (OEO), 3) two ends closed (TEC), and 4) two ends open (TEO) have been applied to simulate reservoir behaviour. The first two boundary condition types are applied on core samples during our experiments. The schematic of these two boundary condition types are shown as Figure 4.1.

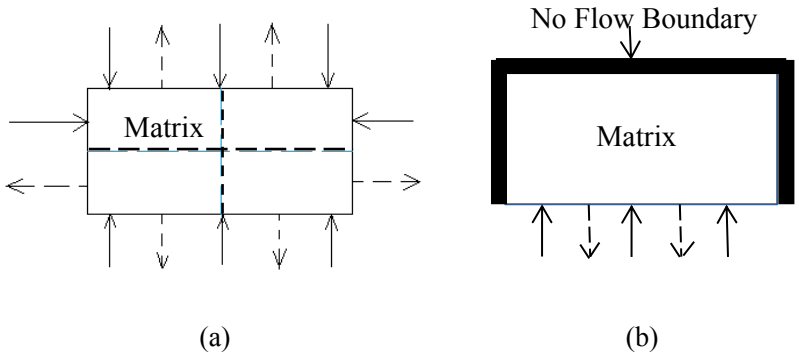

Figure 4.1 Schematic of (a) all face open (AFO) counter-current imbibition and (b) one end open (OEO) counter-current imbibition.

4.3 Experiment Procedure

A total of 69 spontaneous imbibition tests are conducted, which can be categorized into four sets. In sets 1 and 2, large samples with core-size diameter (~10 cm) are immersed in the fluid and all samples faces are open for imbibition. This boundary condition is referred here as all face open (APO). In set 3, small cylindrical plugs cut from the cores by nitrogen are immersed in the fluid, and only one sample end is open for imbibition. This open end face is parallel to the lamination direction in all tests. The other faces are coated by epoxy. This boundary condition is referred here as one end open (OEO). In set 4, both large samples and small samples were immersed into kerosene and iso-octane.

The general test procedure includes the following steps:

(1) Heat the selected samples at 100 ^{o}C in the oven for 24 hours to ensure moisture evaporation.

(2) Measure the dried sample mass and bulk volume.

(3) Place the samples in the imbibition cell and measure the weight gain at selected time intervals.

1. Set 1 (Parallel Imbibition Tests). This set compares the mass of oil and brine of various concentrations imbibed in different shales. A total of 19 samples, with the physical properties listed in table 4.4, were selected from the three formations. Each sample was immersed in oil, DI water or brine, and the mass gain was measured periodically for 72 hours that resulted in 19 imbibition curves. Pictures were taken before and after each test to observe any possible physical alteration.
2. Set 2 (Sequential Imbibition Tests). Set2 compares the mass of DI water and brines of different concentrations sequentially imbibed in identical samples. The basic test procedure is similar to that of set 1. However, for this set, three imbibition tests were conducted on each sample in the following steps:

   (1) Dry the selected sample and measure DI water imbibition profile.

   (2) Dry the same sample and measure brine imbibition profile.

   (3) Dry the same sample and measure DI water imbibition profile again.

   We applied the above procedure on three UOP and three LOP samples for brine with KCl concentrations of 2, 4, and 6wt% separately. Thus, a total of 18 (6×3) imbibition profiles were produced. Samples properties of this set are listed in Table 4.5. It was not possible to conduct the above test on Muskwa samples because they break after the first imbibition test as observed in set 1 results.

3. Set 3 (Comparing Brine and DI Water Imbibition Rate in Small Samples). This set compares the mass gain of DI water and KCl solution with various concentrations in small samples. In previous two sets, all faces of relatively large samples are open for imbibition, and therefore the chance of microfracture induction is relatively high. To address this problem, in this set 3, we use small cylinder plugs with only one end open for imbibition. The other faces are all sealed by epoxy. Using small coated samples has the following advantages over using large and uncoated samples:

(1) It is easier to select intact homogeneous samples with similar size and mass for more accurate comparative experiments.

(2) Sealing the small sample with epoxy reduces the chance for microfracture induction during the test.

(3) The imbibition could be assumed as one-dimensional and primarily counter-current, which can be modeled mathematically.

The experiments in set 3 are divided into two parts:

Part 1 (Sequential Imbibition Test). This part investigates the effect of KCl concentration on the imbibition rate in a Muskwa sample. Sample properties are listed in Table 4.6. The general test procedure is very similar as set 2. One sample, with the properties given in Table 4.6, is sequentially immersed in 6wt. %, 4wt. % and 2wt. % KCl solution then DI water, and the imbibition rate is measured. In contrast to set 2 tests, here we first immerse the samples in brine with high salinity (6wt. %) and finally in DI water to minimize the chance for microfractures induction in the early test.

Part 2 (Parallel Imbibition Tests). This part investigates the effect of KCl concentration on the imbibition rate in separate shale samples of similar size, mass and physical properties. Ternary plugs with similar size were cut from LM, UM, UOP and LOP core sections that resulted in the total of 12 (4×3) samples with the properties given in listed in Table 4.6. The three samples selected from each section were immersed into 6wt%, 4wt% KCl solution and DI water, respectively. The mass gain was measured that resulted in a total of 12 imbibition curves.

4）Set 4 (Parallel Oil Imbibition Tests). This set mainly compares the imbibition rates of kerosene and iso-octane into similar shale samples in two parts:

Part 1. Binary samples, with core-size diameter and similar thickness, from LM and LOP sections, with the properties given in Table 4.7, were immersed in kerosene and iso-octane, and imbibition profiles were measured.

Part 2. Small and coated binary samples from UM, LM, UOP and LOP sections, with the properties given in Table 4.7, were immersed in kerosene and iso-octane, and imbibition profiles were measured. Set 4 resulted in a total of 16 imbibition profiles. The sample boundary conditions in part 1 and 2 were AFO and OEO, respectively.

Table 4.4 Mass, average depth, cross-sectional area, and thickness of the cylindrical samples used in set 1 tests.

Label	mass (g)	area (cm^2)	thickness (cm)	diameter (cm)	depth (m)
FS1	255.2	78.5	1.34	10	1755
FS2	276.2	78.5	1.34	10	1755
UM1	360.7	78.5	1.86	10	1758
UM2	347.2	78.5	1.77	10	1758
LM1	423	78.5	2.23	10	1792
LM2	282.7	78.5	1.59	10	1792
LM3	416.9	78.5	2.2	10	1792
LM4	341.7	78.5	1.85	10	1792
LM5	397	78.5	2.04	10	1792
UOP1	529.5	78.5	2.74	10	2603
UOP2	581	78.5	3	10	2603
UOP3	335.2	78.5	1.7	10	2603
UOP4	592.4	78.5	3.09	10	2603
UOP5	558.4	78.5	2.91	10	2603
LOP1	335.9	78.5	1.21	10	2639
LOP2	416.6	78.5	2.36	10	2639
LOP3	235	78.5	1.21	10	2639
LOP4	398.3	78.5	2.29	10	2639
LOP5	446.9	78.5	2.37	10	2639

"The boundary condition in all samples is AFO."

Table 4.5 Mass, average depth, cross-sectional area, and thickness of the cylindrical samples used in set 2 tests.

Label	mass1 (g)	mass2 (g)	mass3 (g)	area (cm^2)	thickness (cm)	diameter (cm)	depth (m)
UOP6	476.2	475.3	474.5	70.66	2.5	9.48	2608
UOP7	433.6	433.6	433.4	71.83	2.4	9.56	2608
UOP8	465.4	465.2	464.4	73.48	2.4	9.67	2608
LOP6	416.2	416.2	416.3	62.46	2.6	8.91	2642
LOP7	390.5	390.4	390.7	71.83	2.5	8.81	2642
LOP8	394	393.4	393.7	62.46	2.5	8.91	2642

"The boundary condition in all samples is AFO.1,2,and 3 represent first, second and third imbibition tests conducted on each sample."

Table 4.6 Mass, average depth, cross-sectional area, and thickness of the cylindrical samples used in set 3 tests.

Label	mass (g)	area (cm^2)	thickness (cm)	diameter (cm)	depth (m)
UM3	40.6	7.6	1.3	3.11	1722
UM4	9.82	3.8	0.88	2.2	1722
UM5	8.79	3.8	0.79	2.2	1722
UM6	12.82	3.8	1.18	2.2	1722
LM6	16.35	3.8	1.48	2.2	1796
LM7	12.82	3.8	1.25	2.2	1796
LM8	17.46	3.8	1.68	2.2	1796
UOP9	17.46	3.8	1.23	2.2	2608
UOP10	14.73	3.8	1.02	2.2	2608
UOP11	10.99	3.8	1.18	2.2	2608
LOP9	15.22	3.8	1.38	2.2	2642
LOP10	15.07	3.8	1.85	2.2	2642
LOP11	12.82	3.8	1.15	2.2	2642

"The boundary condition in all samples is OEO."

Table 4.7 Mass, average depth, cross-sectional area, and thickness of the cylindrical samples used in set 4 tests.

Label	mass (g)	area (cm^2)	thickness (cm)	diameter (cm)	depth (m)	B.C.
UM7	9.8	3.8	0.88	2.2	1772	OEO
UM8	8.78	3.8	0.79	2.2	1772	OEO
LM9	16.34	3.8	1.48	2.2	1796	OEO
LM10	12.84	3.8	1.25	2.2	1796	OEO
LM11	197.23	73.48	1.3	9.67	1796	AFO
LM12	220.35	73.48	1.3	9.67	1796	AFO
LM13	166.4	73.48	1.1	9.67	1796	AFO
LM14	174.22	73.48	1.17	9.67	1796	AFO
UOP12	14.72	3.8	1.23	2.2	2608	OEO
UOP13	13.4	3.8	1.22	2.2	2608	OEO
LOP12	14.81	3.8	1.85	2.2	2642	OEO
LOP13	15.7	3.8	1.85	2.2	2642	OEO
LOP14	320.57	73.48	1.95	9.67	2642	AFO
LOP15	322.29	73.48	2.03	9.67	2642	AFO
LOP16	216.79	73.48	1.15	9.67	2642	AFO
LOP17	184.25	73.48	0.9	9.67	2642	AFO

4.4 Experiment Results

This section presents and discusses the results of the four sets of imbibition experiments. Moreover, in each subsection, the imbibition profiles are compared to identify the key factors controlling spontaneous liquid intake of dry shale samples.

1. Set 1. Figure 4.2 compares the imbibition profiles of oil and brine of different KCl concentrations. Brine intake of all samples is significantly higher than oil intake. This is more pronounced in FS and M section samples. It is well known that the primary driving force for spontaneous imbibition is capillary suction which at the pore scale is expressed as $(\sigma_{ia}\cos(\theta_i))/D_p$, where σ_{ia}, θ_i, and D_p are the surface tension, contact angle and average pore size diameter, respectively. One may argue that the observed difference is due to the lower surface tension of oil as compared to water. Therefore, we multiply the oil imbibition profiles by

$(\sigma_{wa}\cos(\theta_w))/(\sigma_{oa}\cos(\theta_o))$, which is shown by the dashed curves in Figure 4.2. The approximate values of $(\sigma_{wa}\cos(\theta_w))/(\sigma_{oa}\cos(\theta_o))$ for each section are listed in Table 4.2. If the capillarity is the only factor controlling the water intake, the maximum water intake should be nearby the dash curve. However, the measured brine imbibition is still much above the dashed curve for all of the samples. The difference between oil and water imbibition rate is more pronounced in the dimensionless plots presented in Chapter 5. The excess water intake relative to oil intake, which is more pronounced in clay-rich FS and UM samples, can be due to water adsorption on the surface of dehydrated clay minerals.

Table 4.8 Measured ratio between water and oil capillary pressure based on Young-Laplace equation.

Parameter	FS	UM	LM	UOP	LOP
$(\sigma_{wa}\cos(\theta_w))/(\sigma_{o1a}\cos(\theta_{o1}))$	2.14	1.89	1.7	1.67	1.54
$(\sigma_{wa}\cos(\theta_w))/(\sigma_{o2a}\cos(\theta_{o2}))$	3.42	3.02	2.71	2.66	2.47

"Subscripts o1 and o2 represent kerosene and iso-octane, respectively."

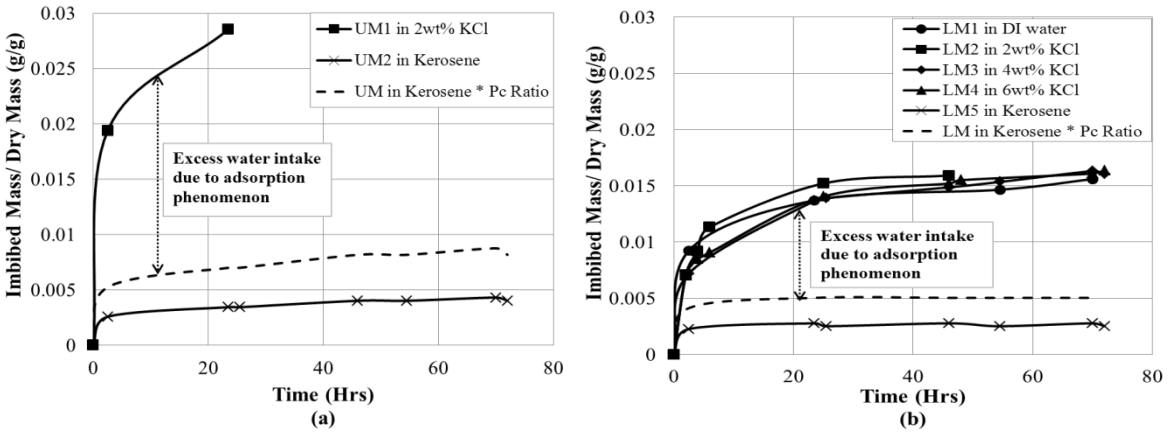

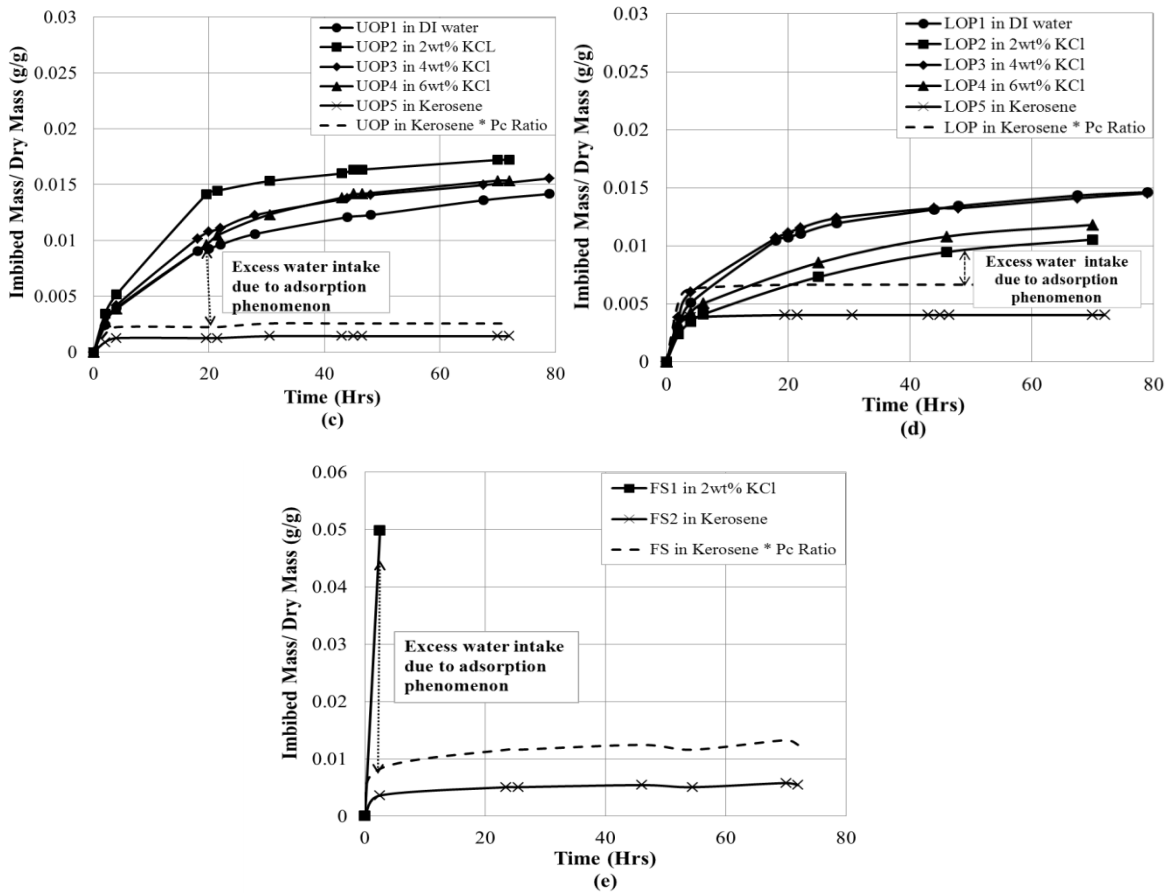

Figure 4.2 Brine and oil normalizes imbibed mass versus time in (a) UM, (b) LM, (c) UOP, (d) LOP, and (e) FS shale samples (set 1). The clay-rich samples from UM (a) and FS (e) completely break after exposure to 2wt. % KCl solution, and therefore the corresponding imbibition profiles are incomplete. Pc ratio is ($\sigma_{wa}\cos(\theta_w)$) / ($\sigma_{o1a}\cos(\theta_{o1})$) that is given in Table 3.10 for each section.

Figure 4.3 shows the pictures of FS and UM samples before and after 3 days of exposure to 2wt. % KCl solution and kerosene. In contrast to oil, brine alters the two samples physically, which indicates the water adsorption by clay minerals present in the two samples. Figure 4.4 shows pictures of LM, UOP and LOP samples before imbibition test and after 3 days of exposure to 2wt. % and 6wt. % brines. Brine dose not destroy the OP samples, although some microfractures are induced which will be discussed later. Increasing the brine salinity from 2wt. % to 6wt. % reduce the degree

of physical alteration of LM samples which indicates the role of KCl in swelling inhibition.

Interestingly, the imbibition mass of 6wt. % KCl in LM, UOP and LOP samples is still unexpectedly higher than that of oil in the same samples (Figure 4.2 b-d), although the pictures of these samples shown in Figure 4.4 do not show a strong swelling. However, we observe some induced microfractures after brine imbibition tests that will be discussed later. Therefore, water adsorption can still be responsible for the excess brine intake, but it is not strong enough to break some of the samples.

Although high brine intake of the shale samples shown in Figure 4.2 indicates the dependence of imbibition rate on KCl concentration. This might be due to the difference in size and mass of the samples used in set 1 tests. To address this problem, we conduct set 2 tests where the imbibition mass of water and brine in the identical samples are measured and compared.

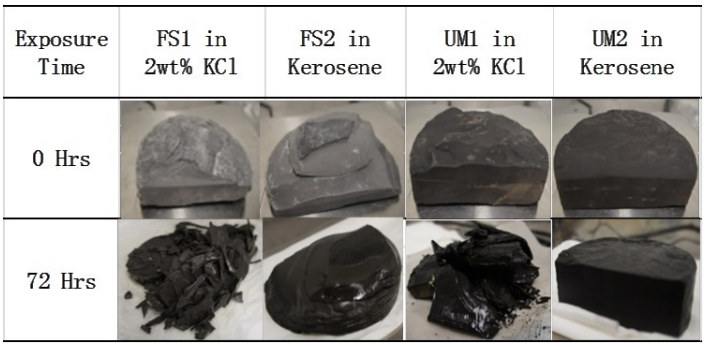

Figure 4.3 Pictures of Fort Simpson and Upper Muskwa samples before and after exposure to oil and 2wt. % KCl brine.

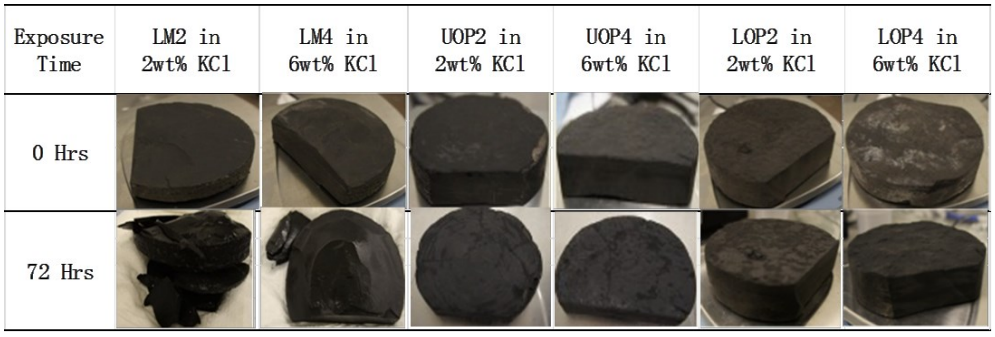

Figure 4.4 Pictures of Lower Muskwa and Otter Park samples before and after exposure to brine of different salinity.

2. Set 2. In this set, each sample is sequentially immersed in DI water, KCl solution with a certain salinity, and DI water again. The tests were conducted on three samples from UOP and there samples from LOP, which resulted in the total of 18 imbibition profiles. Each subfigure in Figure 4.5 compares the imbibition profiles of DI water, brine, and again DI water sequentially imbibed in each sample. In each plot, circles and triangles represent the second imbibition test, where brine with KCl concentration of 2wt. %, 4wt. %, and 6wt. % is used. Figure 4.5 (a), (c), and (e) compare the mass of DI water and KCl solution with respective concentration of 2wt. %, 4wt. %, and 6wt. %, imbibed in UOP samples. Figure 4.5 (b), (d), and (f) compares the mass of similar fluids imbibed in LOP samples.

   In general, the data do not show a strong salinity effect on aqueous phase imbibition in any of the samples. Interestingly, the early time mass intake measured in the first test, where the DI water is used, is relatively lower than that measured in the other two subsequent tests. The trend indicates that in general the imbibition conductance is higher in the second and third tests. One may argue that the drying process does not completely dehydrate the shale samples. Even if some water remains in the sample, one should expect less imbibition rate in the second and third tests because hydrated clay minerals have less affinity for water adsorption. Furthermore, the equilibrium total imbibed mass generally slightly increases from the first immersion to the third immersion. This trend indicates that the accessible pore volume slightly increases after the first immersion. Although OP samples do not swell and break when exposed to water, we observe microfractures induced after the first imbibition test that is shown for example in Figure 4.6. Therefore, the higher imbibition mass observed at the early time scales in the second and third tests can be explained by the presence of microfractures induced in the first test.

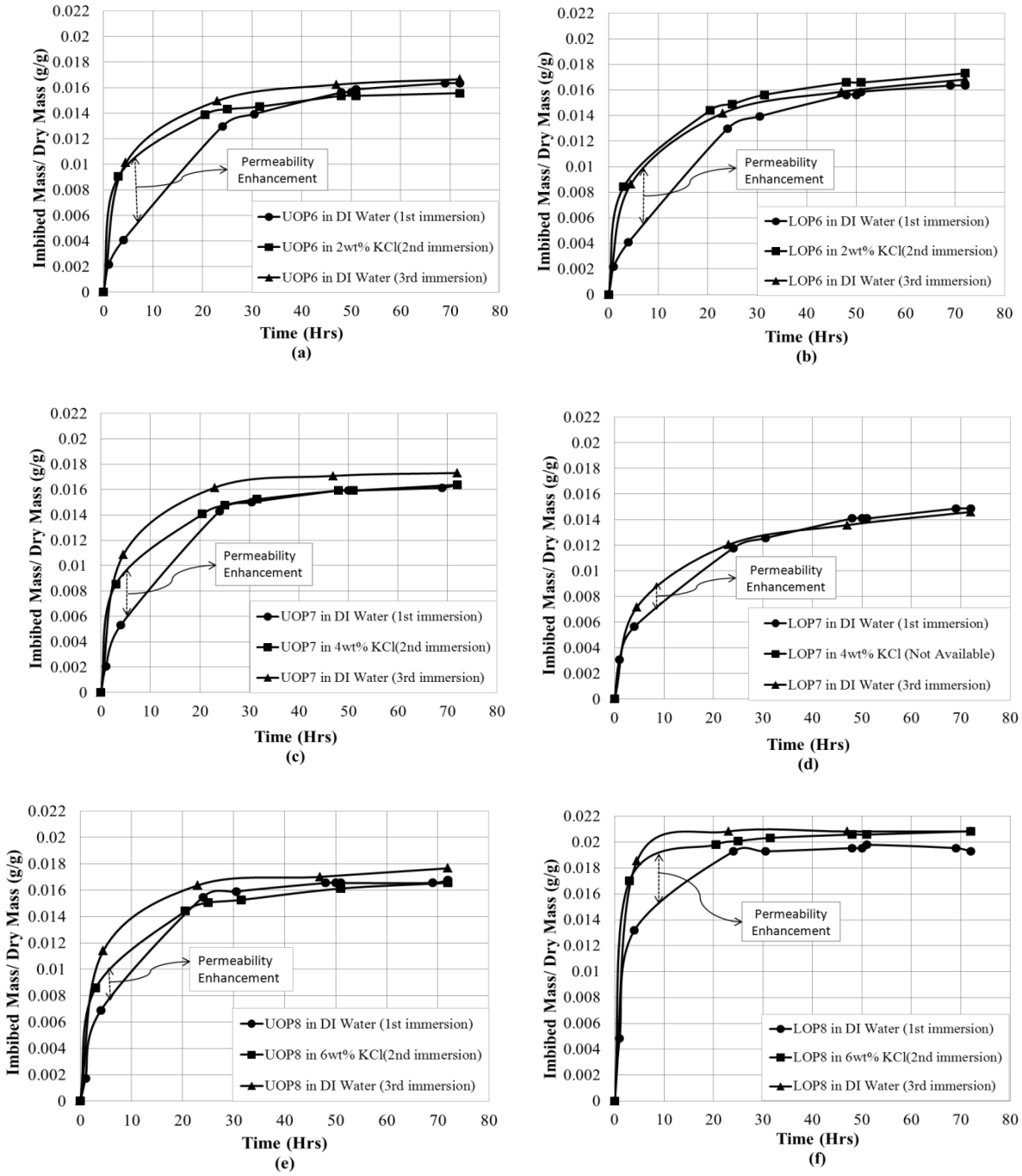

Figure 4.5 The results of sequential imbibition experiments (set 2) conducted on three Upper Otter Park samples (a, c, and e) and three Lower Otter Park samples (b, d, and f).

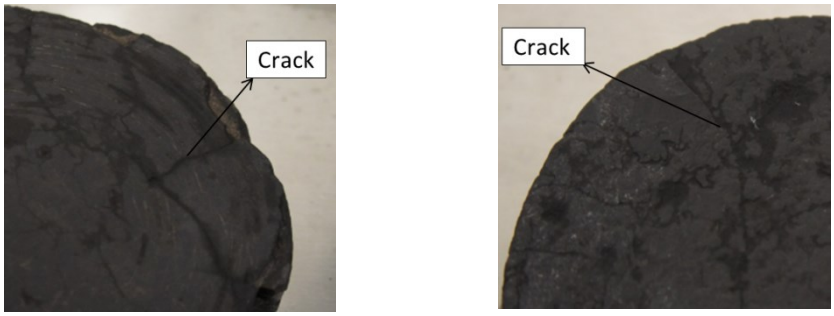

(a) **(b)**

Figure 4.6 Pictures of LOP6 (a) and UOP6 (b) after imbibition tests (set 2) show water-induced cracks.

3. Set 3. In the experiments of set 1, we observed that brine breaks the Muskwa samples. Therefore, it was impossible to conduct sequential imbibition test (set 2) on large Muskwa samples. To address this problem of microfracture induction, and also to minimize the heterogeneity effect, small samples were used in set 3. Here, only one end of the sample is open for imbibition, and the other faces are sealed by epoxy.

   Part 1 (Sequential Imbibition Test). In part 1 if the set, we study the effect of salinity on brine imbibition in a Muskwa sample by conducting sequential imbibition tests similar to set 2 tests. One Muskwa sample was sequentially immersed in 6wt. %, 4wt. % and 2wt. % KCl brines and DI water, and the imbibition profiles were measured, which are compared in Figure 4.7. The data do not suggest any salinity effect, which confirms the results of set 2 experiments. However, in contrast set 2 results, here the first imbibition curve is not lower than other curves at early time scales. This observation indicates the absence of microfractures in this test that can be explained by two reasons: (1) the sides and one end of the small samples are sealed by epoxy that reduces the chance for microfracture induction. (2) the sample is first exposed to 6wt. % brine as opposed to set 2 where the samples are first exposed to DI water.

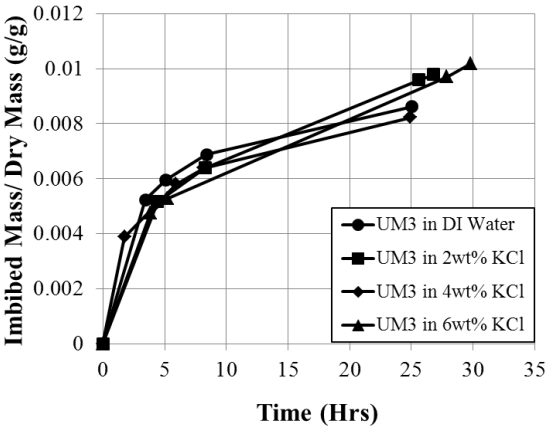

Figure 4.11 Comparsion between the imbibition rate of DI water and KCl brine of different concentrations in one Muskwa sample (related to part 1 of set 3).

Part 2 (Parallel Imbibition Test). In part 2 of this set, we cut ternary samples with almost equal size from each of LM, UM, UOP and LOP sections that resulted in the total of 12 samples. The samples selected from each section are immersed in DI water, 4wt. % and 6wt. % KCl brines, and the imbibition profiles are measured. Each subfigure of Figure 4.8 compares the imbibition profiles of DI water and the two brines. Figure 4.8 (a), (b) and (d) shows that increasing KCl concentration generally slightly decreases the imbibition rate. However, this trend is not observed in Figure 4.7 (c). One should note that the observed differences between the curves may also be due to slight differences in samples size and small-scale heterogeneity.

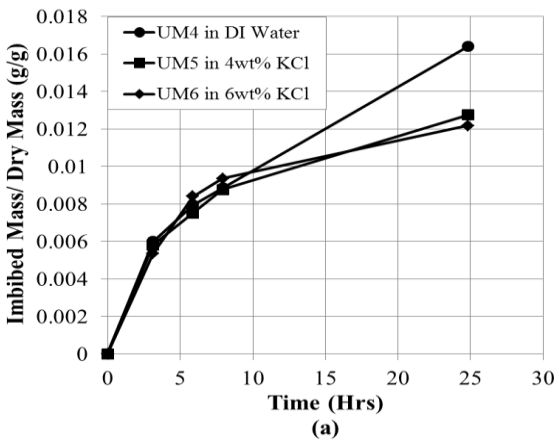

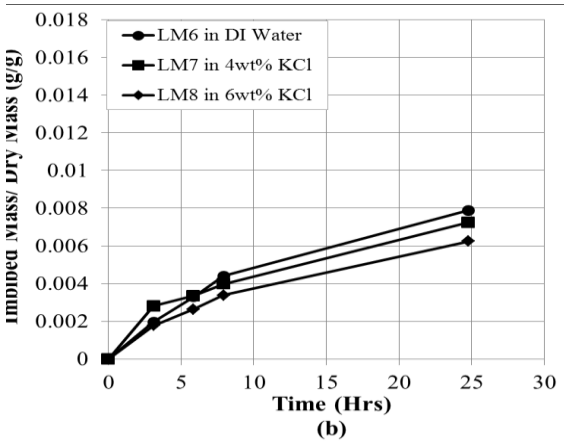

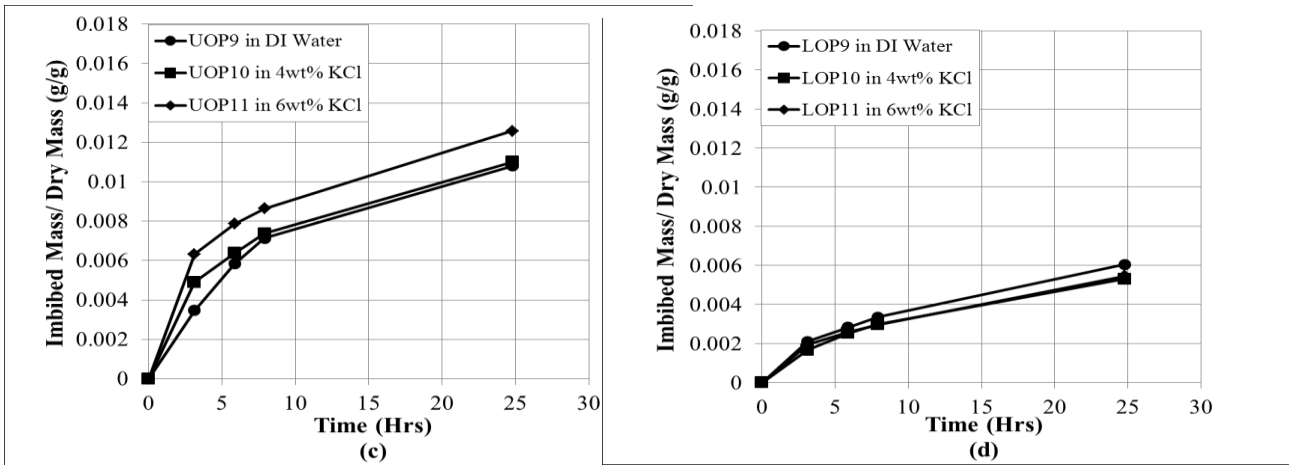

Figure 4.12 Comparison between imbibition rate of DI water and KCl brine of different salinities in ternary samples selected from (a) UM, (b) LM, (c) UOP, and (d) LOP sections.

4. Set 4. The results of kerosene and iso-octane imbibition tests will be presented in the dimensionless plots of Chapter 5.

4.5 Summary

(1) The significant brine intake of Fort Simpson and Muskwa samples results in microfracture induction and sample disintegration. However, brine uptake dose not result in disintegration of the Otter Park samples, although some microfractures are observed. The physical alteration degree is correlated to the amount of brine intake. By increasing the sample depth, from Fort Simpson to Muskwa, and Otter Park formation, the degree of physical alteration, and brine intake decrease. Previous study (Dehghanpour et al. 2012) shows that rock clay content is positively correlated to total brine uptake. Thus the decreased brine uptake can be explained by the change in clay content by increasing the depth. FS has the highest clay concentration followed by UM and LM, while OP samples have the least clay content. Adsorption of water on the surface of negatively charged clay platelets develops internal expansive stresses, and in turn expands and disintegrates the unconfined shale samples (Hensen et al. 2002;

Steiger 1982). However, the XRD results show that Illite is the dominant clay mineral in all of the samples, while the swelling clays such as montmorrillonite are negligible. It is generally believed that Illite having a 2:1 structure with the potassium as the interlayer cation dose not swell. However, previous experiments show that water adsorption can even alter illitic shales (Chenevert 1970). In addition, the presence of a small amount of mixed layer clay (interlayered or interstratified mixtures of illite and montmorrillonite) may be the possible reason for the observed alteration. The hydration tendency of mixed layer clays is greater than that of illite (Hensen et al.2002).

We also observed some dependence of sample alteration on KCl concentration. For example, physical alteration of UM samples exposed to 2wt. % KCl brine is greater than that of the similar samples exposed to 6wt. % KCl. This observation can be explained by the swelling inhibition characteristics of KCl. Simply, increasing the salt concentration reduces the activity difference between shale water and external water, which in turn reduces the water adsorption and shale expansion (Chenevert et al. 1970). In addition, potassium ions in brine can replace cations already present in the shale. Cations with low hydration energy such as K^+ remain unhydrated and interact more strongly with the surface of clay minerals as compared to smaller cations such as Na^+. The reluctance of potassium ions to hydration reduces the swelling tendency of shale and results in better screening of negatively charged clay layers (Steiger 1982; Boek et al. 1995). However, clay-rich FS samples completely disintegrated even when exposed to 6wt. % KCl brine. Furthermore, changing the KCl concentration dose not consistently affect the imbibition rates.

(2) The driving force and also the effective permeability for water intake are higher than that for oil intake in the dry organic shales studied here. This contradicts the observation that oil completely spreads, while brine shows a measureable contact angle on the clean surface of all the samples. The excess driving force can be explained by the adsorption potential of the compacted clay platelets present in

the dry shale samples. Simply, the negatively charged clay platelets strongly attract polar water molecules (Hensen et al. 2002; Chenevert 1970; Fripiat et al. 1984). This driving force is absent in the case of oil imbibition. Therefore, the total water flux during spontaneous imbibition in a dry organic shale consists of capillary-driven (q_{cap}) and adsorption-driven (q_{ads}) components:

$$q_{cap} = D\frac{\partial S_w}{\partial x}, \ \ where\ D = \frac{k_w}{\mu_w}\frac{\partial P_c}{\partial S_w}$$

$$q_{ads} = c\frac{\partial w}{\partial x}$$

Here, q_{cap} is related to the gradient of water saturation in space ($(\partial S_w)/(\partial x)$), while q_{ads} is related to the gradient of water mass fraction in space ($(\partial w)/(\partial x)$). D is a capillary diffusion parameter, which depends on water saturation and rock-fluid multiphase properties, while c is adsorption constant, which depends on rock structure, clay mineralogy, and fluid chemistry. For the samples used in this study, q_{ads} dominates the water intake, while q_{cap} dominates the oil intake. The excess water intake can also be attributed to the enhancement of sample permeability due to water-induced microfractures. The adsorption of water by clay platelets induces large internal stresses in confined samples or expands the unconfined samples (Chenevert 1970).

(3) Brine can spontaneously induce microfracture in organic shales. The induced microfractures, which are possibly the result of water adsorption, enhance the shale permeability, and in turn the imbibition rate. This phenomenon that does not occur during the oil imbibition can partly explain the high ratio of water to oil intake observed in all samples studies here.

(4) The presence of KCl does not consistently influence the imbibition rate in organic shales. However, previous experiments reporting counter-current imbibition of brine into oil-saturated reservoir rocks (Morrow et al. 1998; Tang et al. 1997) show that reducing brine salinity increases water imbibition rate, and in turn oil recovery rate. Although sufficient increase of KCl concentration reduced the

degree of clay swelling and imbibition rate in some of the Muskwa samples, in general we did not observe a strong dependence of imbibition rate on KCl concentration. The lake of consistent correlation between imbibition rate and KCl concentration observed in our experiments is partly because the shale samples are initially dry, and initial water saturation is zero. Furthermore, the dry samples may contain some salt from the initial formation water, and the KCl concentrations used in this study are not high enough to observe a strong salinity effect.

(5) We observed significant brine intake of various dry organic shale samples. It can be argued that in situ shales may have some initial water saturation that has been shown to influence the spontaneous imbibition rate in gas/water/rock system (Li et al. 2006). However, the irreducible water saturation of some gas shale (Wang et al. 2008) and tight gas reservoirs (Bennion et al. 2005; Newsham et al. 2002) is abnormally low. In other words, such reservoirs are in a state known as "sub-irreducible initial water saturation", created by the excessive drying at high paleo temperatures and pressures, and the lack of sufficient water for increasing the irreducible water saturation (Wang et al. 2008). Our measurements indicate that the rock matrix of such reservoirs can adsorb the water in the surrounding fractures, and the adsorbed mass can be more than 1% of the exposed rock mass. The water imbibed into the complex and fine pore structure of shales (Bai et al. 2012; Clarkson et al. 2012) can hardly be drained by gas due to the strong capillary pressure effect. Furthermore, it has been reported that less than 50% of the injected fracturing water is recovered during the flowback operations (Wang et al. 2008; Soeder et al. 2011; Asadi et al. 2008). We conclude that spontaneous imbibition of fracturing water into the shale matrix can partly explain poor load recovery reported in the field. On one hand, the imbibed water can damage the reservoir through various mechanisms (Bennion et al. 2005; Shaoul et al.2011). On the other hand, we observe that strong water adsorption by the shale samples

can induce microfractures that enhance the total rock permeability. This spontaneous permeability enhancement can enhance gas recovery rate from low permeability shale reservoirs (Wang et al. 2011; King et al. 2012). In addition, rapid imbibition of the water into the matrix helps to clean up water in fractures that in turn enhances gas effective permeability. Therefore, extended shut-in can reduce and increase initial production rates of water and gas, respectively (Cheng 2012).

CHAPTER 5

SCALING THE IMBIBITION DATA OF HORN RIVER SHALE

This chapter presents analytical scaling of spontaneous imbibition in shales. Dimensionless scaling has been applied to investigate spontaneous imbibition of various fluids in Fort Simpson, Muskwa and Otter Park shales.

5.1 Dimensionless Scaling of Spontaneous Imbibition

The dimensionless analysis is an essential and useful tool for interpretation of laboratory results and predicting the field performance from laboratory measurements. For conventional rocks, the imbibition rate is usually affected by (1) rock properties such as porosity, permeability and wetting affinity; (2) fluid properties including viscosity, density and interfacial tension; and (3) geometrical parameters such as size, boundary conditions and shape of the test samples (Li and Horn, 2002). Various dimensionless scaling groups have been developed to characterize the spontaneous imbibition in rocks. We applied the dimensionless scaling approach to understand the factors controlling imbibition process in fluid-rock systems and analysis rock wettability.

5.1.1 Dimensionless Time Formulation

Several formulations have been proposed to scale imbibition in gas saturated rocks (Li and Horne, 2006). The most frequently used dimensionless time (t_D) for scaling spontaneous imbibition data was presented by (Mattax and Kyte, 1962; Ma et al. 1997):

$$t_D = t\sqrt{k/\emptyset}\,\frac{\sigma}{\mu_m}\frac{1}{L_c^2} \tag{5.1}$$

where, t_D is dimensionless time, k is matrix permeability, $\emptyset$ is porosity, σ is interfacial tension, μ_m is the geometric mean of water and oil viscosity, and t is the imbibition time. L_c is the characteristic length which depends on sample shape, size and boundary condition.

The dimensionless time (Eq. 5.1) accounts for the rock, fluid and sample's geometrical properties. Besides, in the dimensionless time proposed for gas/ water/ rock systems, only water viscosity is honored. Imbibition ratio is affected by sample geometrical parameters: decrease the ratio of sample volume to surface area open to fluid, the imbibition rate would be increased. Therefore, to compensate for the effect of sample size, shape and boundary conditions, Kazemi et al (1992) proposed the following shape factor:

$$F_s = \frac{1}{V_b}\sum_{i=1}^{n}\frac{A_i}{S_{A_i}} \tag{5.2}$$

Where, V_b is bulk volume of rock, A_i is area open to imbibition fluid in ith direction, S_{A_i} is the distance from A_i to the center of rock matrix, and n is the total number of surface open to imbibition fluid.

A characteristic length L_s that corresponds to this shape factor (Ma et al. 1995) is defined by:

$$L_s = \sqrt{\frac{1}{F_s}} = \sqrt{\frac{V_b}{\sum_{i=1}^{n} A_i/S_{A_i}}} \tag{5.3}$$

A modified characteristic length (L_c) was proposed by Ma et al. (1995) as below:

$$L_c = \sqrt{\frac{V_b}{\sum_{i=1}^{n} A_i/l_{A_i}}} \tag{5.4}$$

Where, l_{A_i} is the distance travelled by the imbibition front from imbibition face to the no flow boundary.

5.1.2 Characteristic Length of Various Boundary Condition Types

Boundary condition can affect the characteristic length (L_c). In the following we calculate the characteristic length for a cylindrical core (Figure 5.1) under different boundary conditions (Table 5.1).

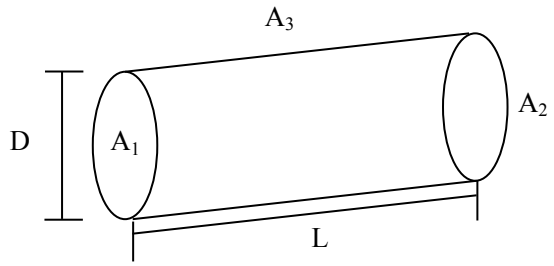

Figure 5.1 Schematic of a cylindrical core

Table 5.1 Characteristic length for a cylindrical core under different boundary conditions

B.C.	A_1	A_2	A_3	V_b	I_{A1}	I_{A2}	I_{A3}	$\sum^{n}_{i=1}$	L_c
AFO	$\pi D^2/4$	$\pi D^2/4$	πLD	$(\pi D^2/4)*L$	$L/2$	$L/2$	$D/2$	$(\pi D^2/L)+2\pi L$	$DL/2\sqrt{(D^2+2L^2)}$
OEO	$\pi D^2/4$	/	/	$(\pi D^2/4)*L$	L	/	/	$(\pi D^2/4)*(1/L)$	L
TEO	$\pi D^2/4$	$\pi D^2/4$	/	$(\pi D^2/4)*L$	$L/2$	$L/2$	/	$\pi D^2/L$	$L/2$
TEC	/	/	πLD	$(\pi D^2/4)*L$	$D/2$	/	/	$2\pi L$	$D/(2\sqrt{2})$

Boundary conditions such as all face open (AFO) and one end open (OEO) were used for our spontaneous imbibition experiments.

5.2 Imbibition Data Scaling of Horn River Shale

In Figure 5.2, we plot the normalized brine and oil mass imbibed in the large uncoated samples of set 1, set 2 and set 4 (Chapter 4) versus the corresponding dimensionless

time. On the basis of the existing theories of spontaneous imbibition, all of the data should sit around one curve. Interestingly, we observed that the brine imbibition data are much above the oil imbibition data. This result confirms the results of set 1 in the dimensional plots of Figure 4.2. The observed differences between brine and oil imbibition data can be explained by (1) water adsorption and (2) increase in sample permeability and effective rock-fluid interface due to induced microcracks that are not accounted for in the dimensionless time given by eq. 5.1 because fixed original values of $\emptyset$, k, L_c are used.

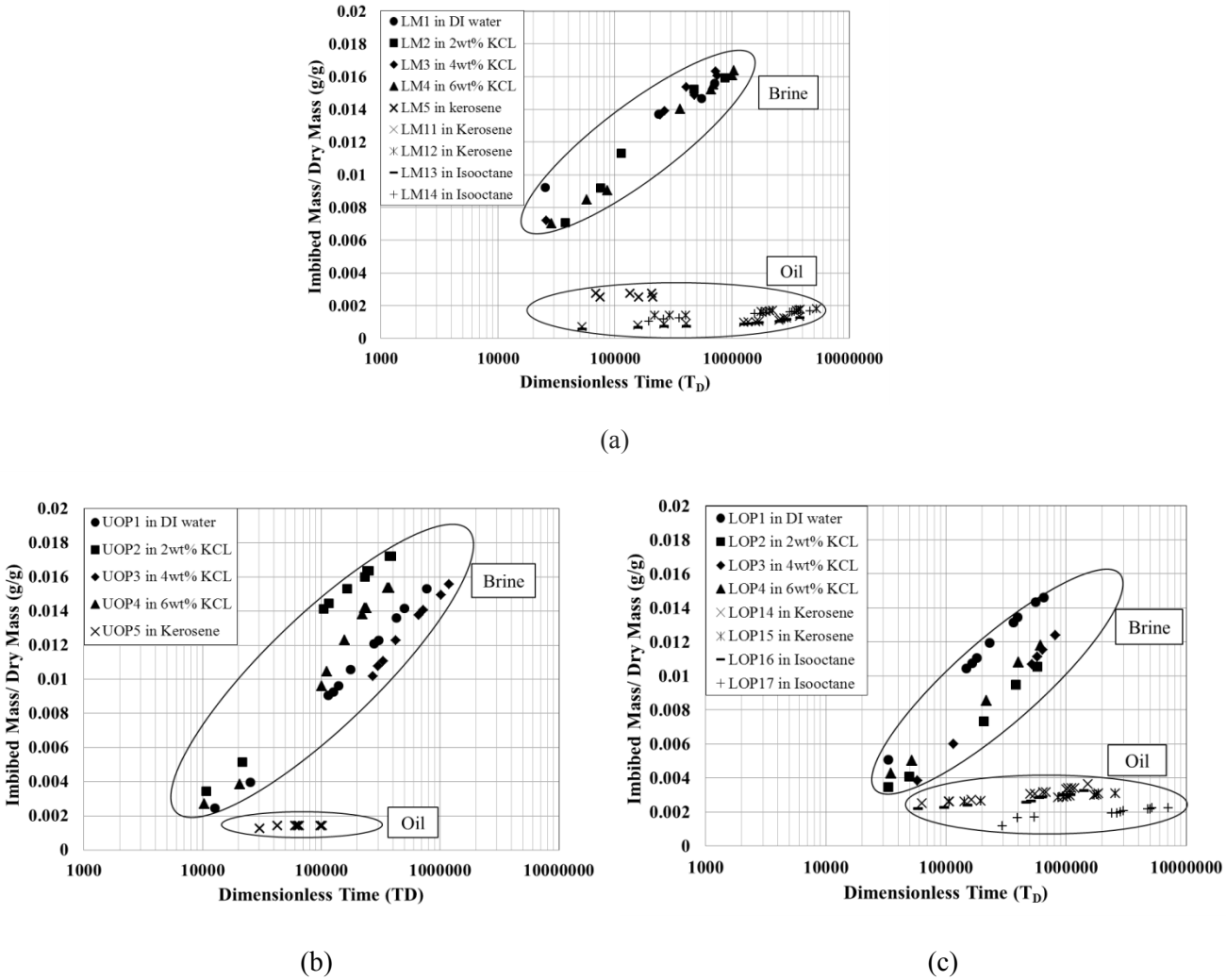

Figure 5.2 Normalized imbibed mass versus dimensionless time for large samples with AFO boundary condition.

To confirm the observations of Figure 5.2, we similarly plot the normalized brine and oil mass imbibed in the small coated samples of set 3 and set 4 (Chapter 3) versus the corresponding dimensionless time in Figure 5.3. Again, we observe that brine imbibition data are above oil imbibition data, although the separation is relatively smaller in this case.

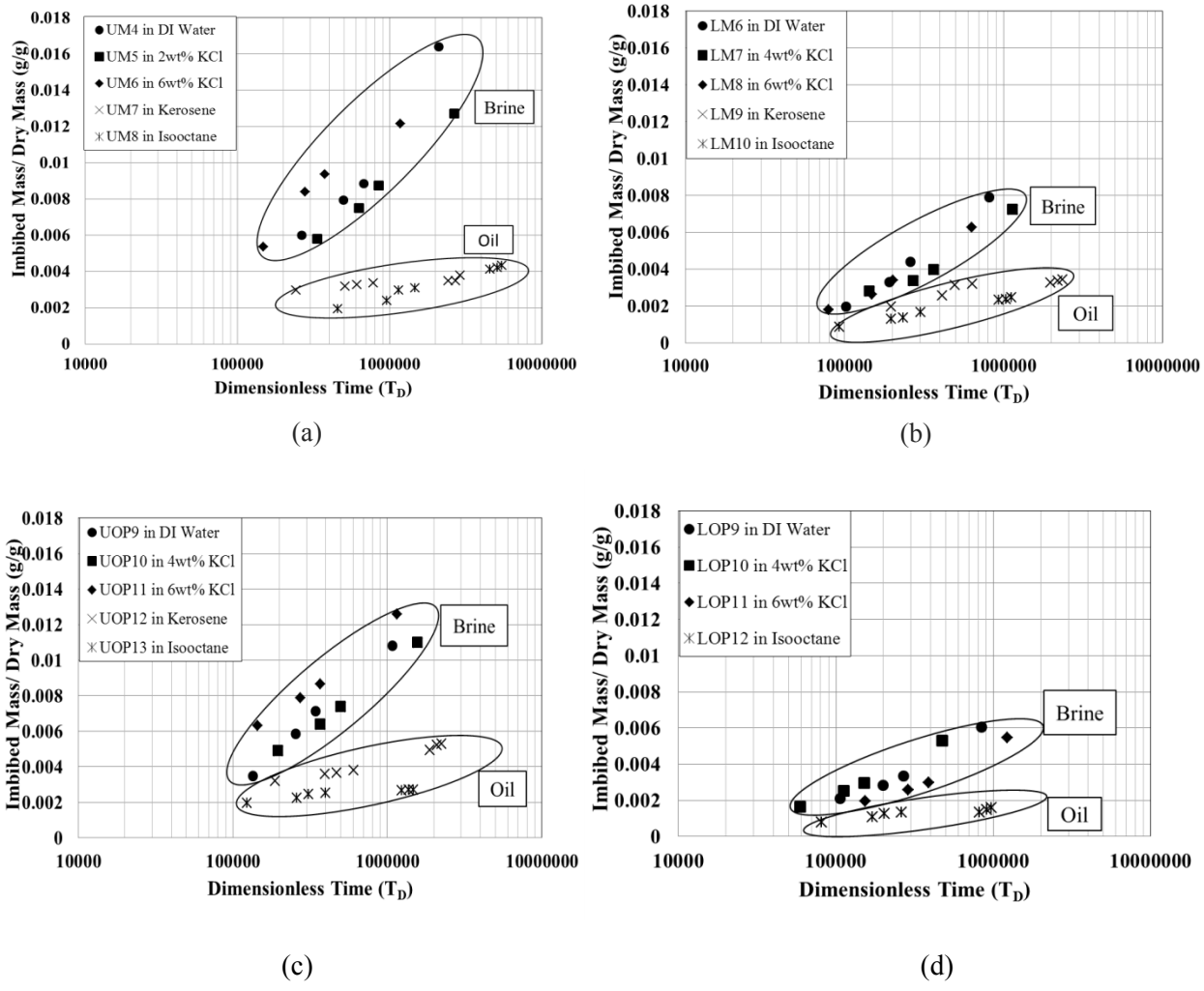

Figure 5.3 Normalized imbibed mass versus dimensionless time for small samples with OEO boundary condition.

For a more consistent comparison, we plot all of the imbibition data versus dimensionless time in Figure 5.4. The data can be classified into three groups: the maximum values relate to brine and DI water imbibition in large uncoated samples with the boundary condition of AFO. The intermediate values relate to brine and DI

water imbibition in small coated samples with the boundary condition of OEO. The minimum values relate to oil imbibition in both large and small samples. The unexpected high values of brine and DI water data relative to oil data can be explained through water adsorption by clay minerals and resulting changes in sample properties that will be discussion later.

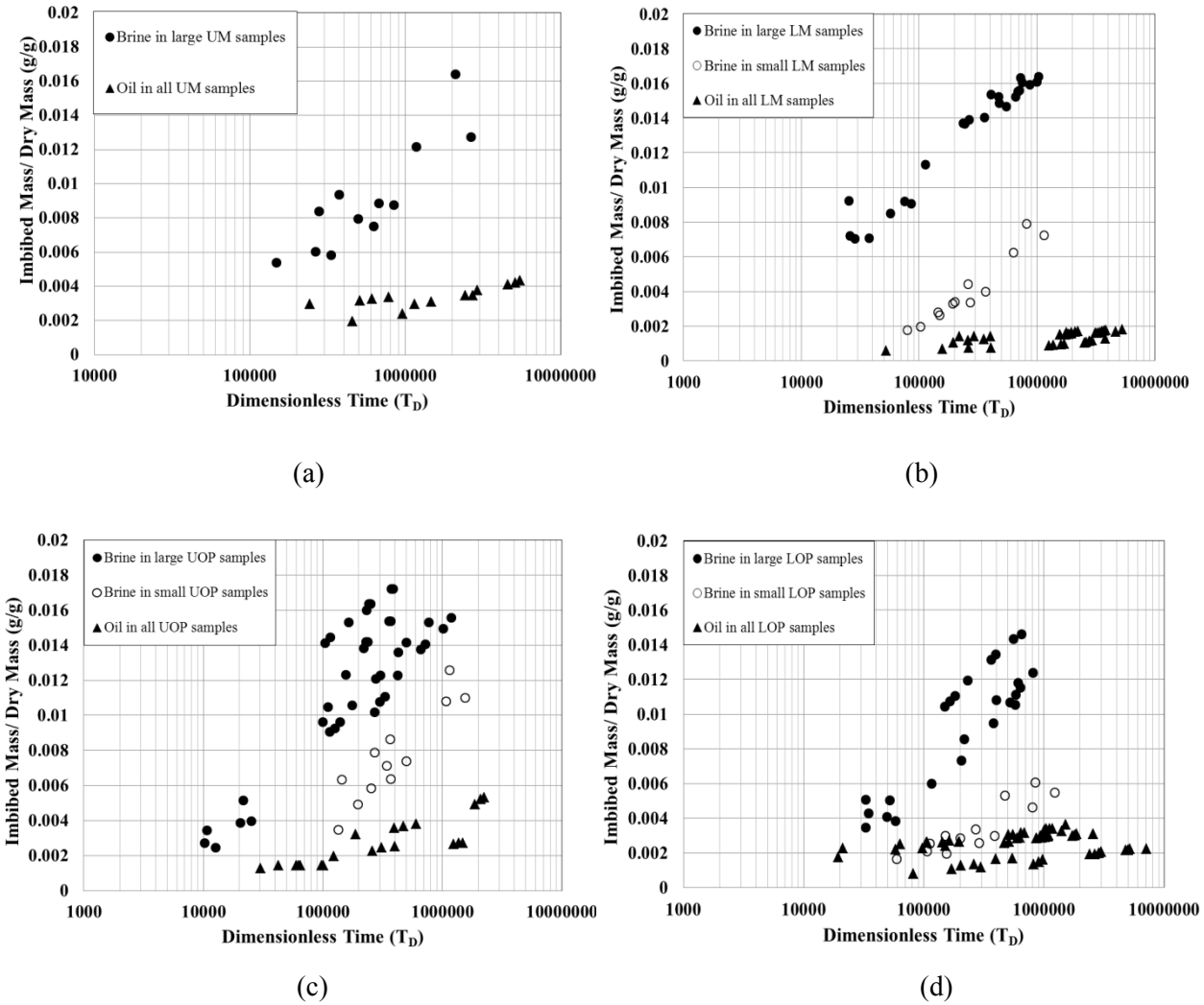

Figure 5.4 Normalized imbibed mass versus dimensionless time for both large and small samples

The separation between normalized brine intake of large and small samples could be explained by two reasons: 1) the chance of microfracture generation in uncoated large samples is higher than that in small coated samples. 2) For large (core-size diameter) samples, water can imbibe through horizontal direction that is parallel to the lamination, and vertical direction that is perpendicular to the lamination. For small

samples (plug), water can imbibed through the vertical dissection that is perpendicular direction. Previous study has shown that the imbibition parallel to the lamination is faster than that of perpendicular to the lamination (Makhanov 2012).

5.3 Summary

On the basis of the existing theory of capillary-dominated spontaneous imbibition, oil and brine imbibed mass should nearby one general curve when plotted versus dimensionless time. The dimensionless time should to some extent account for the change in viscosity, surface tension, sample size / shape, and boundary condition. Therefore, the observed difference can be explained by the physical phenomena discussed above. In other words, oil and brine imbibition data do not scale because the dimensionless time used in this study does not account for water adsorption by clay minerals and the resulting induced micro-fractures that increase the sample effective permeability. Furthermore, the observed scatter in brine data can be explained by the presence of induced micro-fractures in some samples and also small-scale heterogeneity. In conclusion, the existing scaling groups, developed for clean reservoir rocks such as sandstones and carbonates, should be modified for application in organic shales, which remains the subject of future study.

CHAPTER 6

CHARACTERISICS OF MONTNEY TIGHT SANDSTONE

The Early Trassic Montney formation forms an enormous tight gas fairway in the Western Canadian Sedimentary Basin. The application of horizontal drilling and multistage hydraulic fracturing during the past few years has made the Montney tight gas play increasingly essential. This chapter aims to investigate Montney tight sandstone properties obtained from well logs, Rock-Eval and X-Ray diffraction technologies.

6.1 Origin and Geology

The Montney resource play straddles the Canadian provinces of British Columbia and Alberta (Figure 2.3). This formation is one of the largest economically feasible resource plays in North America (Keneti et al. 2010). The study area is in the central portion of the Montney tight gas fairway and is located on the Alberta-British Columbia border. Core plugs range from 2127 m to 2348 m. The formation is up to 320 m thick, and is composed primarily of siltstone, shaly siltstone, and very fine-grained sandstone (Wood 2013). Generally, as Montney rock depth increases, the corresponding values of porosity, bulk volume water (BVW), and initial water saturation decrease, and the rock becomes less laminated and bioturbated (Wood 2012).

6.2 Montney Sample Properties

In this section, I describe the physical and petrophysical properties of Montney tight sandstone. Rock properties were obtained primarily through log measurement, Rock-Eval technique and x-ray diffraction. Tables 6.2, 6.3 and 6.4 summarize the specific rock properties obtained from these measurements.

6.2.1 Well Logging Properties

The logs for Upper and Lower Montney samples from the Sunrise field are shown in Figure 6.1. The measurements show no pronounced difference between the Upper and Lower Montney samples. Gamma ray (GR) log data positively correlate to the amount of organic materials in a reservoir (TOC data of MT samples will be shown later). Thus the high total gamma ray value shown in Figure 6.1 indicates that the study samples are organic rocks, with an average GR response of 113 API. The thorium radioactivity response on the spectral GR log remains fairly steady among all samples with an average value of 8.2 ppm, with potassium radioactivity response varying from 0.027 to 0.033 fractions. Average bulk densities of studied cores are 2.53 gm/cm^3. Table 6.2 presents the log responses at depths from which the study samples were obtained.

Upper Montney

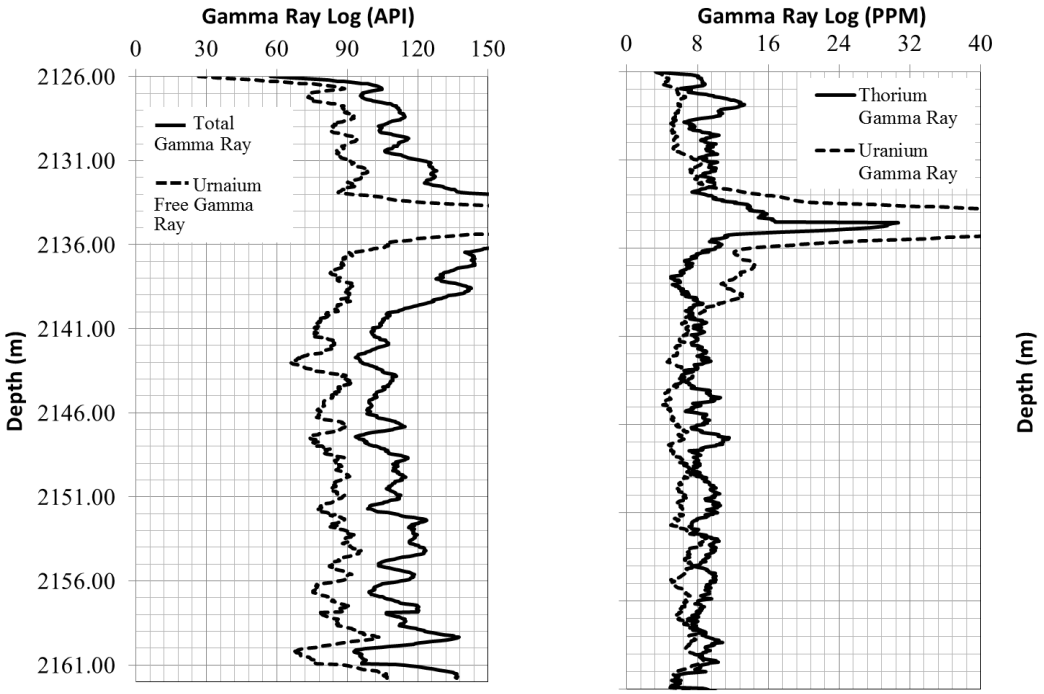

(a) (b)

Upper Montney

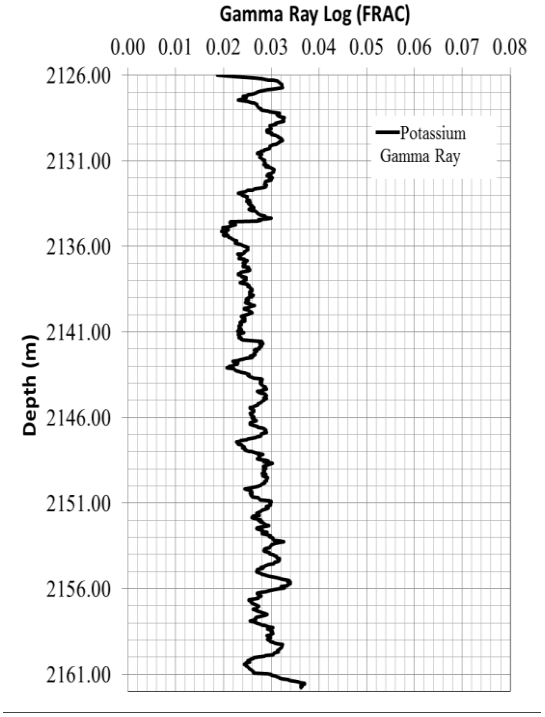

(c)

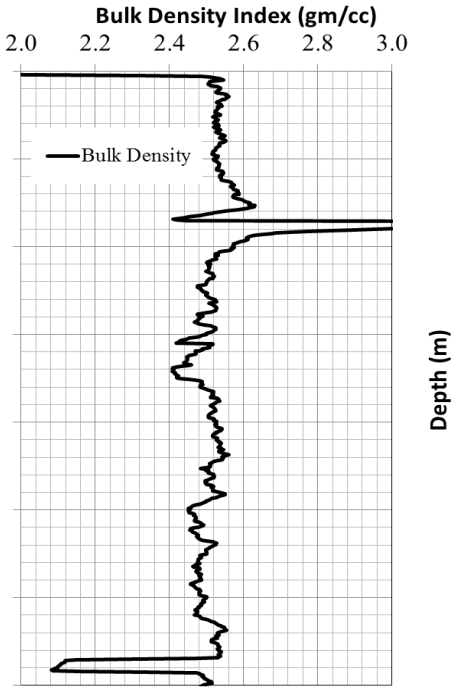

(d)

Lower Montney

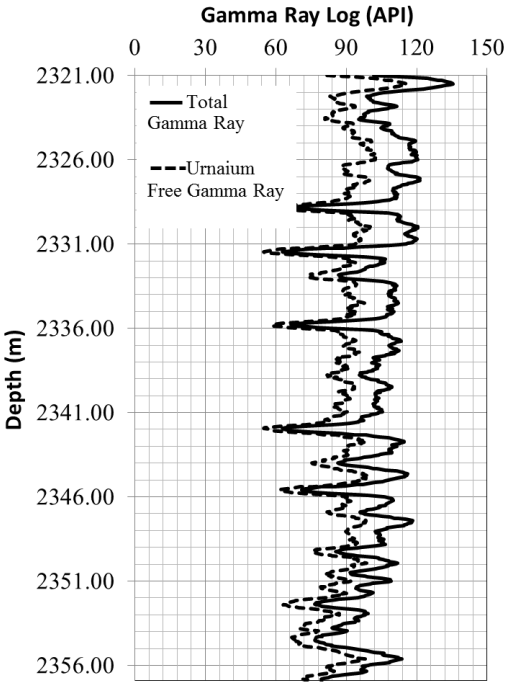

(e)

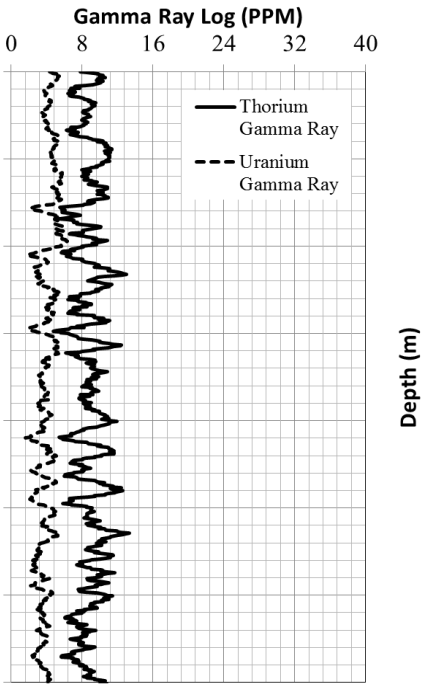

(f)

Lower Montney

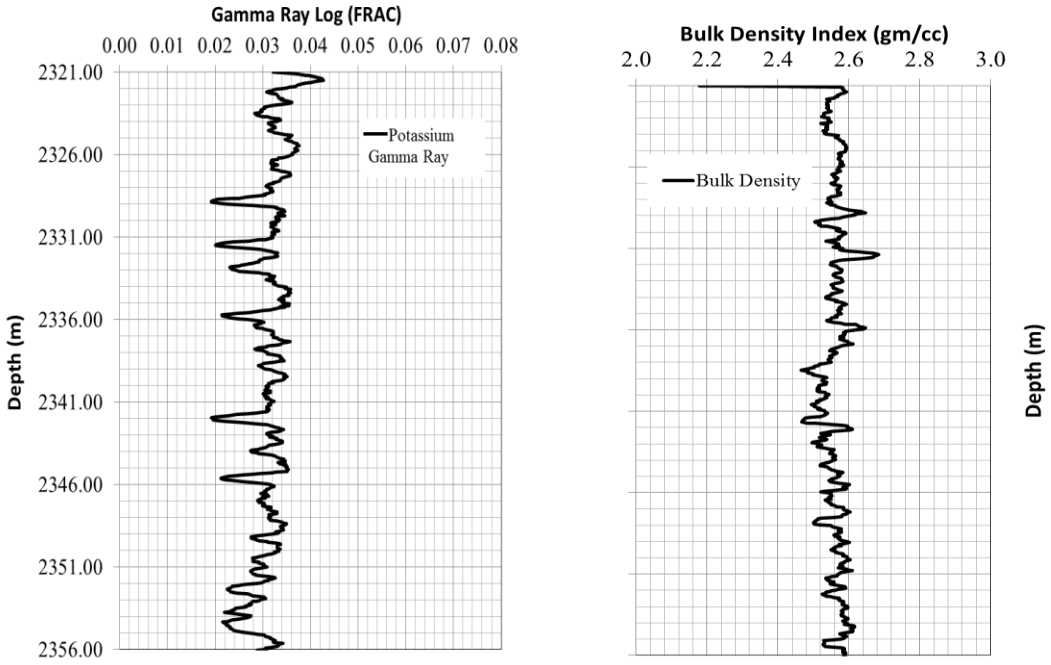

(g) (h)

Figure 6.1 Well logs recorded in Upper Montney samples (a) to (d), and Lower Montney samples (e) to (h).

Table 6.1 Log responses of Montney core samples

Label	Depth (m)	Total gamma (API)	Uranium free gamma (API)	Thorium (ppm)	Potassium (fraction)	Uranium (ppm)	Bulk density (gm/cc)
UMT1	2127.4	97	75	6	0.027	5.6	2.54
UMT2	2130.4	111	90	9	0.032	5.7	2.55
UMT3	2137.6	142	88	7	0.024	14.5	2.51
UMT4	2144.2	110	90	8.5	0.027	5	2.49
UMT5	2150.9	111	89	9.5	0.03	5.9	2.45
LMT1	2323.4	110	90	9	0.032	4.2	2.54
LMT2	2330.1	120	100	9	0.033	5	2.59
LMT3	2340.4	105	90	8	0.031	2.9	2.54
LMT4	2347.1	109	90	8.5	0.032	4	2.52

"UMT6 was broken after overburden porosity measurement, no well logging data could be measured."

6.2.2 Rock-Eval Measurement Data

Rock-Eval technique is primarily used to identify the type and maturity of organic matter and to detect petroleum potential in sediments. Rock-Eval is the trade name for a set of equipment used in the lab to measure organic content of rocks, as well as other properties of the organics that help to identify the kerogen type. The Montney samples have moderately high TOC content (0.86 – 1.81 wt. %) with an average value of more than 1.33 wt. % which qualifies them as representing a source rock. Table 6.3 details the TOC Rock-Eval test results of samples obtained from depths nearest to those of our studied samples.

Table 6.2 Rock-Eval results of core samples

Label	TOC (wt. %)	S_1	S_2	S_3	HI	OI	PI	T_{max}
UMT1	0.96	3.61	0.88	0.18	94	19	0.8	445.5
UMT2	0.86	3.93	0.77	0.14	88.5	15.5	0.81	443
UMT3	1.17	2.69	0.67	0.22	57.5	19.5	0.8	452.5
UMT4	0.93	3.32	0.77	0.22	83.5	23.5	0.82	430
UMT5	1.3	3.61	1.1	0.15	84	12	0.77	463.5
LMT1	1.7	3.26	1.19	0.14	70.5	8	0.73	458
LMT2	1.8	3.27	1.21	0.09	67	4.5	0.72	458.5
LMT3	1.81	3.47	1.14	0.11	62.5	5.5	0.75	457
LMT4	1.44	2.55	0.89	0.12	62	8.5	0.74	295

"UMT6 was broken after overburden porosity measurement, no Rock-Eval data could be measured."

Parameters of the Rock-Eval measurement process that yielded the data in Table 6.3 are briefly described as follows:

(1) S_1 is amount of free hydrocarbons (gas and oil) in a sample (mg/g). They are distilled out of the sample at initial heating;

(2) S_2 is amount of hydrocarbons generated through thermal cracking of nonvolatile organic matter (mg/g). S_2 provides the quantity of hydrocarbons that the rock has the potential to produce at thermal maturity;

(3) S_3 is amount of CO_2 (mg of CO_2/g of rock) produced during pyrolysis of kerogen (mg/g). S_3 represents the amount of oxygen in the oxidation step. This value is proportional to the oxygen present in the kerogen;

(4) T_{max} is the temperature (^oC) yielding the maximum hydrocarbon generation rate during pyrolysis. Moreover, T_{max} is also a useful indicator of maturity, higher values being more maturity; while

hydrogen index (HI) = 100 * S_2 / TOC%;

oxygen index (OI) = 100 * S_3 / TOC%; and

production index (PI) = S_1 / (S_1 + S_2).

6.2.3 XRD Analysis

X-ray diffraction (XRD) measurements were used to identify the bulk and clay mineralogies of our studied samples. In Table 6.4, I present the concentrations of different minerals comprising the Montney samples as determined by XRD technology. The x-ray diffraction of clay measurement indicates that the clay species is illite/mica, chloride and kaolinite. The dominant clay is illite/mica, and the dominant non-clay is quartz. Samples also contain feldspar (3.5-9.5%), plagioclase (8-15%) and traces of calcite and pyrite.

Table 6.3 Average bulk mineral concentration (wt. %) of core samples determined by XRD

Label	Quartz (wt. %)	Feldspar (wt. %)	Plagioclase (wt. %)	Calcite (wt. %)	Dolomite (wt. %)	Pyrite (wt. %)	Chlorite (wt. %)	Illite/Mica (wt. %)	Kaolinite (wt. %)
UMT1	45	9.5	11	7	13	1	1.5	12.5	1
UMT2	47	7	13	6	7	1	2	14.5	2
UMT3	56.5	8	13	5.5	11.5	1	0	4	0
UMT4	55	6	15	5.5	5.5	1	2	10.5	1
UMT5	54.5	4.5	14	7	7	1	0	10.5	1
LMT1	56.5	5	8	7	5.5	1	2	13.5	2
LMT2	51.5	3.5	13	4	6.5	1	2	17.5	2
LMT3	55.5	4	8.5	5.5	4	1	2	16.5	2
LMT4	51.5	3.5	11.5	3.5	6	1	2.5	19.8	2.5

"UMT6 was broken after overburden porosity measurement; no mineral concentration could be measured."

CHAPTER 7

WETTABILITY OF MONTNEY TIGHT GAS FORMATION

The abundant hydrocarbon resources in low-permeability formations are now technically accessible due to advances in drilling and completion of multi-lateral/multi-fractured horizontal wells. However, measuring and modeling of petrophysical properties, required for reserve estimation and reservoir-engineering calculations are the remaining challenges for the development of tight formations. In particular, characterizing wettability (wetting affinity) of tight rocks is challenging due to their complex pore structure, which can be either in hydrophobic organic materials or in hydrophilic inorganic materials. In this chapter, we measure and compare spontaneous imbibition of oil and brine into fresh (uncleaned) binary core plugs selected from different depths of one vertical well drilled in the Montney formation. The samples are characterized by measuring porosity, permeability, pore size distribution, TOC, mineralogy, and oil/water equilibrium contact angles.

7.1 Materials Used

Ten pairs of binary core plugs were dilled using a dry-cut machine and nitrogen gas. It is believed that nitrogen does not change the surface properties of plugs. The samples are characterized by measuring equilibrium contact angle, porosity, pore size distribution, mineralogy, TOC and SEM imaging. Dodecane and 2wt. % potassium chloride (KCl) were used as oleic and aqueous phases for the imbibition experiments.

7.1.1 Core Samples

The depth of selected Montney plugs ranges from 2127 m to 2348 m as detailed in Table 7.1. The Montney formation crosses through a large area of British Columbia (B.C.) trending towards North West from the Alberta border to Fort St. John (Nieto 2009). This formation is one of the largest economically feasible resource plays in

North America (Keneti et al 2010). The study area is in the central portion of the Montney tight gas fairway and is located in the border of Alberta and British Columbia. The Montney formation is in general composed of siltstone, and contains minor intervals of shaly siltstone and very fine-grained sandstone (Wood 2012). The formation thickness can reach to 320 m in some locations. Based on properties of the observed clinoform units, the formation can be divided into Upper Montney and Lower Montney. In general, by increasing the depth from Upper Montney to Lower Montney, the values of porosity, bulk volume water (BVW), and initial water saturation decrease (Wood 2012).

Six pairs of the samples (UMT1 to UMT6) are selected from the Upper Montney (UMT) cores and four (LMT1 to LMT4) from the Lower Montney (LMT) cores. The mass, cross-sectional area, thickness, diameter, depth, TOC content, petrophysical properties and average mineral concentration of the samples are summarized in Tables 7.1, 7.2, 7.3 and 7.4. All samples are fresh and have neither been cleaned nor exposed to air.

The total organic content of the bulk dried, as-received rock samples (70 mg after being finley powderized) were measured using Rock-Eval 6 analysis (Vinci Technologies, France) in the Geological Survey of Canada. Organic petrolgy was conducted on selected samples using reflected light microscopy (Zeiss Axioimage II) on the polished block made by a cold-setting epoxy-resin mixture.

The quantitative bulk mineralogy of the samples is measured using X-ray diffraction (XRD) method. The dried, bulk, as-received samples (1.2 gr) are crushed in a ball mill and then homogenized to approximately <80 micron grain size. The resulting ground powder was then packed in the sample holders and run up to 600^{o}C. The X-ray diffractograms of the unreduced samples were recorded at a scan speed of 1^{o} (2 per minute).

Table 7.2 Original mass, cross-sectional area, thickness, diameter and depth of core samples from Upper Montney formation

Label	Mass (g)	Cross-sectional area (cm^2)	Thickness (cm)	Diameter (cm)	Depth (m)
$UMT1_o$	205.79	10.752	6.6	3.7	2127.21
$UMT1_w$	198.03	10.752	6.6	3.7	2127.55
$UMT2_o$	195.57	10.752	6.8	3.7	2130.2
$UMT2_w$	200.72	10.752	6.9	3.7	2130.57
$UMT3_o$	192.20	10.752	6.6	3.7	2137.45
$UMT3_w$	191.98	10.752	6.7	3.7	2137.83
$UMT4_o$	192.86	10.752	6.7	3.7	2144.01
$UMT4_w$	199.37	10.752	6.95	3.7	2144.37
$UMT5_o$	198.26	10.752	6.75	3.7	2150.74
$UMT5_w$	190.52	10.752	6.5	3.7	2151.17
$UMT6_o$	195.25	10.752	6.7	3.7	2157.9
$UMT6_w$	193.01	10.752	6.5	3.7	2158.29

"Subscripts o and w represent dodecane and brine, respectively."

Table 7.2 Original mass, cross-sectional area, thickness, diameter and depth of core samples from Lower Montney formation

Label	Mass (g)	Cross-sectional area (cm^2)	Thickness (cm)	Diameter (cm)	Depth (m)
$LMT1_o$	199.06	10.752	6.75	3.7	2323.2
$LMT1_w$	195.55	10.752	6.7	3.7	2323.53
$LMT2_o$	201.73	10.752	6.9	3.7	2329.8
$LMT2_w$	202.53	10.752	6.95	3.7	2330.22
$LMT3_o$	192.06	10.752	6.55	3.7	2340.29
$LMT3_w$	194.01	10.752	6.6	3.7	2340.61
$LMT4_o$	199.50	10.752	6.75	3.7	2346.98
$LMT4_w$	196.88	10.752	6.6	3.7	2347.28

"Subscripts o and w represent dodecane and brine, respectively."

Table 7.3 TOC content, permeability and porosity of Montney samples

Label	TOC (wt. %)	Permeability (md)	Porosity (fraction)
UMT1	0.96	/	0.063
UMT2	0.86	3.89E-03	0.062
UMT3	1.17	2.35E-02	0.066
UMT4	0.93	1.05E-01	0.081
UMT5	1.3	4.42E-03	0.063
LMT1	1.67	1.50E-02	0.043
LMT2	2.09	2.33E-03	0.02
LMT3	1.43	2.04E-03	0.049
LMT4	1.74	1.01E-02	0.045

"UMT6 was broken after overburden porosity measurement, no overburden air permeability could be measured."

Table 7.4 Average mineral concentration (wt. %) of the Montney samples determined by X-ray diffraction

Label	Quartz (wt. %)	Feldspar (wt. %)	Plagioclase (wt. %)	Calcite (wt. %)	Dolomite (wt. %)	Pyrite (wt. %)	Chlorite (wt. %)	Illite/Mica (wt. %)	Kaolinite (wt. %)
UMT1	45	9.5	11	7	13	1	1.5	12.5	1
UMT2	47	7	13	6	7	1	2	14.5	2
UMT3	56.5	8	13	5.5	11.5	1	0	4	0
UMT4	55	6	15	5.5	5.5	1	2	10.5	1
UMT5	54.5	4.5	14	7	7	1	0	10.5	1
LMT1	56.5	5	8	7	5.5	1	2	13.5	2
LMT2	51.5	3.5	13	4	6.5	1	2	17.5	2
LMT3	55.5	4	8.5	5.5	4	1	2	16.5	2
LMT4	51.5	3.5	11.5	3.5	6	1	2.5	19.8	2.5

"UMT6 was broken after overburden porosity measurement, no mineral concentration could be measured."

7.1.2 Fluids

Dodecane and 2wt. % KCl solution were used as imbibing fluids. Density, viscosity and surface tension of the test fluids are listed in Table 7.5.

Table 7.5 Properties of different fluids used for imbibition experiments at 25°C

Fluid	Density (g/cm^3)	Viscosity (cp)	Surface tension (dyn/cm)
Dodecane	0.749	1.374	25.35
2wt. % KCl	1.02	0.89	72.7

7.2 Experimental Procedure

The general procedure for the imbibition experiments includes the following steps:

(1) Cut binary plugs from different depths of the cores using a dry-cut machine for oil and water imbibition tests.

(2) Cut an end piece from each side of each core plug and keep it for measuring TOC, mineral concentration and other petrophysical properties.

(3) Measure the original weight of each plug sample.

(4) Measure contact angle of oil and brine on the clean surface of the plugs prior to imbibition experiments.

(5) Place each core plug vertically on a mesh screen inside the imbibition cell and make sure only the sample bottom face contacts with the wetting liquid as shown in Figure 7.1.

(6) Seal the imbibition cell to avoid liquid evaporation and measure the weight gain periodically.

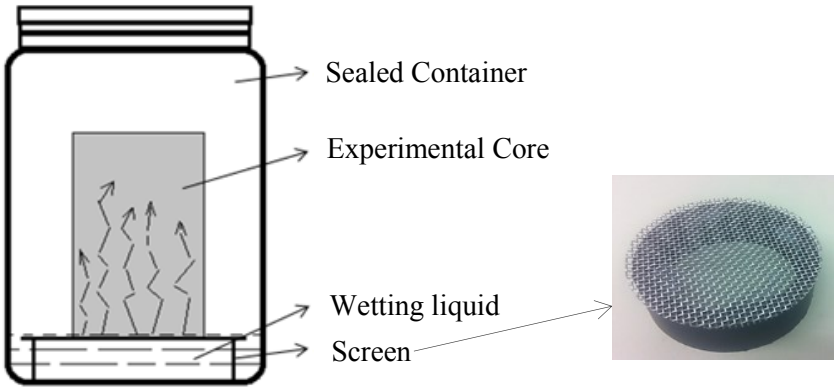

Figure 7.1 The schematic illustration of the imbibition set-up.

7.2.1 Contact Angle Measurement

Contact angle for various rock-fluid combinations was obtained by analyzing the droplet profile equilibrated on the rock surface (Rao 1997). A high-resolution camera is used to visualize the profile of the droplet injected by a needle on the rock surface. The profile is analyzed using software (Image J) to obtain the contact angle, as shown in Figure 7.2 for an example case.

7.2.1 Spontaneous Imbibition Experiments

Ten of the total twenty plugs are placed inside the imbibition cells partly filled with brine and the other ten inside those filled with oil. The mass gain by each sample is periodically measured and recorded for thirty days.

7.3 Experimental Results

This section presents and discusses the experimental results.

7.3.1 Contact Angle Measurement

When brine (2wt. % KCl) droplets contact with the clean core surface, they retain their identity as droplets. However, the oil (dodecane) droplets completely spread on the rock surface. These phenomena for random samples are shown in Figure 7.2. The measured contact angle of oil on all samples is zero, and that of water is listed in Table 7.6. These data indicate that the affinity of the Montney samples to oil is higher than that to water.

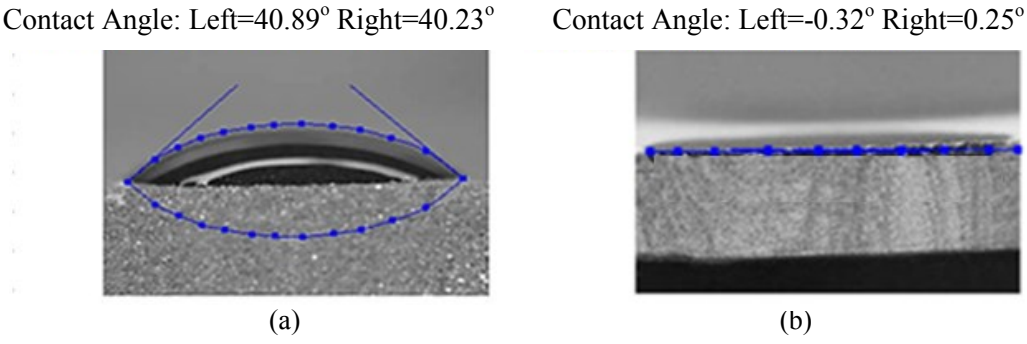

Figure 7.2 Contact angles of (a) brine and (b) oil on the clean surface of rock samples.

Table 7.6 Equilibrium contact angles of oil and brine for all binary plugs.

Label	$UMT1_o$	$UMT1_w$	$UMT2_o$	$UMT2_w$	$UMT3_o$	$UMT3_w$	$UMT4_o$	$UMT4_w$	$UMT5_o$	$UMT5_w$
θ_w (deg)	---	45.2	---	46.5	---	36.7	---	41.6	---	44.5
θ_o (deg)	0	---	0	---	0	---	0	---	0	---
Label	$UMT6_o$	$UMT6_w$	$LMT1_o$	$LMT1_w$	$LMT2_o$	$LMT2_w$	$LMT3_o$	$LMT3_w$	$LMT4_o$	$LMT4_w$
θ_w (deg)	---	48	---	37	---	40	---	45	---	37
θ_o (deg)	0	---	0	---	0	---	0	---	0	---

"Subscripts o and w represent brine and dodecane, respectively."

7.3.2 Qualitative Interpretation of Imbibition Results

Figure 7.3 shows pictures of an example binary sample before, during, and after the imbibition of oil and water. Interestingly, both oil and water spontaneously imbibe against gravity into the two samples, which immediately indicates the mixed-wet characteristics of these samples. The samples are relatively homogenous and we did not observe any induced or natural cracks. In contrast to the Horn River shale samples (Dehghanpour et al. 2012; Dehghanpour et al. 2013), the Montney samples do not expand when exposed to water.

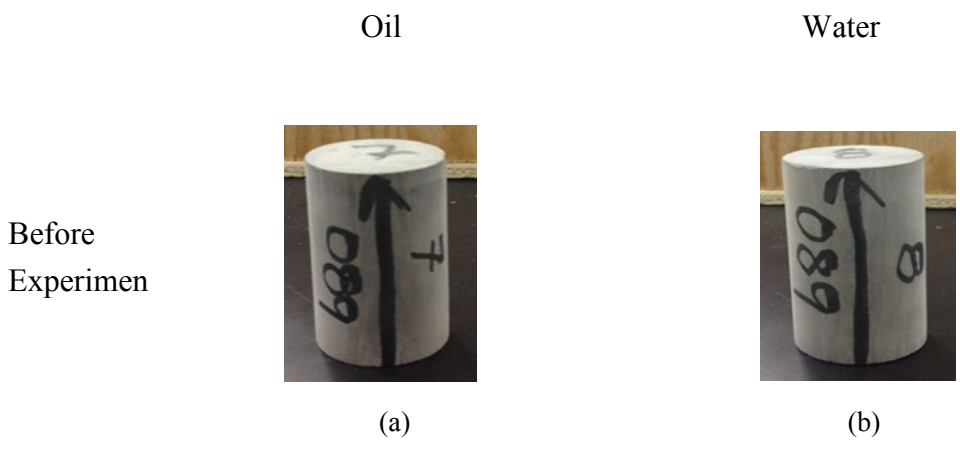

During Experiment

(c) (d)

After Experiment

(e) (f)

Figure 7.3 Pictures of Montney samples before (a, b), during (c, d), and after (e, f) exposure to dodecane and 2wt. % KCl solution.

Figure 7.4 compares the normalized mass and volume of oil and water imbibed into the twenty plugs. The imbibition profiles reach to an equilibrium state after an initial transition period. The equilibrium imbibed mass/volume of oil is higher than that of water for all twenty samples. This indicates that the natural affinity of these samples to oil is higher than that to water. This observation is consistent with the contact angle results. Furthermore, the relative separation between water and oil equilibrium values for Lower Montney (LMT) samples is considerably higher than that for Upper Montney (UMT) samples. This observation indicates that the relative affinity of LMT samples to oil is higher than that of UMT samples. However, the equilibrium oil and water uptake of UMT samples is higher than that of LMT samples. This observation can be explained by the higher porosity of UMT samples, which will be discussed later in details. We also observe that UMT profiles reach to the equilibrium state much faster than LMT profiles. This simply indicates higher permeability of UMT samples, and this argument is backed with their higher porosity. Figure 7.5 shows that

LMT is in general less laminated and less bioturbated than UMT, and the plugs are drilled parallel to the bedding plain. It is well known that the vertical permeability and even imbibition rate (Makhanov et al. 2012) are affected by lamination. Therefore, the lower rate of oil and specifically water imbibition in LMT samples compared with UMT samples can also be explained be the change in lamination with depth. In subsequent section, we will show that the liquid uptake of MT samples correlated to the rock fabric, petrophysical and petrographic properties of these samples.

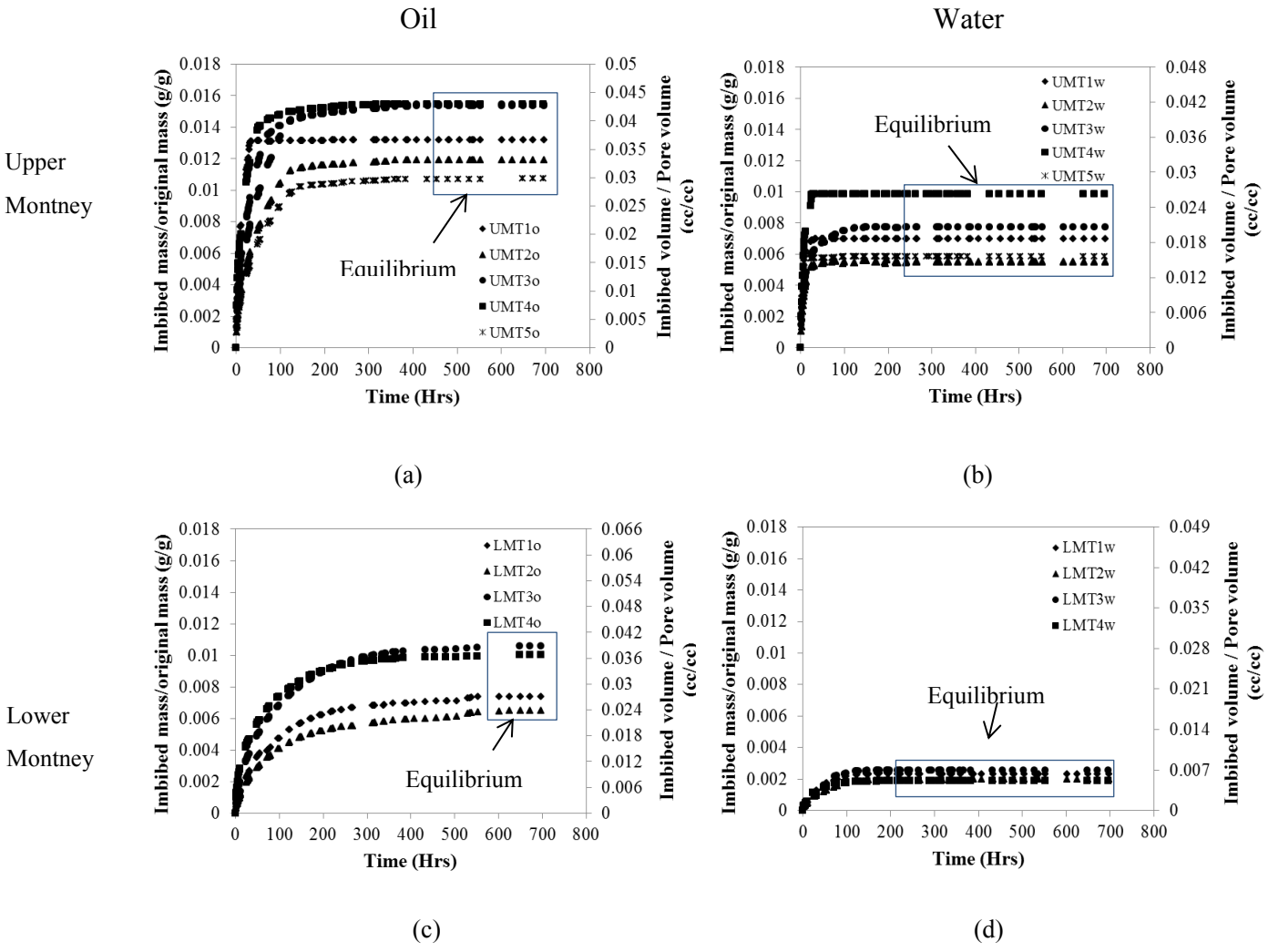

Figure 7.4 Normalized mass and volume of oil (a and c) and water (b and d) into UMT and LMT samples.

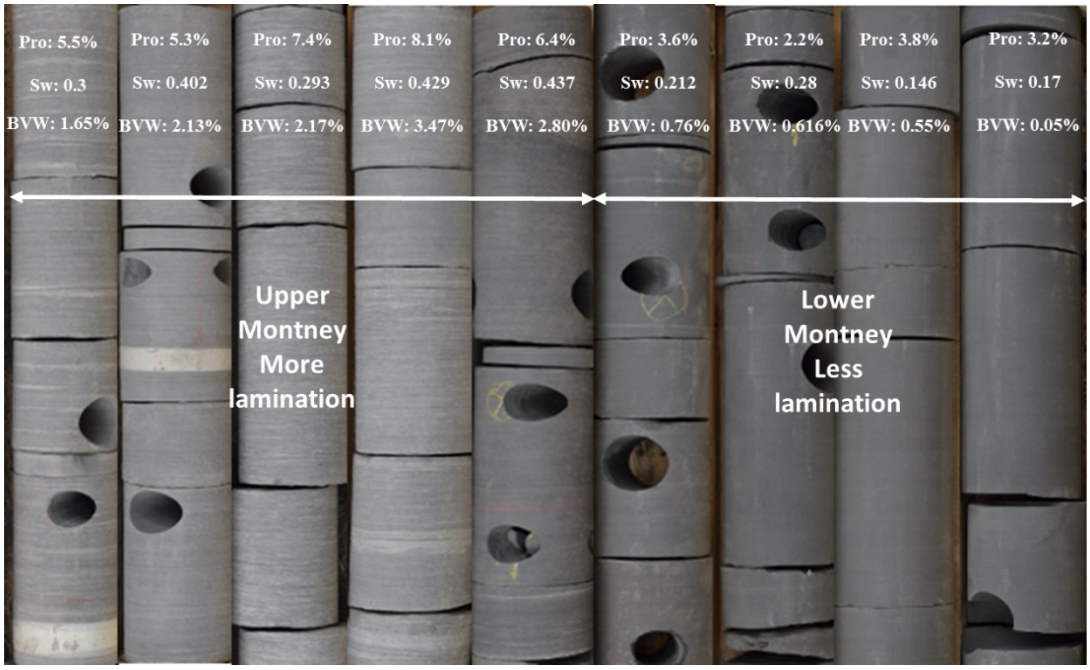

Figure 7.5. Photographs of the cores sampled for the imbibition study.

7.4 Quantitative Analysis of Imbibition Data

In this section, we analyze the imbibition data for characterizing petrophysical properties of the rock samples.

7.4.1 Effective versus Total Porosity

The total porosity of the twenty samples was obtained by analyzing the end pieces in a Helium Porosimeter. The porosity values are listed in Table 7.7 and plotted versus depth in Fig. 7.6. The reported porosity value for each sample is the mean value of four measurements. The separation between the porosity of the two pieces cut from the two ends of one plug can be explained by the small-scale heterogeneity.

Table 7.7 Porosity of core plugs measured by Helium Porosimeter

Label	$UMT1_o$	$UMT1_w$	$UMT2_o$	$UMT2_w$	$UMT3_o$	$UMT3_w$	$UMT4_o$	$UMT4_w$	$UMT5_o$	$UMT5_w$
Porosity Value	0.051	0.047	0.057	0.0485	0.064	0.069	0.072	0.078	0.0565	0.0505
Label	$UMT6_o$	$UMT6_w$	$LMT1_o$	$LMT1_w$	$LMT2_o$	$LMT2_w$	$LMT3_o$	$LMT3_w$	$LMT4_o$	$LMT4_w$
Porosity Value	0.0485	0.051	0.036	0.04	0.029	0.032	0.036	0.0395	0.041	0.0452

"Subscripts o and w represent brine and dodecane, respectively."

Figure 7.6 shows that in general the porosity of UMT samples is higher than that of LMT samples. This observation is correlated to the higher and faster brine and oil uptake of UMT samples compared with that of LMT samples.

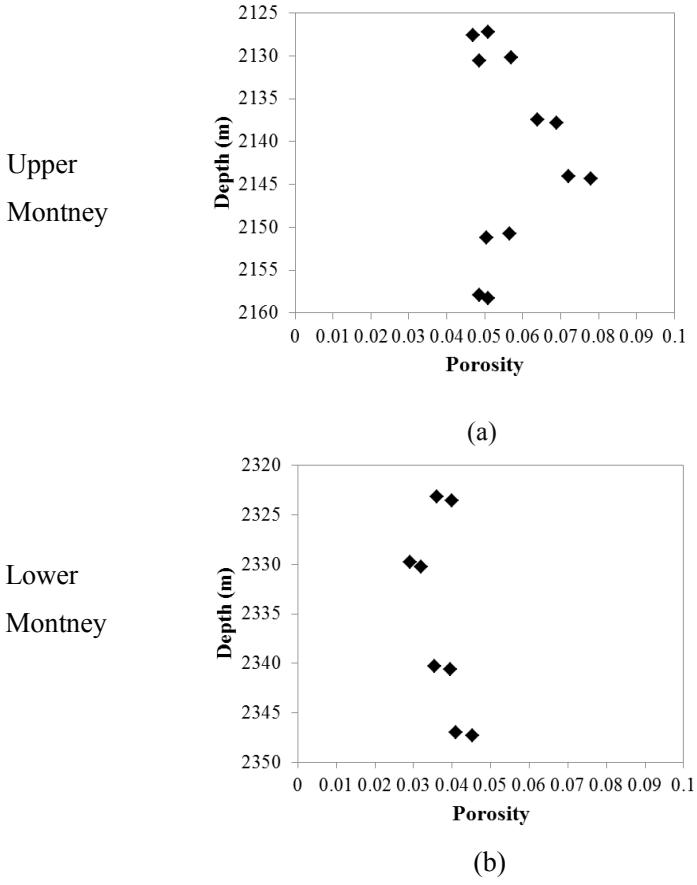

Figure 7.6 Porosity of core plugs versus depth.

Considering the extremely small pore size and the relatively short length of the plugs, the effect of gravity on imbibition is negligible compared with the strong capillary pressure. Therefore, the water and oil imbibition profiles shown in Figure 7.4 reach to an equilibrium state when the connected hydrophilic and hydrophobic pore networks are fully invaded by water and oil, respectively, as a result of capillary suction. Therefore, the equilibrium imbibition value can be used to define an effective porosity for each sample and fluid as the ratio of total imbibed volume to the total sample pore volume: $\text{Effective porosity}(\emptyset_e) = \left(\frac{\text{Cumulative imbibed volume}}{\text{Sample pore volume}}\right) * \text{Total porosity}$. Pore volume of the samples was measured independently and the cumulative imbibed liquid volume was obtained from the imbibition data presented in Figure 7.4. For each binary plug, we calculate an effective porosity for oil ($\emptyset_{eo}$) and an effective porosity for water ($\emptyset_{ew}$), as listed in Table 7.8.

Table 7.8 Effective porosity of core plugs obtained from spontaneous imbibition experiments

Label	$UMT1_o$	$UMT1_w$	$UMT2_o$	$UMT2_w$	$UMT3_o$	$UMT3_w$	$UMT4_o$	$UMT4_w$	$UMT5_o$	$UMT5_w$
$Ø_{eo}$	0.049	---	0.043	---	0.056	---	0.055	---	0.039	---
$Ø_{ew}$	---	0.019	---	0.015	---	0.020	---	0.026	---	0.016
Label	$UMT6_o$	$UMT6_w$	$LMT1_o$	$LMT1_w$	$LMT2_o$	$LMT2_w$	$LMT3_o$	$LMT3_w$	$LMT4_o$	$LMT4_w$
$Ø_{eo}$	0.011	---	0.027	---	0.024	---	0.031	---	0.037	---
$Ø_{ew}$	---	0.010	---	0.006	---	0.005	---	0.007	---	0.005

"Subscripts o and w represent brine and dodecane, respectively."

The data show that $\emptyset_{eo}$ is higher than $\emptyset_{ew}$ for all samples. It is important to note that the surface tension (as the dominant driving force for imbibition) of water is almost three times higher than that of oil. Therefore the observations indicate that the hydrophobic part of the pore network is significantly larger than the hydrophilic part. In other words, the data suggest that oil imbibes into parts of the rock pore space where water can hardly imbibe. For a more careful analysis, we plot $\emptyset_{eo}$ and $\emptyset_{ew}$ versus measured total porosity of the samples in Figure 7.7. Figure 7.7(a) shows that

in general most of the total pore space is imbibed by oil, while only a small fraction of the total pore space is imbibed by water as shown in Figure 7.7(b).

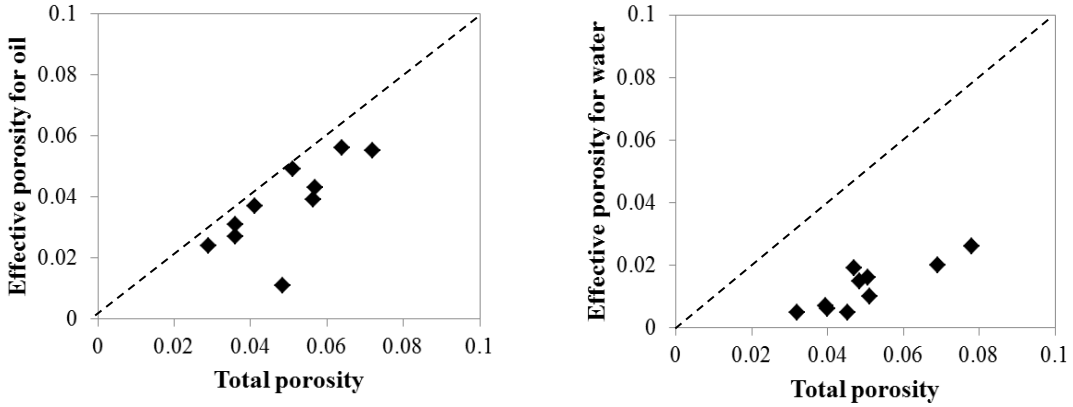

(a) (b)

Figure 7.7 Effective porosity for oil (a) and water (b) versus measured total porosity.

7.4.2 Wettability Index

As discussed in the previous section, the separation between the equilibrium water and oil imbibed mass (or volume) is an indication of rock wettability. Therefore, we define the following wettability indices for water and oil:

$$\text{Wetting Affinity Index of Brine } (WI_w) = \frac{I_w}{I_w + I_o}$$

$$\text{Wetting Affinity Index of Oil } (WI_o) = 1 - \frac{I_w}{I_w + I_o}$$

Here, I_w and I_o are the normalized volume of oil and brine imbibed into a binary plug. I_w (or I_o) is calculated by dividing the total imbibed volume of water (or oil) by the sample pore volume. The imbibed volume is obtained through dividing the imbibed mass by the water or oil density. Table 7.9 lists the total imbibed mass of water and oil for the ten binary plugs. The calculated wettability indices for the nine binary plugs (UMT6 was broken) are listed in Table 7.10.

Table 7.9 Cumulative imbibed mass of oil and water after equilibrium for the ten binary plugs.

Label	$UMT1_o$	$UMT1_w$	$UMT2_o$	$UMT2_w$	$UMT3_o$	$UMT3_w$	$UMT4_o$	$UMT4_w$	$UMT5_o$	$UMT5_w$
Mass Uptake (g)	2.615	1.382	2.336	1.105	2.969	1.483	2.983	1.962	2.127	1.114
Label	$UMT6_o$	$UMT6_w$	$LMT1_o$	$LMT1_w$	$LMT2_o$	$LMT2_w$	$LMT3_o$	$LMT3_w$	$LMT4_o$	$LMT4_w$
Mass Uptake (g)	0.579	0.712	1.473	0.457	1.308	0.398	2.032	0.499	1.999	0.37

"Subscripts o and w represent brine and dodecane, respectively."

Table 7.10 Wettability index of oil and brine for the ten binary plugs

Label	Wettability index of oil (WI_o)	Wettability index of brine (WI_w)
UMT1	0.645	0.355
UMT2	0.685	0.315
UMT3	0.667	0.333
UMT4	0.611	0.389
UMT5	0.647	0.353
LMT1	0.761	0.239
LMT2	0.767	0.233
LMT3	0.804	0.196
LMT4	0.842	0.158

7.4.2.1 Correlation between Wettability and TOC

In Figure 8(a), we plot WI_w versus depth, and observe that the affinity of both UMT and LMT samples to oil is stronger than that to water ($WI_o > WI_w$). Furthermore, the wettability index of oil for the LMT samples is higher than that for UMT samples ($WI_{o_{LMT}} > WI_{o_{UMT}}$), although the total oil uptake of LMT samples is lower than that of UMT samples ($I_{o_{LMT}} < I_{o_{UMT}}$). To investigate the observed behavior, one should

consider the major differences in petrophysical and petrographic properties of UMT and LMT samples. In general, the water saturation and the lamination degree of LMT samples are lower than those of UMT samples, as shown in Figure 7.5. Furthermore, TOC values of LMT samples are in general higher than those of UMT samples, as shown in Figure 7.8(b). For a more careful analysis, we plot the WI_o data versus TOC and Bulk Volume Water (BWV) in Figures 7.8(c) and 7.8(d), respectively. Interestingly, WI_o is positively correlated to TOC and negatively correlated to BVW. Figure 7.9 indicates the photomicrograph of a LMT sample under white reflected light using immersion oil showing distribution of organic carbon within the intergranular pore spaces in the rock matrix. The higher TOC content indicates the higher pyrobitumen content. Besides, oil uptake is primarily in pores within or bordering degraded bitumen. Thus, increasing the TOC content increases the wetting affinity to oil (or WI_o).

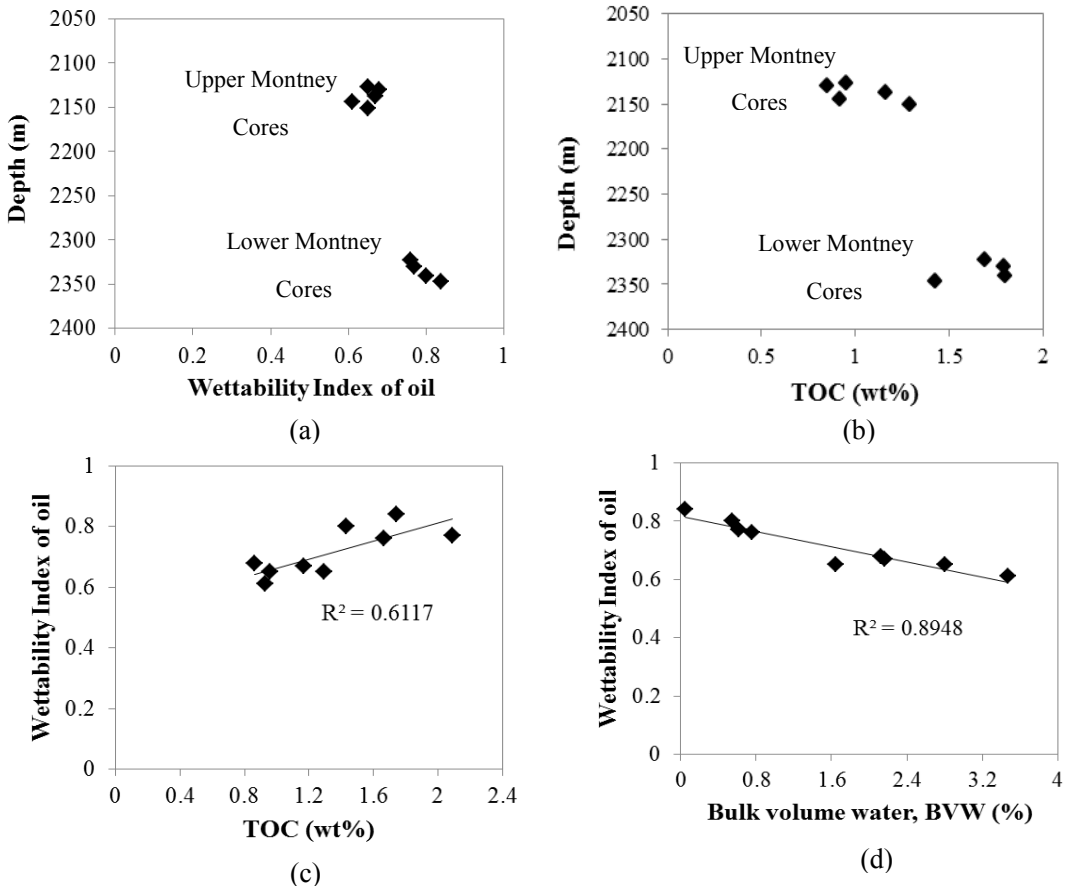

Figure 7.8 Samples TVD versus (a) wettability index of oil, and (b) TOC; wettability index of oil versus (c) TOC, and (d) BVW.

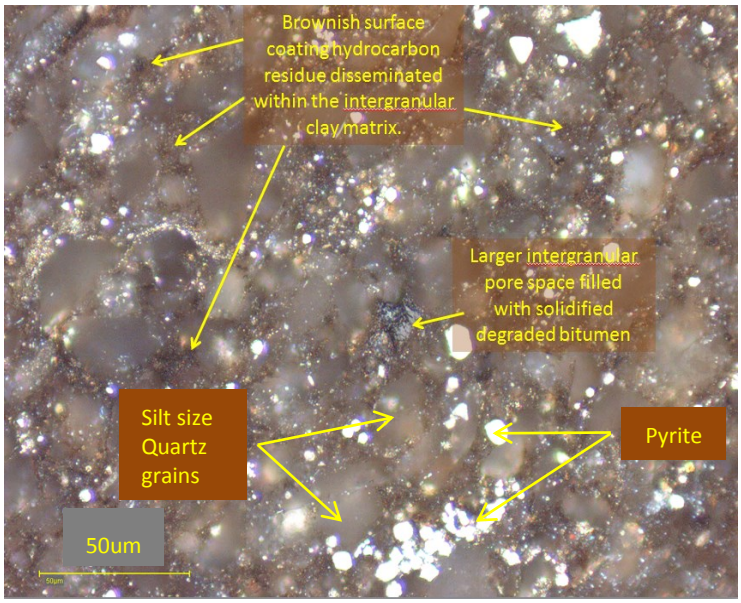

Figure 7.9 Photomicrograph of a LMT sample under white reflected light using immersion oil showing distribution of organic matter within the intergranular pore spaces in the rock matrix.

7.4.2.2 Correlations among Normalized Imbibed liquid Mass, Clay Concentration and TOC.

Figures 7.10(a) and (b) show that both oil and water uptake of the samples is in general negatively correlated with total clay concentration, although the data are quite scattered. One may argue that this correlation exists because clays reduce the effective porosity and permeability of the rock samples. However, Figures 7.10(c) and (d) show a stronger negative correlation between the liquid uptake (both oil and water) and TOC. This observation is in agreement with the theory that degraded bitumen can clog the rock pore space. The higher TOC content of LMT samples indicates the higher saturation of degraded pyrobitumen, which can block the pore space and reduce the effective porosity/permeability. Therefore, the observed correlation between liquid uptake and clay concentration is mainly due to the natural positive correlation between TOC and clay concentration, as shown in Figure 7.10(e). The grain size of LMT samples with higher clay fraction is smaller than that of UMT samples. Therefore, there have been more surface area and larger physical substrate in

LMT samples for surface coating organic matter, and this fact explains the positive correlation between TOC and clay concentration.

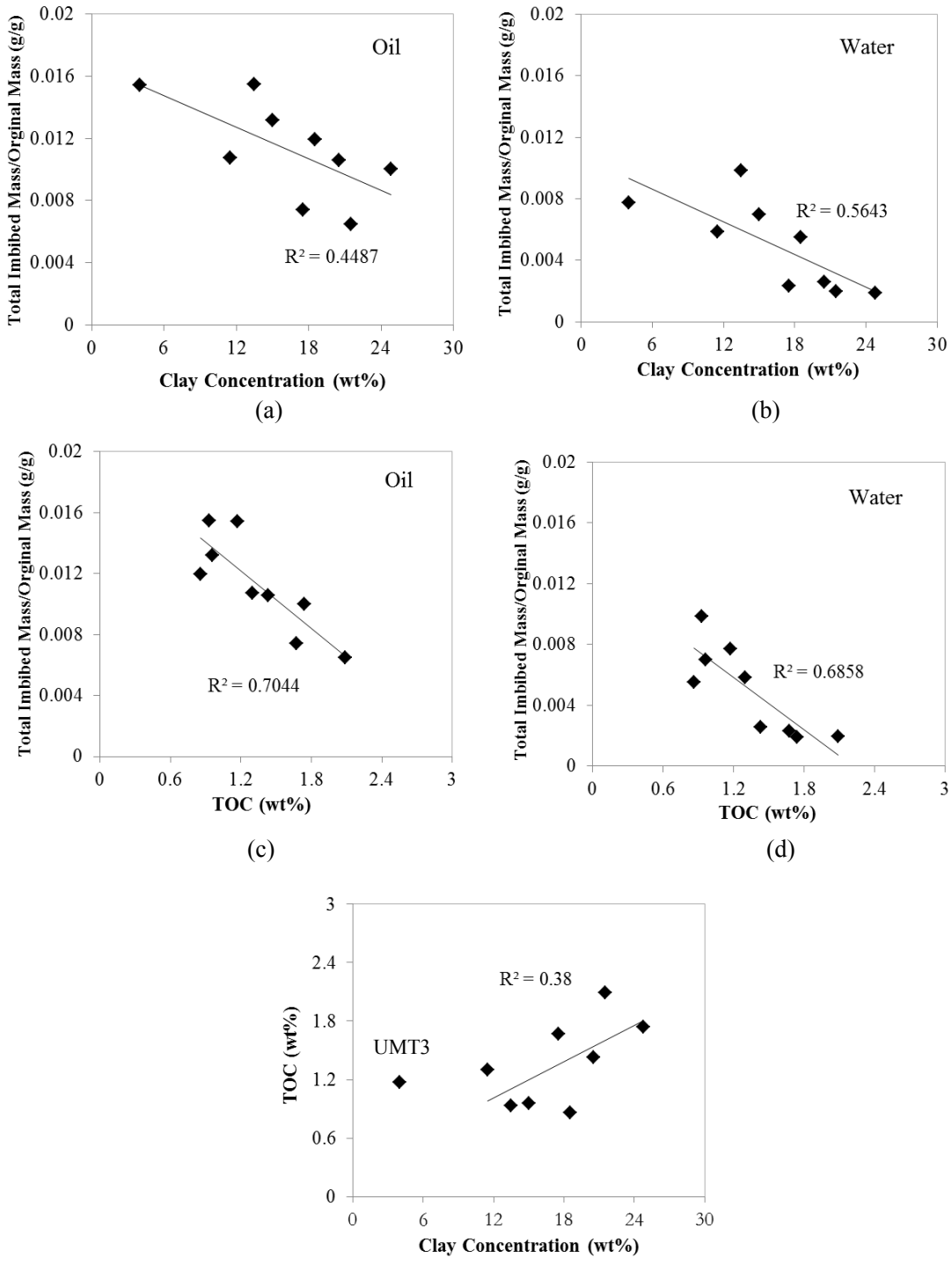

Figure 7.10 Normalized imbibed mass of oil (left) and water (right) versus total clay concentration (a), (b) and TOC (c), (d), TOC versus clay concentration (e) (UMT3 is not used

for calculation of R^2).

7.4.2.3 Correlation between Wettability and Clay Concentration

Figures 7.11(a) and (b) plot WI_o and WI_w data versus clay concentration of Montney samples, respectively. Interestingly, WI_o is positively correlated to clay concentration, while WI_w is negatively correlated to clay concentration. We do not consider UMT3 data here, because it is an obvious outlier. Again, this correlation can be explained by the positive correlation between TOC and clay concentration as discussed above.

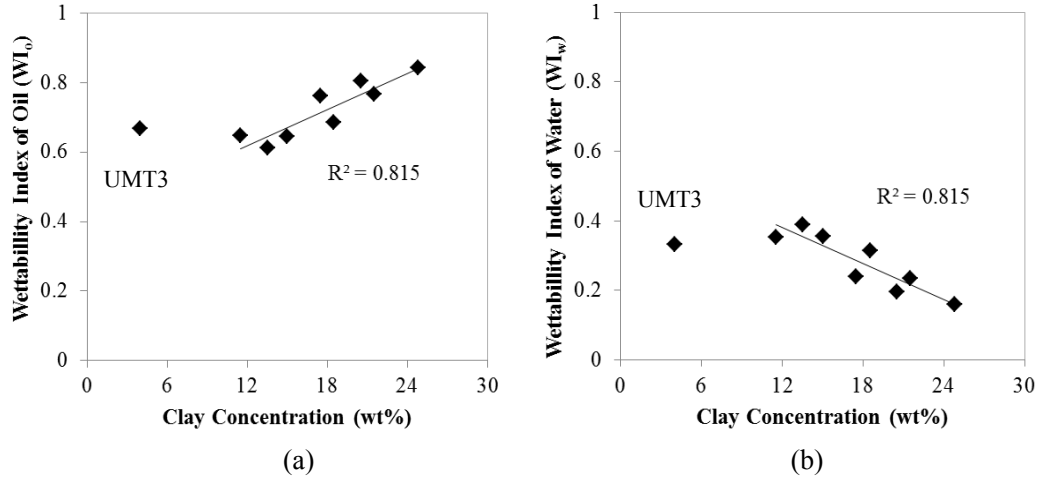

Figure 7.11 Correlation between wettability of oil (a) and water (b) versus clay concentration (UMT3 is not used for calculation of R^2).

7.4.3 Effect of Pore Size Distribution on Liquid Uptake and Wettability

We observe that (1) uptake of oil is always greater than that of brine and (2) uptake of both oil and brine is greater for UMT samples than that for the LMT samples. One may argue that the observed difference between oil and water uptake is due to the almost separate oil and water imbibition pathways. Oil imbibes primarily in pores within or bordering degraded pyrobitumen, while water imbibes in "clean" pores which lack significant pyrobitumen. This argument can be fleshed out by Figure 7.12. Subfigures 7.12(a) to (f) show that the UMT samples have a very different pore size distribution. Their pore size distribution curves are composed of two parts: a

bell-shaped part and a tail part. Figure 7.12(a) shows a well-developed peak at about 0.03 microns radius and a long tail extending from about 0.02 down to 0.002 microns. The peak of the bell-shaped part represents "clean" pore throats and the tail part represents pore throats with pyrobitumen. Interestingly, the tail part is not observed in the pore size distribution curves of LMT samples, as shown in Figures 7.12(g) to (j). For example, Figure 7.12(h) shows that the peak pore throat radius is about 0.005 micros and all the pore throats are less than 0.01 microns. This observation indicates that there are few pores without pyrobitumen influence in this sample.

Figure 7.13 compares example SEM images of samples selected from UMT and LMT cores. In general, the grains and pores observed in the UMT sample are larger than those in the LMT sample. This observation is consistent with the pore size distribution curves shown in Figure 7.12. Moreover, according to SEM images, the average grain size for UMT samples is 35.6 microns and 26.6 microns for LMT samples. The pore size results are in agreement with the imbibition results. The slope of oil and water imbibition profiles for LMT samples is lower than that for UMT samples. This indicates that the effective permeability of both oil and water for LMT is lower than that for UMT. Also we observe that the final (equilibrium) volume of water and oil in LMT is lower than that in UMT.

UMT

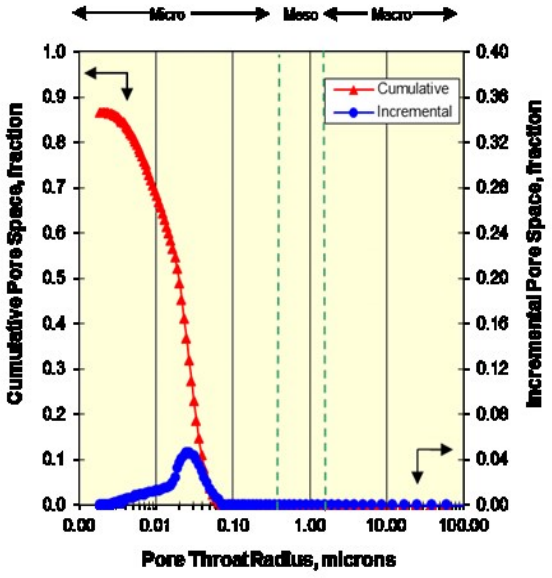

(a)

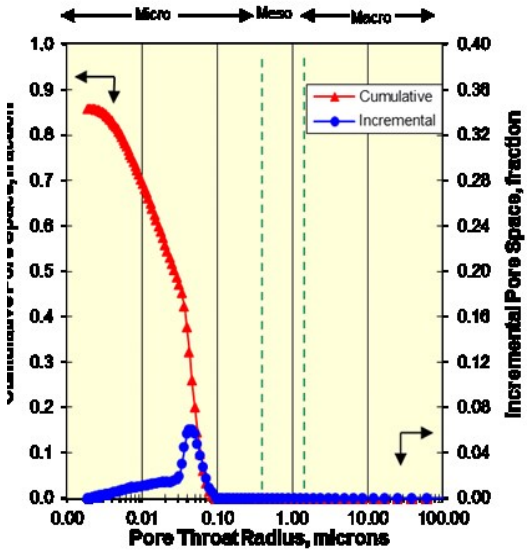

(b)

UMT

UMT

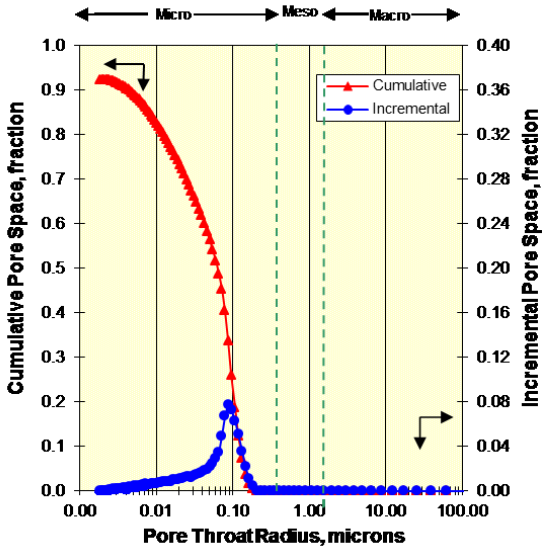

(c)

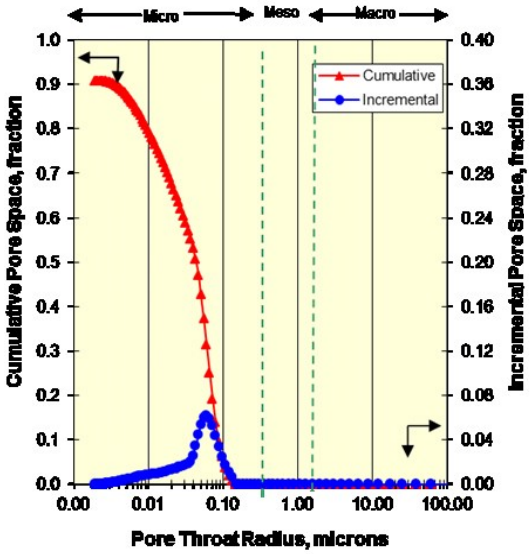

UMT

UMT

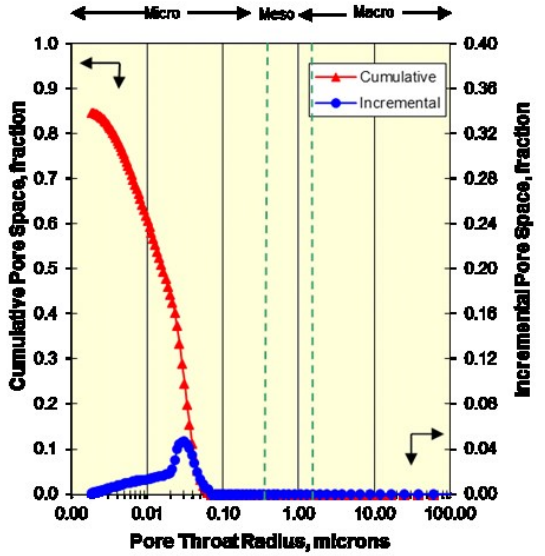

(e)

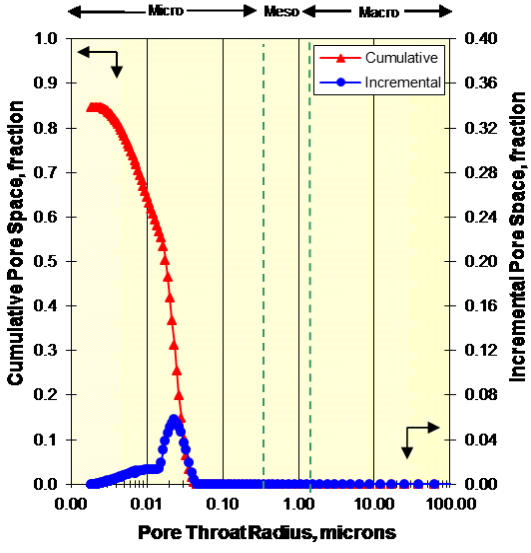

(f)

UMT

LMT

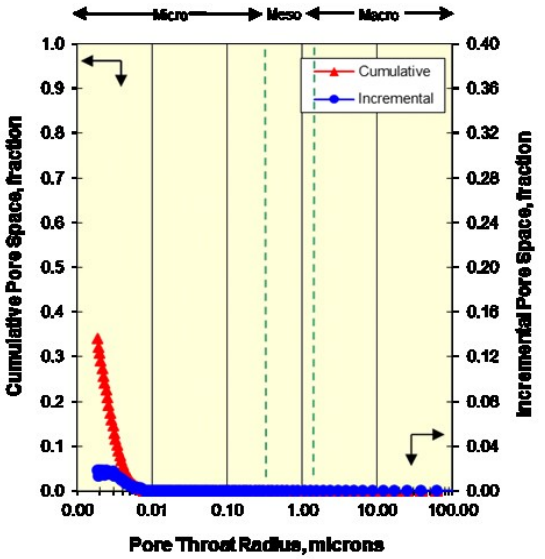

(g)

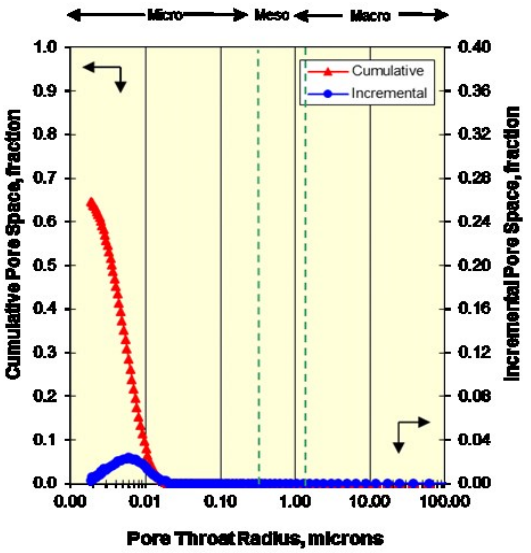

(h)

LMT

LMT

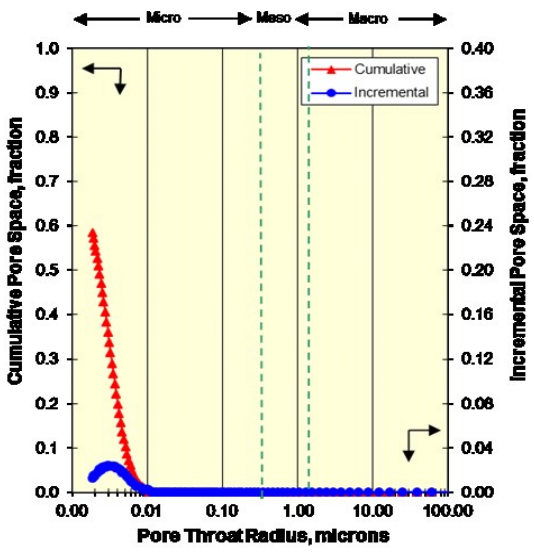

(i)

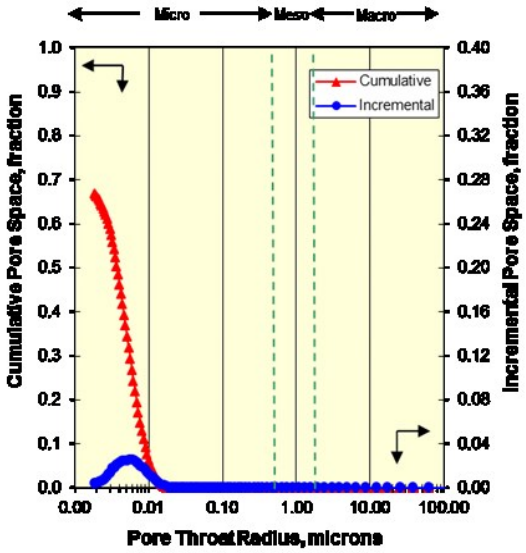

(j)

LMT

Figure 7.12. Pore size distributions of UMT samples (a) to (f) and LMT samples (g) to (j).

UMT

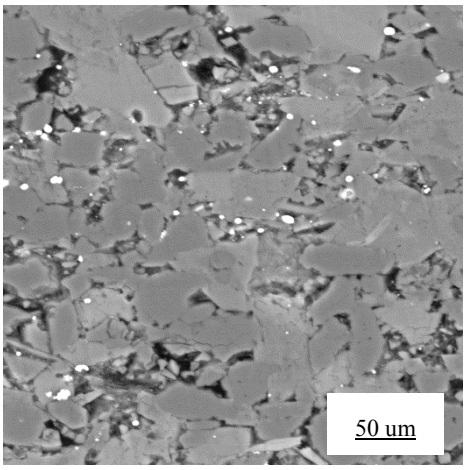

(a)

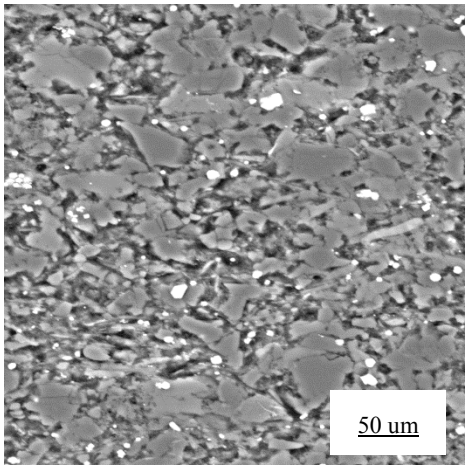

(b)

LMT

Figure 7.13. SEM images of (a) UMT sample and (b) LMT sample.

7.5 Summary

(1) The affinity to the oleic phase is so strong that in some samples more than 90% of the void space becomes invaded spontaneously by oil. Considering the possibility of air trapping due to snap off during the imbibition, the results

indicate that similar experiments under vacuum conditions can be a practical way to estimate connected porosity of tight rocks such as Montney samples. On the other hand, the volume of imbibed water is considerably less than the total pore volume, which indicates that only a small fraction of the pore network is hydrophilic.

(2) The measured wettability index may depend on the rock fabric, and TOC. In general, by increasing the depth, and moving from UMT to LMT, clay content of the rocks increases. This temporal variation in clay content from UMT to LMT is likely controlled by the sedimentation behavior. The results also show that the variations in clay content are weakly correlated with TOC. Clay material provides fine grain matrix with potentially large surface area, which serve as substrate for accumulation of surface-coating amorphous organic matter at the time of deposition. More importantly, large surface area of clay serves as sponge by retaining significant quantity of migrating oil after being exuded from kerogen due to thermal maturity. This fraction of liquid hydrocarbon is disseminated within the clay matrix and later consolidated and solidified due to thermal and possibly bacterial degradation. Higher values of TOC also indicates a higher fraction of secondary cracked light free hydrocarbon, condensate, and residual heavy oil which occur as surface coating within the fine grain matrix of the LMT. Therefore, the relative increase of oil-wetness in LMT can be related to the increase in TOC.

(3) The strong oil uptake of the Montney samples cannot be fully described by the capillary-driven imbibition models. Based on the Young-Laplace equation and assuming identical pore sizes for oil and water flow, the driving force for water uptake almost two times of that for oil uptake. However, the measurements show that the imbibition rate and the final imbibed volume of oil are considerably higher than those of water. The observed discrepancy suggests that in addition to the surface tension, adsorption of oil on the surface of organic matter may act as

a strong driving force for the oil uptake of these samples. Further investigation of this phenomenon remains the subject of future studies.

CHAPTER 8

MODELING THE IMBIBITION DATA OF MONTNEY TIGHT ROCKS

This chapter primarily applies measured spontaneous imbibition data coupled with mathematical models to prove our hypothesis of oil and water imbibed through different pore networks and estimate average pore size of Montney samples.

8.1 Imbibition Rate Analysis

Combing the Darcy equation and diffusion equations, Handy (1960) derived a famous linear relationship between spontaneous imbibition mass and the square root of time.

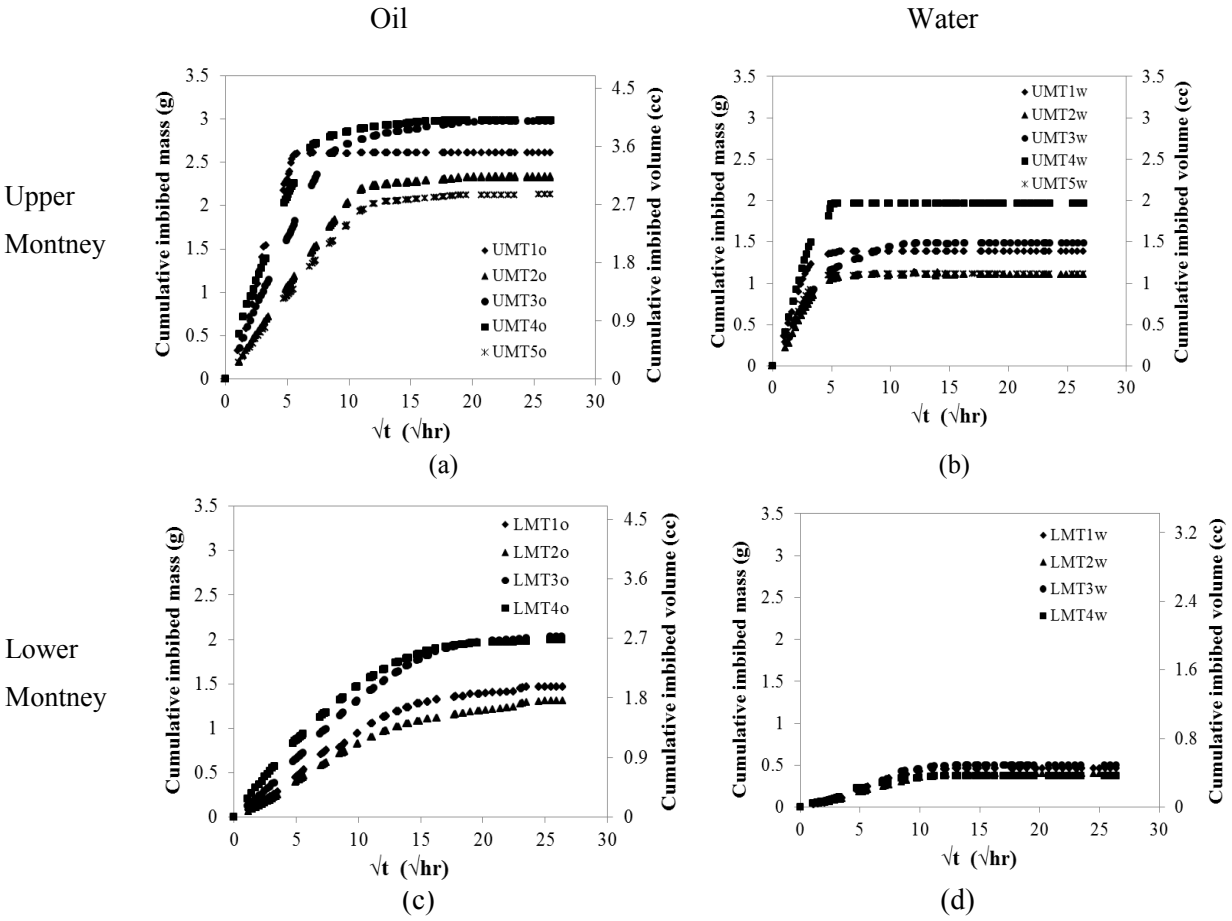

Figure 8.1 Plots of imbibed mass and volume of oil ((a) and (c)) and water ((b) and (d)) versus square root of time for the ten binary plugs.

Therefore, in Figure 8.1, we plot the cumulative imbibed mass (and volume) of oil and water into the binary plugs versus the square root of time. In general, each profile can be divided into an initial linear part (Region 1), a non-linear transition part (Region 2), and a plateau representing the equilibrium conditions (Region 3) as shown Figure 8.2. The slope of Region 1 represents the imbibition rate, which primarily depends on the sample effective permeability and fluid viscosity. The cumulative imbibed mass after equilibrium (Region 3) represents the effective porosity of the sample for each liquid phase. In Figure 8.3, we plot the slope of Region 1 versus the equilibrium value (Region 3) for the imbibition profiles. In general, the slope value is positively correlated to the equilibrium value for both oil (Figure 8.3(a)) and water (Figure 8.3(b)). This correlation can be explained by the natural correlation between effective porosity and effective permeability of the rock samples to oil and water.

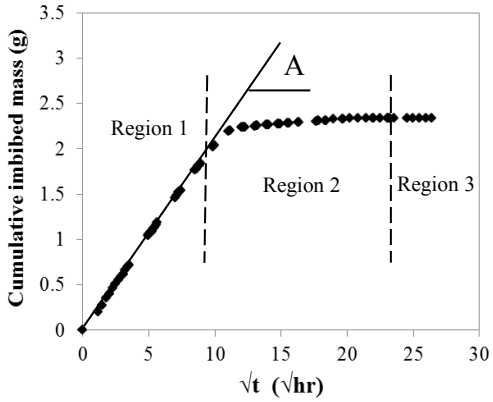

Figure 8.2 An example plot of total imbibed liquid mass vs. square root of time.

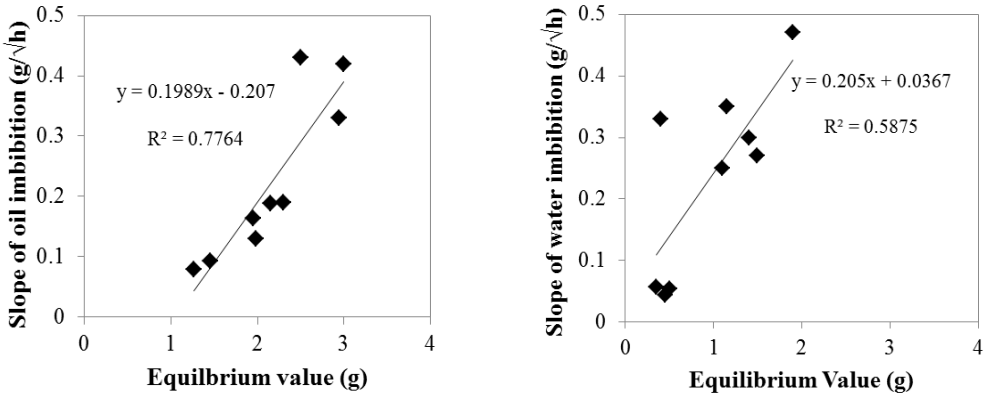

(a) (b)

Figure 8.3 Correlation between slope of linear region (Region 1) and the total imbibed mass after equilibrium (Region 3).

8.2 Handy Model

Various one-dimensional models have been proposed for liquid imbibition into gas-saturated rocks (Handy 1960; Li et al., 2004; Cai et al., 2011; 2013). For an upward piston-like imbibition process into a vertical core, the front velocity is given by

$$v = \frac{K}{\mu}\left(\frac{P_c}{x} - \Delta\rho g\right) \tag{8.1}$$

Where, P_c is the capillary pressure at S_{wf}, μ is viscosity of the wetting fluid, K is permeability of each core. From the material balance equation, the front velocity is also given by

$$v = \phi S_{wf}\frac{\partial x}{\partial t} \tag{8.2}$$

Where, S_{wf} is the imbibition front saturation. Submitting Eq. (8.2) into Eq. (8.1) yields:

$$\frac{dx}{dt} = \frac{K}{\phi\mu S_{wf}}\left(\frac{P_c}{x} - \Delta\rho g\right) \tag{8.3}$$

During early time scales (Region 1), the gravity effect is much smaller than capillary effect, especially for low-permeability rocks studied here. Therefore, neglecting $\Delta\rho g x$ and integrating Eq. (8.3) with respect to time yields:

$$x^2 = \frac{2KP_c}{\mu\emptyset S_{wf}}t \tag{8.4}$$

Since $x = \frac{Q}{\emptyset A S_{wf}}$, and $M = \rho Q$, the total imbibed mass is proportional to the square root of time (Handy 1960):

$$M = \sqrt{\frac{2{S_A}^2\emptyset K\rho^2 S_{wf}P_c}{\mu}}\sqrt{t} \tag{8.5}$$

Where, M is the imbibed wetting fluid mass, ρ is density of wetting liquid, $\emptyset$ is the plug, S_A is the cross-sectional area of the core plug, and t is the imbibition time. We name the slope of initial period (Region 1) as parameter "A" (Figure 8.2). The "A" values for oil and water imbibition in each binary set can be obtained from 1) the imbibition data, 2) and the above model: $\mathrm{A} = \sqrt{\frac{2{S_A}^2 \emptyset K \rho^2 S_{wf} P_c}{\mu}}$.

The ratio between the imbibition slope for oil (A_o) and water (A_w) is mathematically given by

$$m = \frac{\mathrm{A_o}}{\mathrm{A_w}} = \frac{\sqrt{\frac{2{S_A}^2 \emptyset_o \rho_o^2 K_o S_{wfo} P_{co}}{\mu_o}}}{\sqrt{\frac{2{S_A}^2 \emptyset_w \rho_w^2 K_w S_{wfw} P_{cw}}{\mu_w}}} \tag{8.6}$$

$$\text{Or } m = \frac{A_o}{A_w} = \sqrt{\frac{\emptyset_o \rho_o^2 K_o S_{wfo} P_{co} \mu_w}{\emptyset_w \rho_w^2 K_w S_{wfw} P_{cw} \mu_o}} \tag{8.7}$$

If we assume $\emptyset_o = \emptyset_w$, $K_o = K_w$, and $S_{wfo} = S_{wfw}$ for a binary set, the ratio between oil and water capillary pressures is given by $(\frac{P_{co}}{P_{cw}})_{\mathrm{im}} = (\frac{\mathrm{A_o}}{\mathrm{A_w}})^2 \frac{\rho_w^2 \mu_o}{\rho_o^2 \mu_w}$. Therefore, we can calculate the effective capillary ratio $(\frac{P_{co}}{P_{cw}})_{\mathrm{im}}$ using this equation and $\frac{\mathrm{A_o}}{\mathrm{A_w}}$ values obtained from the imbibition data. The density and viscosity of oil and brine, at 25°C listed in Table 7.6 are used to calculate $(\frac{P_{co}}{P_{cw}})_{\mathrm{im}}$ values listed in Table 8.1. The average capillary pressure can also be estimated using Young-Laplace equation $P_c = \frac{\sigma \cos\theta}{r}$. If we assume that the average pore diameter for oil flow through one plug of the binary set is equal to that for water flow in the other plug ($r_o = r_w$), the capillary pressure ratio is given by $(\frac{P_{co}}{P_{cw}})_{\mathrm{YL}} = \frac{\sigma_o \cos\theta_o}{\sigma_w \cos\theta_w}$. Table 8.1 lists $(\frac{P_{co}}{P_{cw}})_{\mathrm{YL}}$ values for the binary plugs using the surface tension and contact angles listed in Tables 7.6 and 7.7. In Figure 8.4, we plot $(\frac{P_{co}}{P_{cw}})_{\mathrm{YL}}$ versus $(\frac{P_{co}}{P_{cw}})_{\mathrm{im}}$, and observe a surprising behavior. Based on the Young-Laplace equation the capillary pressure for

oil imbibition is almost half of that for water imbibition i.e. $(\frac{P_{co}}{P_{cw}})_{\mathrm{YL}} \approx 0.5$. However, based on the imbibition data of all LMT and two of UMT samples, the effective capillary pressure for oil imbibition is higher than that for water imbibition i.e. $(\frac{P_{co}}{P_{cw}})_{\mathrm{im}} > 1$. This observation is correlated with the strong oil-wetness of these samples. The discrepancy between $(\frac{P_{co}}{P_{cw}})_{\mathrm{im}}$ and $(\frac{P_{co}}{P_{cw}})_{\mathrm{YL}}$ values observed in Figure 8.4 can be explained by considering the assumptions made for deriving the expressions for the two ratios. The main assumption is that both oil and water flow through identical pore networks ($\emptyset_o = \emptyset_w,\ K_o = K_w$ and $r_o = r_w$). Furthermore, we assume that imbibition is only driven by capillary pressure defined through Young-Laplace equation. The strong oil uptake of these samples can partly be due to adsorption of oil by the organic material (primarily pyrobitumen) which is not accounted for as a driving force here.

Table 8.1 The ratio between oil and water capillary for each binary core

Label	Slope ratio (A_o/A_w)	(P_{co}/P_{cw})$_{im}$ (Slope Analysis)	(P_{co}/P_{cw})$_{YL}$ (Young-Laplace Eq.)
UM1	1.33	1.480	0.505
UM2	0.75	0.468	0.507
UM3	1.00	0.832	0.435
UM4	0.88	0.637	0.466
UM5	0.6	0.299	0.489
UM6	1.50	1.873	0.521
LM1	2.50	5.203	0.437
LM2	1.67	2.312	0.455
LM3	2.50	5.203	0.493
LM4	4.29	15.29	0.437

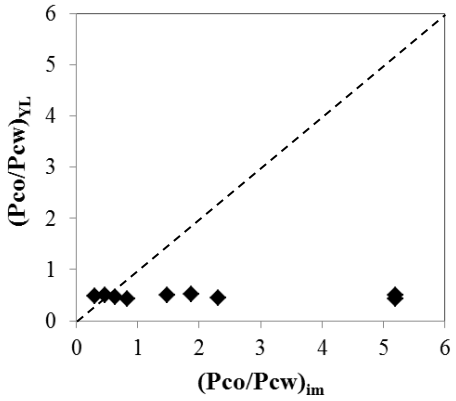

Figure 8.4 $(P_{co}/P_{cw})_{YL}$ versus $(P_{co}/P_{cw})_{im}$

8.3 Lucas-Washburn Model

Randomly distributed pores in a solid matrix may be connected to form tortuous capillaries, through which fluid flows (Cai et al. 2011). The accumulated weight of liquid imbibed into a single tortuous capillary is

$$m = \frac{1}{4}\rho\pi\lambda^2 L_f \tag{8.8}$$

Where, m is the imbibed wetting fluid mass of one capillary, ρ is density of wetting liquid, λ is pore size diameter of the capillary and L_f is actual length of the capillary.

Wheatcraft and Tyler (1988) applied simple scaling arguments to characterize the tortuous streamlines through heterogeneous media by fractal geometry, and developed a scaling relationship for actual length L_f versus the straight-line distance L_s (Cai et al. 2011):

$$L_f = \varepsilon^{1-D_T} L_s^{D_T} \tag{8.9}$$

Where, D_T is the fractal dimension for tortuosity, ε is the length scale L_s is straight-line distance of the capillary.

Lucas (1918) and Washburn (1921) assume the $D_T = 1$, which means the capillary of porous medium is straight tube. Eq. 8.9 could be modified by:

$$L_f = L_s \tag{8.10}$$

If we assume the quasi-steady state, the fully developed laminar flow of an incompressible Newtonian liquid is affected by gravity, viscous and interfacial tension. Then the flow can be represented by the Hagen-Poiseuille law (Washburn 1921):

$$\frac{dL_f}{dt} = \frac{\lambda^2}{32\mu L_f}\left(\frac{4\sigma\cos\theta}{\lambda} - \rho g L_s\right) \tag{8.11}$$

In the initial stage of imbibition, the gravity factor is negligible. Thus Eq. (8.8) can be simplified as

$$\frac{dL_f}{dt} = \frac{\lambda^2}{32\mu L_f} * \left(\frac{4\sigma\cos\theta}{\lambda}\right) \tag{8.12}$$

Integrating the Eq. (8.12), yields Lucas-Washburn (LW) equation:

$$L_f = L_s = \sqrt{\frac{\lambda\sigma\cos\theta}{4\mu}t} \tag{8.13}$$

Submitting Eq. 8.13 into Eq. 8.8, the accumulated mass imbibed into a pore/capillary can be expressed by:

$$m = \frac{\rho\pi\lambda^2}{8}\sqrt{\frac{\lambda\sigma\cos\theta}{\mu}}\sqrt{t} \tag{8.14}$$

For the total mass imbibed into a porous medium, all the pores should be included. Suppose a porous medium has *n* pores/capillaries, the accumulated weight of imbibed liquid can be calculated as

$$M = \sum_{i=1}^{n}\frac{\rho\pi\lambda_i^2}{8}\sqrt{\frac{\lambda_i\sigma\cos\theta}{\mu}}\sqrt{t} \tag{8.15}$$

Since $\sum_{i=1}^{n}\frac{\pi\lambda_i^2}{4} = A_p = \phi A_{area}$, here A_p is the total pore cross-sectional area, A_{area} is cross-sectional area and ϕ is porosity of the porous medium. Thus the accumulative imbibed mass of the porous medium can be expressed by:

$$M = \frac{\rho\phi A_{area}}{2}\sqrt{\frac{\lambda\sigma\cos\theta}{\mu}}\sqrt{t} \tag{8.16}$$

In this model parameter A= $\frac{\rho\phi A_{area}}{2}\sqrt{\frac{\lambda\sigma\cos\theta}{\mu}}$. The unknown parameter in this fractal model is average core pore diameter λ.

$$\lambda = \frac{4\mu \mathrm{A}^2}{\phi^2\rho^2 A_{area}^2\sigma\cos\theta} \tag{8.17}$$

Coupled with "A" parameter values and known parameter values for fluid density, fluid viscosity, rock cross-sectional area, rock porosity, surface tension and contact angle between fluid and rock, the average pore size diameter for oil and water can be expressed by:

$$\lambda_o = \frac{4\mu_o {\mathrm{A}_o}^2}{\phi^2\rho_o^2 A_{area}^2\sigma_{oa}\cos\theta_o} \tag{8.18}$$

$$\lambda_w = \frac{4\mu_w {\mathrm{A}_w}^2}{\phi^2\rho_w^2 A_{area}^2\sigma_{wa}\cos\theta_w} \tag{8.19}$$

The average pore size diameter is estimated in nanometer scale by Eq. (8.18), (8.19) and listed in Table 8.2. Table 8.2 shows that the average pore size diameter for water imbibition is much smaller than that for oil. Although we assume oil and water go through the identical pores ($\phi_o = \phi_w = \phi$), the majority of large pore networks are within or coated by degraded pyrobitumen and water can hardly be imbibed into these hydrophobic networks. In other words, the hydrophilic diameter of the pore network should be significantly smaller than the hydrophobic part shown as Figure 8.5. This observed discrepancy is keeps consistent with the effective porosity for water is lower than effective porosity for oil (Table 7.8).

Table 8.2 Average pore size diameter estimation of Montney core plugs by LW model.

label	$UMT1_o$	$UMT1_w$	$UMT2_o$	$UMT2_w$	$UMT3_o$	$UMT3_w$	$UMT4_o$	$UMT4_w$	$UMT5_o$	$UMT5_w$
λ_o (um)	0.0196	/	0.0039	/	0.0105	/	0.0113	/	0.0037	/
λ_w (um)	/	0.0017	/	0.0012	/	0.0011	/	0.0024	/	0.0009
label	$UMT6_o$	$UMT6_w$	$LMT1_o$	$LMT1_w$	$LMT2_o$	$LMT2_w$	$LMT3_o$	$LMT3_w$	$LMT4_o$	$LMT4_w$
λ_o (um)	/	/	0.0019	/	0.0066		0.0186	/	0.0056	/
λ_w (um)	/	/	/	0.0007	/	0.0008	/	0.0009	/	0.0001

"Subscripts o and w represent brine and dodecane, respectively. UMT6 was broken after overburden porosity measurement, no pore size diameter could be measured. "

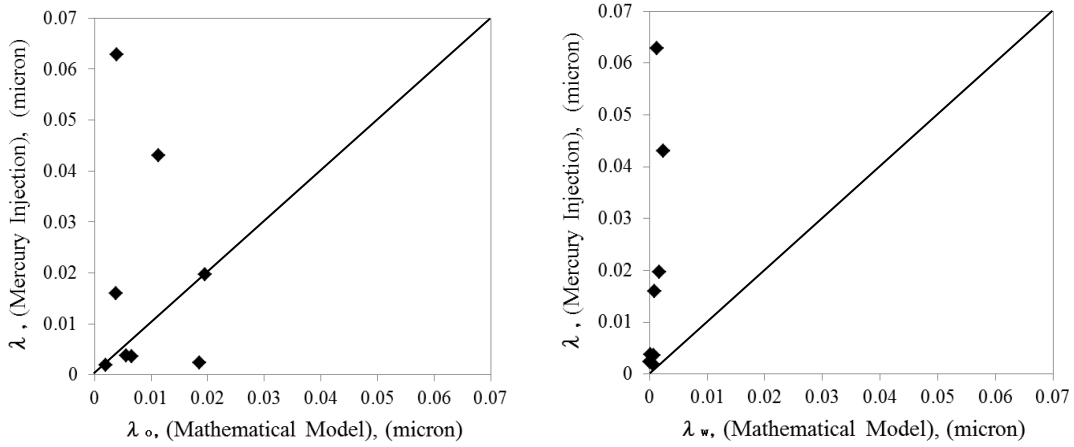

Figure 8.5 Average pore size diameter λ (Mercury Injection)versus (a) average pore size diameter for oil λ_o and (b) average pore size diameter for water λ_w (Mathematical Model).

8.4 Summary

(1) The strong oil uptake of the Montney samples cannot be fully described by the capillary-driven imbibition models. Based on the Young-Laplace equation and assuming identical pore sizes for oil and water flow, the driving force for water uptake is two times of that for oil uptake. However, the measurements show that the imbibition rate and the final imbibed volume of oil are considerably higher than those of water. The observed discrepancy suggests that in addition to the surface tension, adsorption of oil on the surface of organic matter may act as a

strong driving force for the oil uptake of these samples. Further investigation of this phenomenon remains the subject of future studies.

(2) Montney rocks average pore size diameter measured by LW model is smaller than that measured by mercury injection. This discrepancy is primarily due to: 1) ultra-tight characteristics of the samples and their complex inherent pore structures; 2) the fact that many pore spaces are clogged by pyrobitumen (or degraded bitumen). However, the measured values still reveal one general trend: increased sample depth is generally associated with decreased porosity, rock pores for oil imbibition is larger than that for water. This observation is consistent with the results of our previous porosity test and effective porosity measurement for Montney samples.

CHAPTER 9

ADVANCES IN UNDERSTANDING WETTABILITY OF MONTNEY TIGHT GAS AND HORN RIVER SHALE GAS FORMATIONS

The wetting state of a reservoir rock can be identified by measuring equilibrium contact angle, the Amott wettability index (Amott, 1959), the United States Bureau of Mines (USBM) wettability index (Donaldson et al., 1969), spontaneous imbibition rate/volume (Morrow, 1990), hysteresis of the relative permeability curves (Jones and Roszelle, 1978), and Nuclear Magnetic Relaxation (NMR) (Brown and Fatt, 1956). Characterizing the wettability of tight rocks is challenging due to their complex pore structure, which can be either in hydrophobic organic materials or in hydrophilic inorganic materials. Furthermore, the conventional techniques involving forced displacements can hardly be applied for characterizing wettability of tight rocks, due to their ultra-low permeability.

In this chapter, we conduct comparative and systematic imbibition experiments on several core plugs and crushed powder packs from Montney tight gas play and Horn River Basin. We investigate the correlation between the imbibition behavior and other petrophysical properties and discuss the factors controlling the wettability of these samples.

9.1 Samples

Experimental materials include the Montney ultra-tight sand and the Horn River shale samples, and the test fluids used for the spontaneous imbibition experiments.

9.1.1 Montney Tight Rocks

The Montney (MT) resource play straddles across the Canadian provinces of British Columbia and Alberta, as shown in Fig. 9.1. This formation is one of the largest economically feasible resource plays in North America (Keneti et al., 2010). The

study area is in the central portion of the Montney tight gas fairway and is located in the border of Alberta and British Columbia. This formation is up to 320 m thick, and is composed overwhelmingly of siltstone, shaly siltstone, and very fine-grained sandstone (Wood, 2013). Generally, by increasing the depth, porosity, bulk volume water (BVW), and initial water saturation decrease, and the rock becomes less laminated and bioturbated (Wood, 2013).

A total of 6 binary core plugs are selected from depths between 3723 m - 3770 m in the lower Montney Group. Table 9.1 summarizes the main physical, petrophysical properties and the TOC of the samples selected for the study. Table 9.2 and 9.3 summarize the rock properties as obtained from downhole logs and the mineralogy obtained from XRD analysis, respectively.

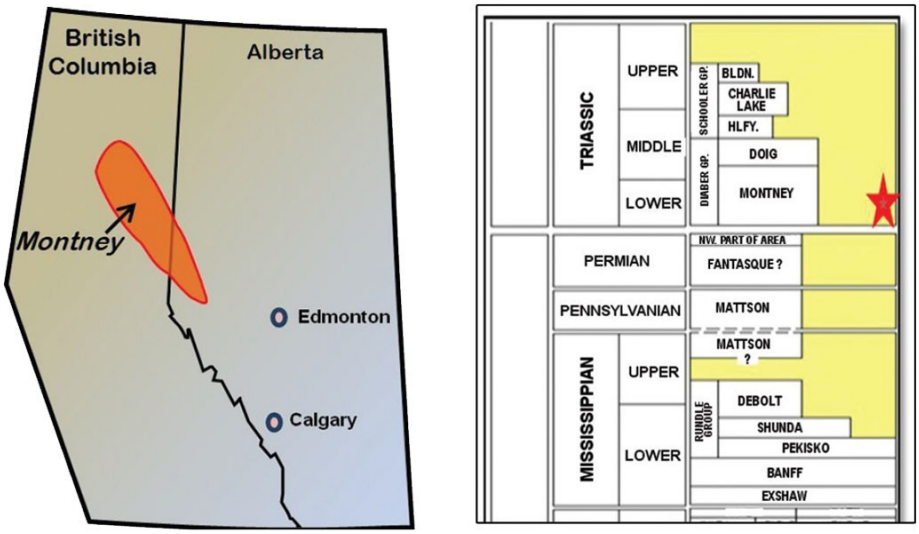

Figure 9.1 Location and depositional stratigraphy of the Montney formation (the star sign highlights the location of the Montney formation, Source: Neito, 2013).

9.1.2 Horn River Shales

The Horn River (HR) formation is a stratigraphic unit of Devonian age in the Western Canadian Sedimentary Basin. This Basin is located in northeastern British Columbia and extends northward into the Northwest Territories (Fig. 9.2). Horn River is the

third largest North American natural gas accumulation discovered prior to 2010, with estimated 500 Tcf of original gas in place and 110 Tcf of recoverable gas in place (Johnson et al., 2011; Mauger and Bozbiciu, 2011). Total organic carbon (TOC) in the Horn River formation has been reported to be up to 5 wt. % (Reynolds and Munn, 2010; Chalmers et al., 2012). The formation is in general composed of dark-colored argillaceous limestone, and calcareous to siliceous shale, which is often bituminous (Reynolds and Munn, 2010). The Horn River formation consists of several subsurface members including Muskwa (M), Otter Park (OP) and Evie (EV) members, as shown in Fig. 9.2.

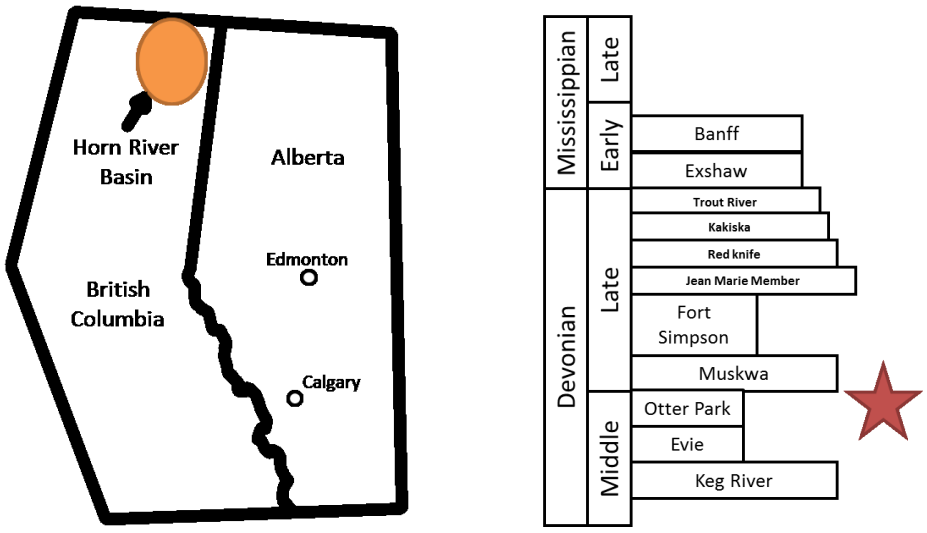

Figure 9.2 Location and depositional stratigraphy of the Horn River Basin (the star sign highlights the location of Muskwa, Otter Park and Evie members).

The core samples were selected from three wells drilled in Muskwa, Otter Park and Evie formations and were dry-cut by using nitrogen gas to obtain binary plugs. Table 9.4 and 9.5, respectively, summarize the average petrophysical properties and mineralogy of the samples selected for the study. A total of 8 samples were crushed to produce shale powder packs for the complementary imbibition tests. Table 9.6 summarizes the average properties of shale packs.

9.2 Fluids

Isopar and 2wt. % sodium chloride (NaCl) solution are used for the imbibition experiments on the MT samples. Kerosene and 2wt. % potassium chloride (KCl) solution are used for the imbibition experiments on the HR shale samples. Kerosene and deionized (DI) water are used for the imbibition experiments on the crushed HR shale samples. The density, viscosity and surface tension of the five fluids are listed in Table 9.7.

Table 9.1 Depth, diameter, cross-sectional area, thickness, TOC, porosity and permeability of the Montney samples used for the imbibition experiments

Label	Depth (m)	Diameter (cm)	Cross-sectional Area(cm^2)	Thickness (cm)	TOC (wt. %)	Porosity (fraction)	Permeability (md)
MT1	3723.5	3.45	9.35	9.25	1.09	0.056	5.36E-03
MT2	3736.5	3.45	9.35	9.44	3.22	0.055	1.66E-03
MT3	3741.8	3.45	9.35	9.62	2.76	0.039	5.38E-03
MT4	3743.8	3.45	9.35	9.32	4.33	0.045	5.38E-03
MT5	3761.9	3.45	9.35	8.55	2.53	0.058	3.77E-03
MT6	3769.2	3.45	9.35	7.51	1.96	0.046	2.00E-02

Table 9.2 Log response of the Montney samples

Label	Total Gamma (API)	Uranium-free Gamma(API)	Thorium (ppm)	Potassium (fraction)	Uranium (ppm)	Bulk Density (gm/cc)
MT1	129.4	81.1	8.9	3.23	8.98	2.351
MT2	95.7	46.5	6.05	2.2	8.89	2.301
MT3	105.5	60.6	6.77	2.75	8.19	2.314
MT4	113	70.9	7.48	3.1	7.86	2.396
MT5	90.8	59.9	8.28	2.76	5.17	2.06
MT6	86.8	63.3	7.47	2.61	4.16	2.286

Table 9.3 Average mineral concentration of the Montney samples determined by XRD

Label	Dolomite (wt. %)	Quartz (wt. %)	Calcite (wt. %)	K-feldspar (wt. %)	Plagioclase (wt. %)	Pyrite (wt. %)	Illite (wt. %)	Matrix Density
MT1	38	23.1	8.4	11.4	7.5	1.4	10.3	2.35
MT2	52	21.1	0	11.8	3.8	1.2	10.1	2.32
MT3	81.5	6	6.5	3.3	2.8	0	0	2.31
MT4	24.8	27.9	3.1	19.4	7.1	2.2	15.4	2.4
MT5	25.4	19.6	10.3	26.5	3.6	1	13.6	2.06
MT6	29.4	17.9	9.4	23.3	11.5	0.6	7.9	2.33

Table 9.4 Depth, diameter, cross-sectional area, thickness, TOC and porosity of the intact Horn River samples used for the imbibition experiments.

Label	Depth (m)	Diameter (cm)	Cross-sectional Area(cm^2)	Thickness (cm)	TOC (wt. %)	Porosity (fraction)
M1	1792	10	78.5	2.04	3.91	0.071
M2	1792	10	78.5	1.59	3.91	0.071
OP1	2639	10	78.5	2.37	3.01	0.087
OP2	2639	10	78.5	2.36	3.01	0.087
EV1	2679	10	78.5	2.89	4.1	0.06
EV2	2679	10	78.5	2.76	4.1	0.06

Table 9.5 Average mineral concentration of intact Horn River samples determined by XRD

Label	Dolomite (wt. %)	Quartz (wt. %)	Chlorite (wt. %)	Calcite (wt. %)	Illite (wt. %)	Plagioclase (wt. %)	Pyrite (wt. %)	Matrix Density
M	5.2	36.7	4.4	0	48.3	3.6	1.7	2.744
OP	2.2	43.6	0	12.9	33.8	4.4	3.2	2.772

Table 9.6 The average depth, diameter, cross-sectional area, thickness, TOC and porosity of the crushed-shale packs.

Label	Depth (m)	Diameter (cm)	Cross-sectional Area (cm^2)	Thickness (cm)	TOC (wt. %)	Porosity (fraction)	Permeability (md)
M1	1758	2.54	5.067	25	3.91	0.27	35
M2	1758	2.54	5.067	25	3.91	0.27	35
M3	1758	2.54	5.067	25	3.91	0.27	35
M4	1758	2.54	5.067	25	3.91	0.27	35
OP1	2639	2.54	5.067	25	3.01	0.274	32
OP2	2639	2.54	5.067	25	3.01	0.274	32
OP3	2639	2.54	5.067	25	3.01	0.274	32
OP4	2639	2.54	5.067	25	3.01	0.274	32

Table 9.7 Density, viscosity and surface tension of different fluids at 25^{o}C used for the imbibition experiments

Fluid	Density (g/cm^3)	Viscosity (cp)	Surface Tension (dyn/cm)
Isopar	0.69	2.06	20.7
Kerosene	0.8	1.32	28
2wt. % NaCl	1.02	0.91	73.6
2wt. % KCl	1.02	0.89	72.7
DI water	1	0.9	72

9.3 Methodology

We conduct a series of comparative oil/water imbibition tests on several dry plugs, which were dry-cut from the cores of the Montney, Muskwa, Otter Park, and Evie formations. We also conduct similar imbibition tests on crushed shale packs produced from Muskwa and Otter Park cores.

9.3.1 Contact Angle Measurement

Contact angle for various rock-fluid combinations is obtained by analyzing the droplet profile equilibrated on the rock surface (Rao, 1997). A high-resolution camera is used

to visualize the profile of the droplet injected by a needle on the rock surface, as shown in Fig. 7.6 for several example cases.

9.3.2 Imbibition Experiments on Intact Samples

A total of 18 spontaneous imbibition experiments are conducted on Montney (MT) and Horn River (HR) samples. Half of the total 18 dry plugs are completely immersed in the oil and all the sample faces are open for oil imbibition. The other half are placed inside the imbibition cells filled with brine. The imbibed mass of each sample is periodically measured using a weight balance and recorded for two days. The imbibition data are used for comparing wetting affinity to oil and brine. The general procedure for the imbibition experiments includes the following steps:

1) Dry-cut binary plugs using nitrogen for the comparative oil and water imbibition tests.

2) Heat the samples at 100^{o}C in the oven until the weight is stabilized. Measure the dried weight and bulk volume of each plug sample.

3) Place each plug sample into the imbibition cell and make sure samples were completely immersed into fluids as shown in Fig. 9.3.

4) Seal the imbibition cell to avoid liquid evaporation and measure the weight gain periodically.

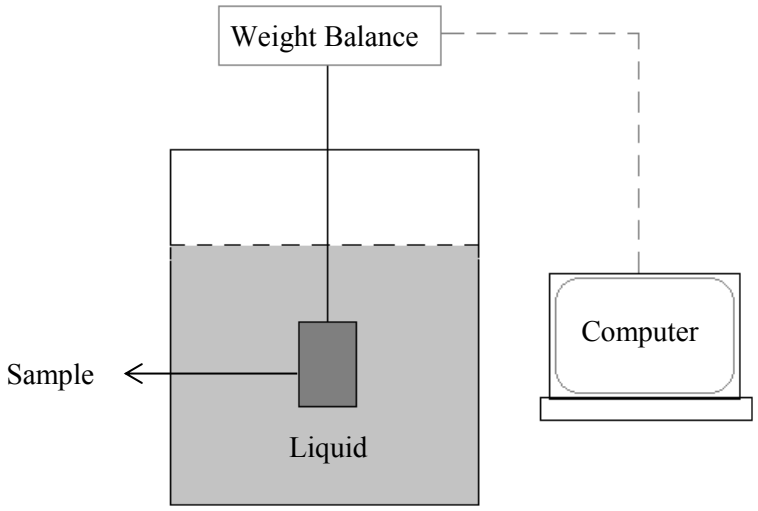

Figure 9.3 The schematic illustration of the imbibition set-up.

9.3.3 Imbibition Experiments on Crushed Samples

Two different set-ups are designed to measure and compare the rate of water and oil imbibition into horizontal and vertical crushed packs, as shown in Figure 9.4 and 9.5, respectively. For horizontal tests, the crushed-shale pack is fully immersed into an imbibition cell filled with DI water or kerosene. The fluid gradually imbibes from the screen-side to the plug-side. The volume of the liquid imbibed into the pack is obtained by measuring the volume of air displaced by the liquid and collected in the inverted cylinder located at the inlet part. For the vertical imbibition tests, the crushed shale pack is placed vertically inside an imbibition cell. The volume of the liquid imbibed into the pack is obtained by measuring the pack weight at different times during the imbibition.

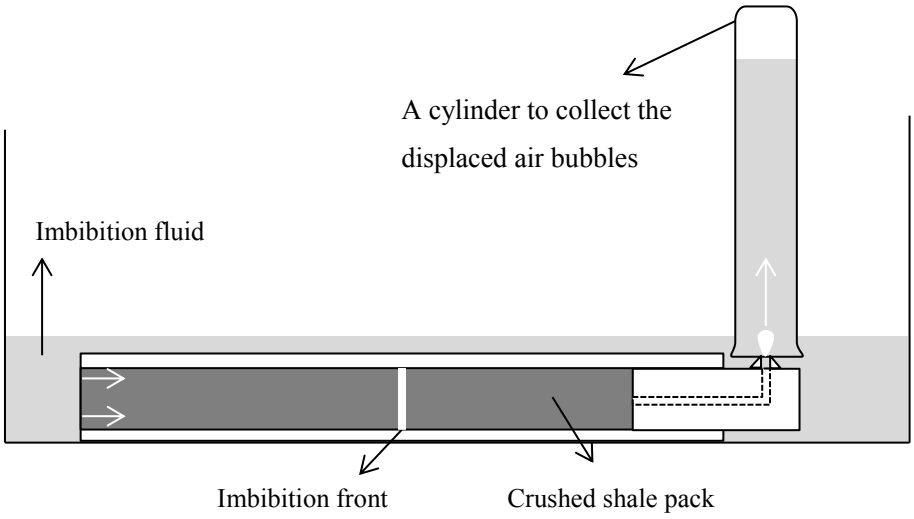

Figure 9.4 The schematic illustration the set-up for the horizontal imbibition experiments. The fluid imbibes from the left to the right and displaces the air in the crushed-shale pack. The air is collected in an inverted cylinder (Xu and Dehghanpour, 2014).

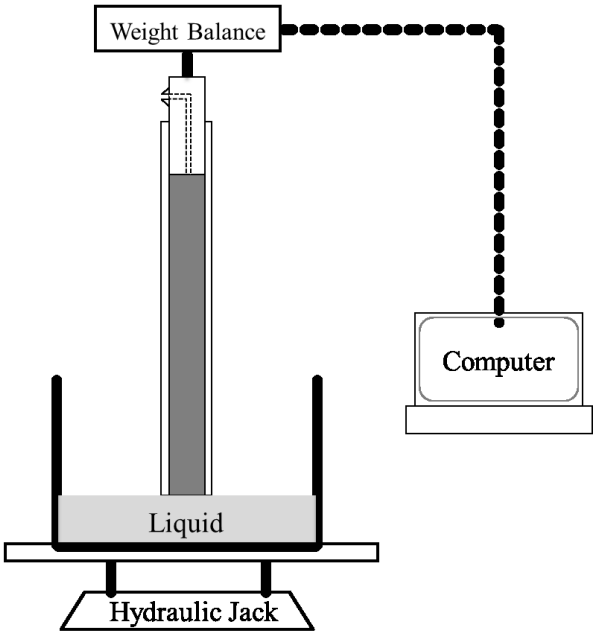

Figure 9.5 The schematic illustration the set-up for the vertical imbibition experiments. The fluid imbibes from the bottom to the top. The mass of imbibed liquid is recorded by weight balance (Xu and Dehghanpour, 2014).

9.4 Experimental Results

This section presents and discusses the experimental results.

9.4.1 Contact Angle Results

When brine (2wt. % NaCl) droplets are in contact with the clean surface of the MT samples, they retain their identity as droplets. However, the oil (Isopar) droplets completely spread on the rock surface. These phenomena for random samples are shown in Figure 9.6 (a) and (b). A similar behavior is observed for M, OP, and EV samples, as illustrated in Figure 9.6 (c) to (h). Table 9.8 lists the average values of contact angle of each formation. Thus, based on the contact angle results, all the rock samples studied here are strongly oil-wet.

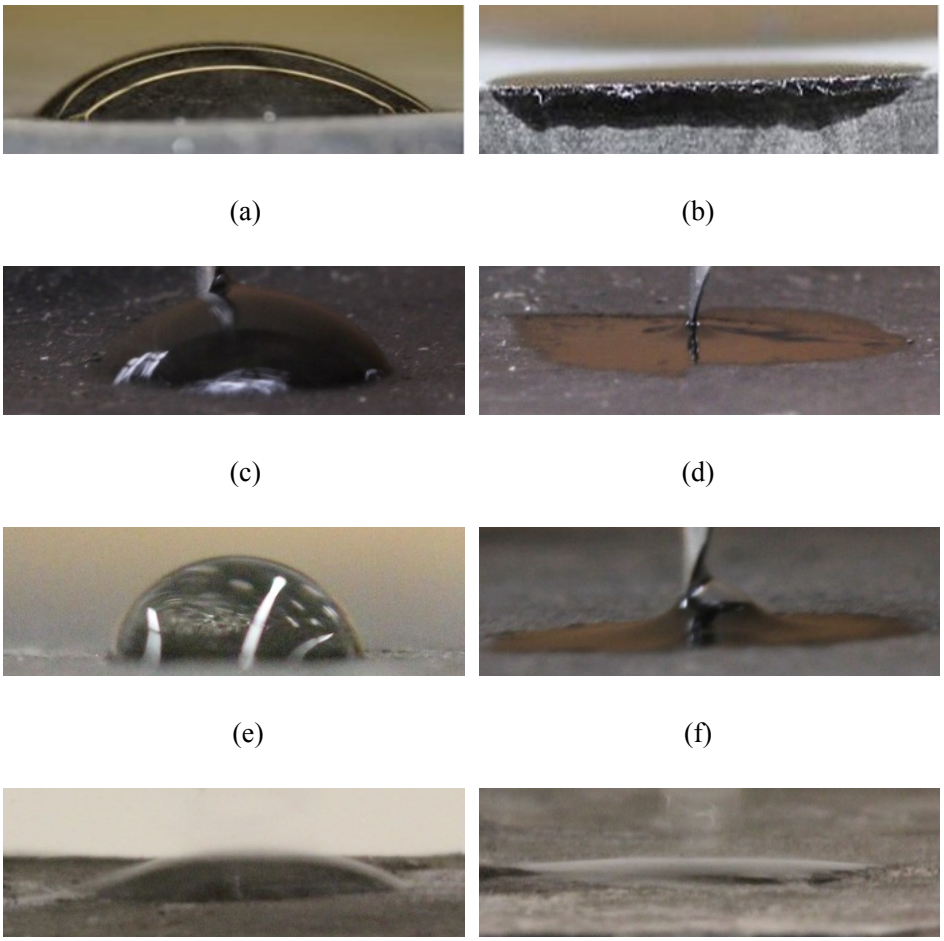

(a) (b)

(c) (d)

(e) (f)

(g) (h)

Figure 9.6 Equilibrated droplets of water (left) and oil (right) on the fresh surface of MT (a, b), M (c, d), OP (e, f) and EV (g, h) samples. Oil completely spreads on the surface of all samples.

Table 9.8 Average contact angle of oil and water droplets equilibrated on the surface of rock samples from Montney, Muskwa, Otter Park and Evie formations.

Formation	Montney	Muskwa	Otter Park	Evie
θ_o(deg)	45	58	73	37
θ_w(deg)	0	0	0	0

9.4.2 Imbibition Results for the MT Samples

Figure 9.7 shows the normalized volume of oil and brine imbibed into the MT plugs. The final imbibed volume of oil is higher than that of brine for all samples. Since the surface tension of brine (2wt. % NaCl) is more than three times higher than that of oil (Isopar), the imbibition data indicate that the wetting affinity of the MT samples to oil is higher than that to brine. This observation is consistent with the contact angle results.

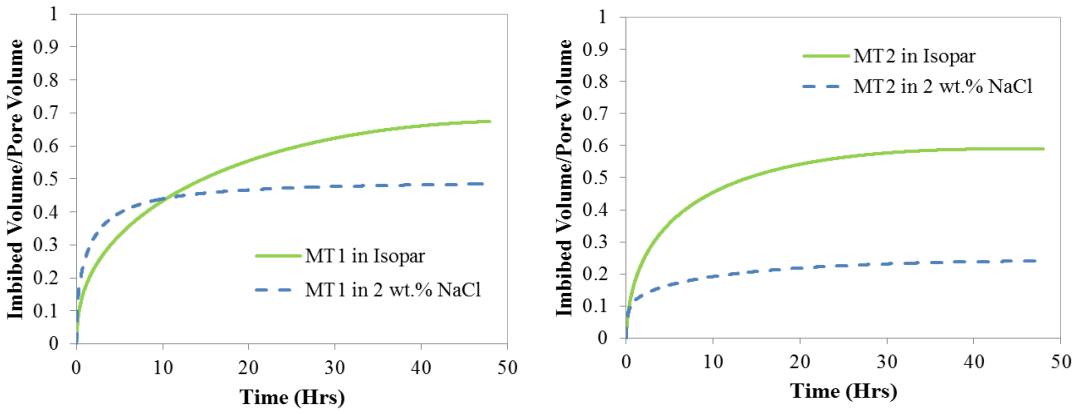

(a) (b)

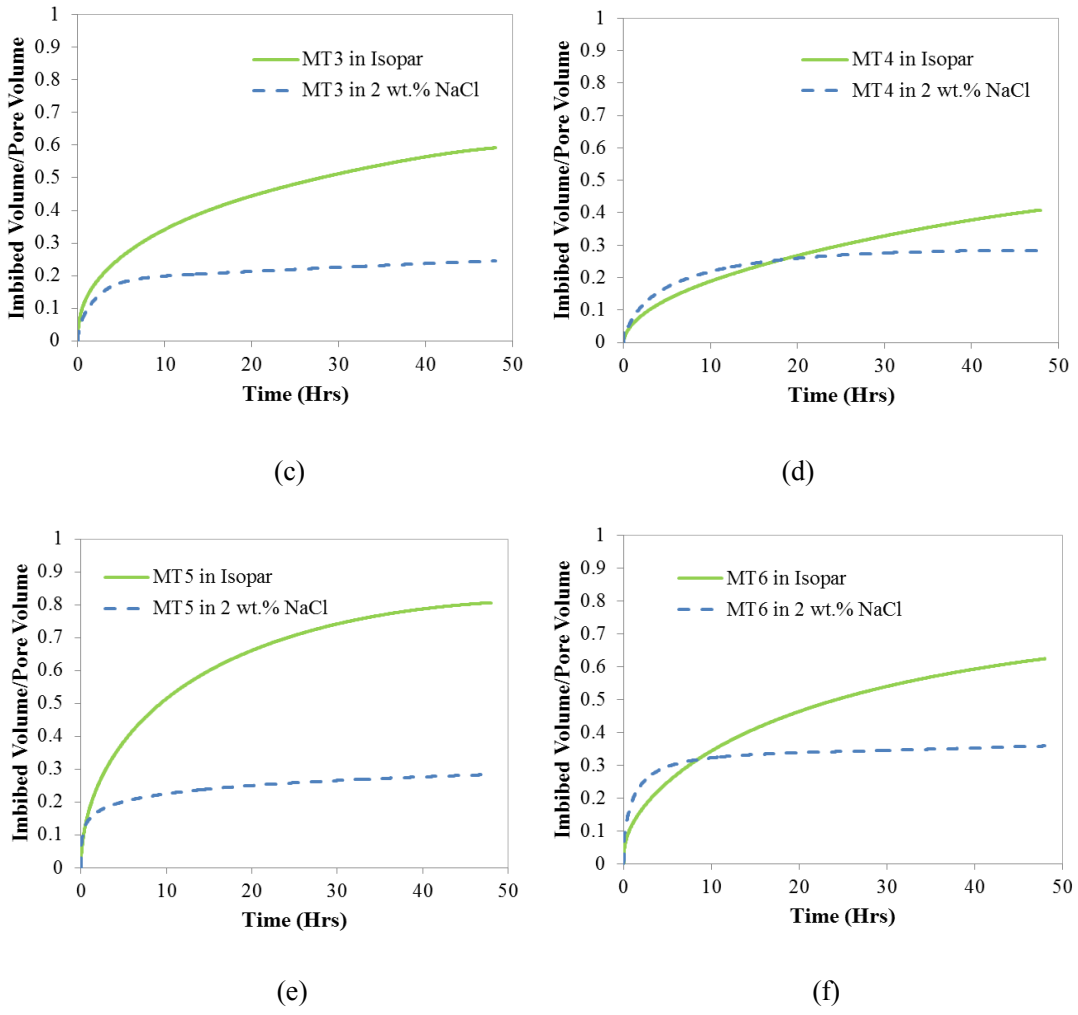

Figure 9.7 Normalized volume of oil (Isopar) and brine (2wt. % Nacl) into the Montney core samples.

9.4.3 Imbibition Results for the Intact HR Samples

Figure 9.8 shows the normalized volume of oil and brine imbibed into the HR plugs. Interestingly, in contrast to the MT samples, the HR samples imbibe more water than oil. This observation is contrary to the contact angle results, which indicate the samples are strongly oil-wet. It is well-know that the primary driving force for spontaneous imbibition is capillary pressure, which at the pore scale is approximated by $(\frac{\sigma_{ia}\, cos(\theta_i)}{D_p})$, where σ_{ia}, $\theta_i$and D_p are the surface tension, contact angle and average pore diameter of the porous medium, respectively. One may argue that the observed difference is due to the lower surface tension of oil as compared to water.

For a more consistent analysis, the imbibition data should be plotted and compared on dimensionless plots.

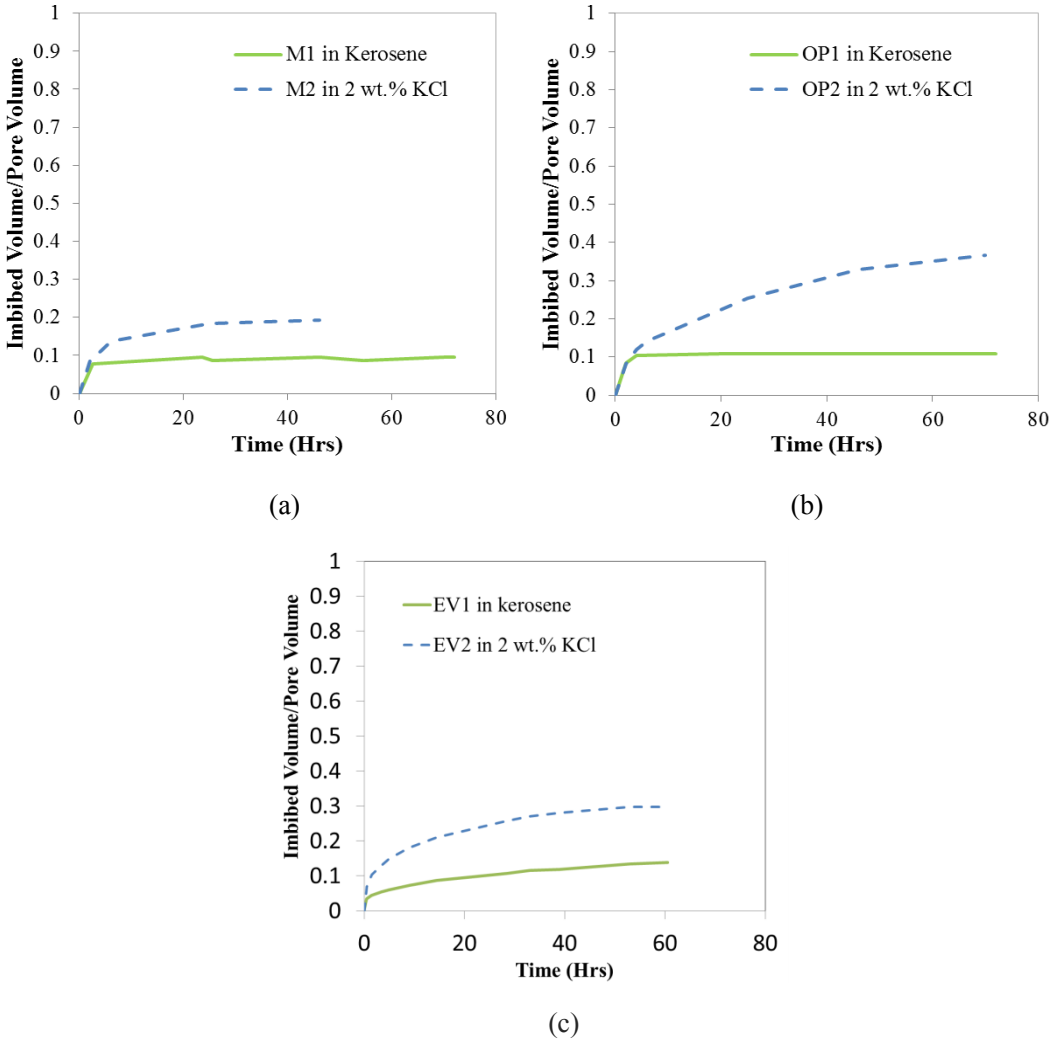

Figure 9.8 Normalized volume of oil (Kerosene) and brine (2wt.%KCl) into intact HR samples.

9.5 Scaling the Experimental Data

The objective of this section is to compare consistently the imbibition behavior of oil and brine in the MT and HR samples. As we discussed in Chapter 5 the imbibition behavior in general depends on (1) rock properties such as porosity, permeability and pore structure, (2) fluid properties such as viscosity, surface tension and density, (3) physical parameters such as size, shape and boundary conditions of the samples, and (4) wettability which is a rock-fluid property. In order investigate the wetting affinity

of the samples, one should scale the imbibition data to exclude the other parameters controlling the imbibition behavior. Various expressions have been proposed for the dimensionless time that can be used for scaling the imbibition data (Rapoport, 1955; Zhang et al., 1996; Shouxiang et al., 1997; Li and Horne, 2004; Schmid and Geiger, 2012). The most frequently used dimensionless time (t_D) for scaling spontaneous imbibition data is (Mattax and Kyte, 1962):

$$t_D = t\sqrt{k/\emptyset}\frac{\sigma}{\mu}\frac{1}{L_c^2} \tag{9.1}$$

Where, μ is fluid viscosity, σ is fluid interfacial tension, k is permeability, $\emptyset$ is porosity and L_c is the characteristic length which depends on sample shape and boundary conditions. If all faces of the samples are open for imbibition (AFO boundary condition), the characteristic length is given by:

$$L_c = DL/\sqrt[2]{(D^2 + 2L^2)} \tag{9.2}$$

Where, *D* and *L* are diameter and length of the samples, respectively.

Figures 9.9 and 9.10, respectively, show the normalized oil/brine volume imbibed in the MT and HR samples versus the corresponding dimensionless time. Based on the existing models of the spontaneous imbibition, the oil and water data for each binary plug should be close together. However, Figure 9.9 shows that the oil imbibition curves of all MT samples are consistently above the water curves. The excess oil uptake of the MT samples can be interpreted by their excess affinity to oil compared with water. It should be noted that the dimensionless time defined by Eq. 9.1 does not account for the rock wettability. On the other hand, Figure 9.10 shows that the water imbibition curves of all HR samples are consistently above the oil curves. Similarly, the excess water uptake of the HR samples can be interpreted by their excess affinity to water compared with oil.

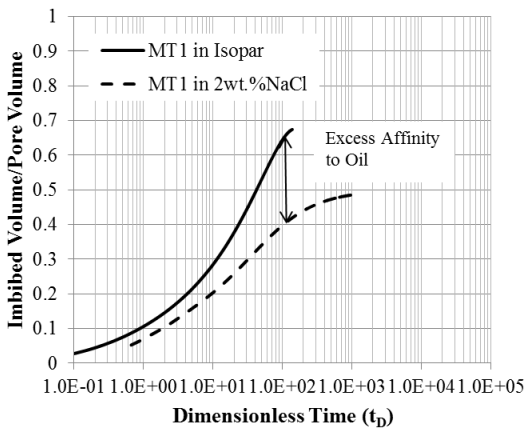

(a)

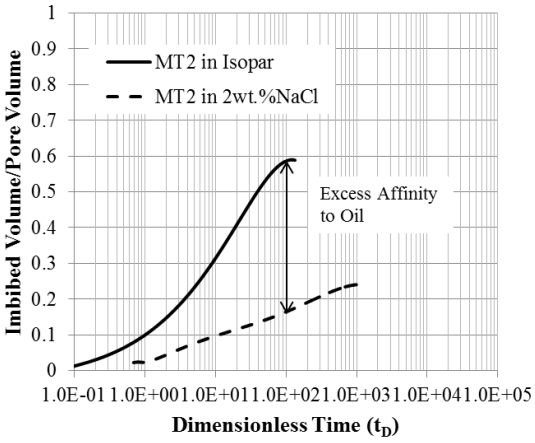

(b)

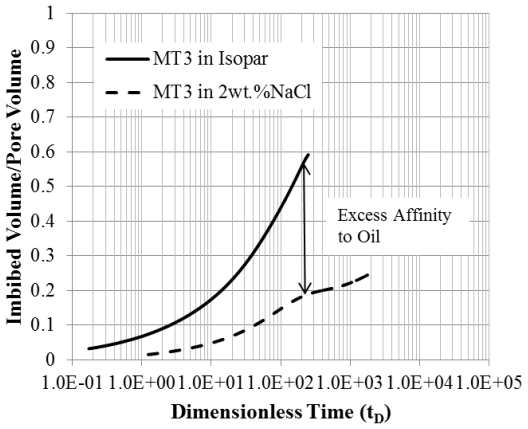

(c)

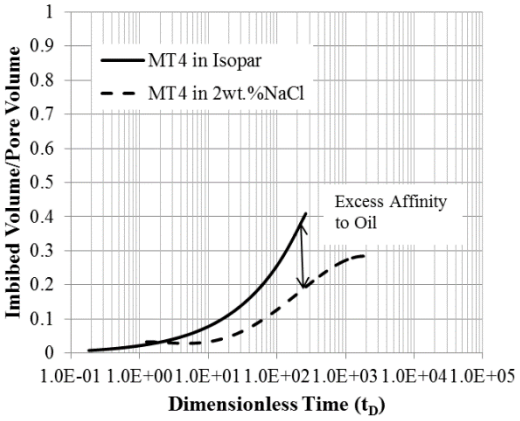

(d)

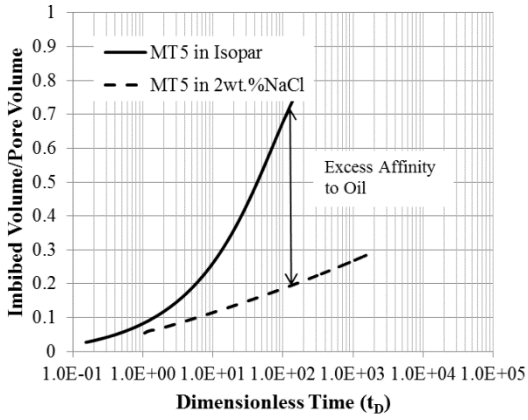

(e)

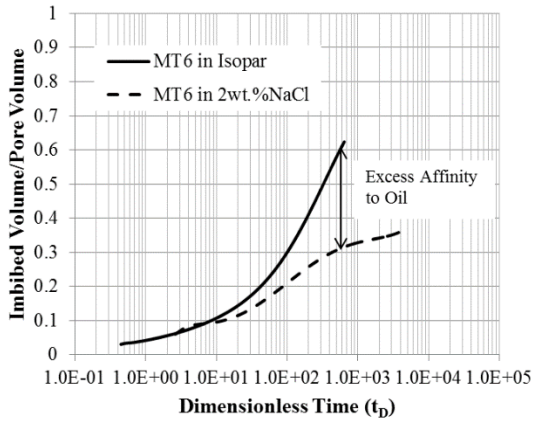

(f)

Figure 9.9 Normalized imbibed oil and brine volume versus dimensionless time for MT tight samples.

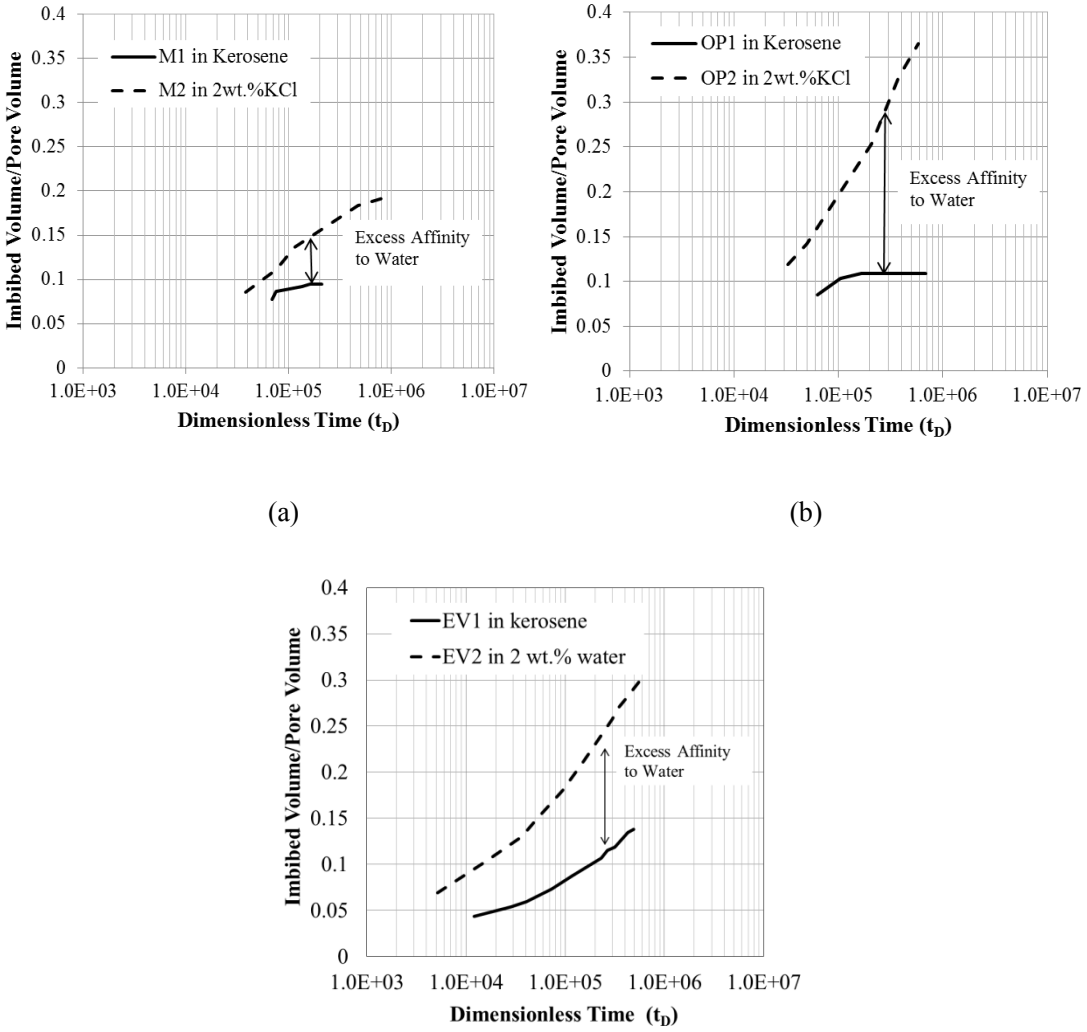

Figure 9.10 Normalized imbibed oil and brine volume versus dimensionless time for HR shale samples.

9.6 Discussion of Imbibition Results

The results of the experiments presented above can be summarized by three key observations:

1) Oil completely spreads on the fresh break of all samples, while water droplets show a measurable contact angle which is less than 90 degree.

2) Both oil and water spontaneously imbibe into the MT samples. However, the imbibition rate and the total imbibed volume of oil are considerably higher than those of water for all MT samples. This difference is more pronounced in the dimensionless plots.

3) Both oil and water spontaneously imbibe into the HR samples. However, the imbibition rate and the total imbibed volume of water are significantly higher than those of oil for all intact HR samples. This difference is more pronounced in the dimensionless plots.

Observation 1 indicates that both HR and MT samples are strongly oil-wet, and should spontaneously imbibe the oleic phases.

Observation 2 confirms the strong affinity of the MT samples to oil, however, the large separation between water and oil uptake, especially on the dimensionless plots, is interesting and needs further investigation. We hypothesize that oil preferentially flows through the organic pore network of the MT samples, which is mainly coated by pyrobitumen. In the next section we will examine this hypothesis by 1) investigating the possible correlation between the oil wettability index and TOC and 2) interpreting the thin sections and SEM images of the MT samples.

Observation 3 is surprising because oil which completely spreads on the fresh break of HR samples can hardly imbibe into their pore network, while their water uptake is significantly high. It should be noted the shale pores can be either in organic or inorganic materials (Sondergeld et al., 2010). The organic part of the rock is hydrophobic (Mitchell et al., 1990), while the non-organic part can be hydrophilic, especially in the presence of clay minerals. Therefore, organic shales are usually a mixture of hydrophilic and hydrophobic materials. Significant water uptake of the HR samples may indicate that the hydrophilic pore network is relatively well-connected. Furthermore, the significant water uptake of the HR samples can be explained by the clay hydration (Dehghanpour et al. 2012), depositional lamination (Makhanov et al.,

2014), imbibition-induced microfractures (Dehghanpour et al., 2013), and osmotic potential (Xu and Dehghanpour 2014). On the other hand, insignificant oil uptake of these samples may indicate that the hydrophobic pore space, partly coated by organic carbon, is poorly connected. In the next section, we will compare oil and water imbibition in crushed shale packs to investigate this hypothesis.

9.6.1 Imbibition Experiments on Crushed Samples

We hypothesize that the unexpected low oil uptake of the HR samples, with a significant water uptake, is primarily due to the poor connectivity of the organic pore network. To test this hypothesis, we compare oil and water imbibition behavior in the crushed shale packs. Figure 9.11 compares the normalized volume of oil and water imbibed into several HR shale packs. Evidently, the imbibed volume of oil is higher than that of water for all samples. Figure 9.12 shows that the separation between the oil and water imbibition values is even more pronounced when plotted versus scaling dimensionless time. Therefore, the wetting affinity of crushed samples to oil is higher than that to water, in contrast to the behavior of the intact samples. Evidently, in a crushed sample, both hydrophilic and hydrophobic pores are artificially connected. Therefore, oil, which hardly flows though the intact samples, easily wets the created hydrophobic surfaces and imbibes into the crushed pack. This observation is in agreement with the complete spreading of oil on the fresh break of the HR samples.

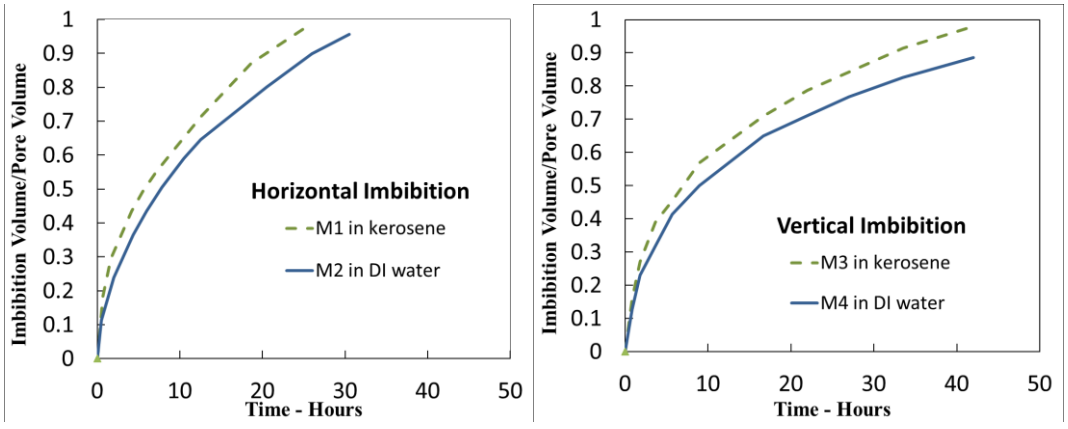

(a) (b)

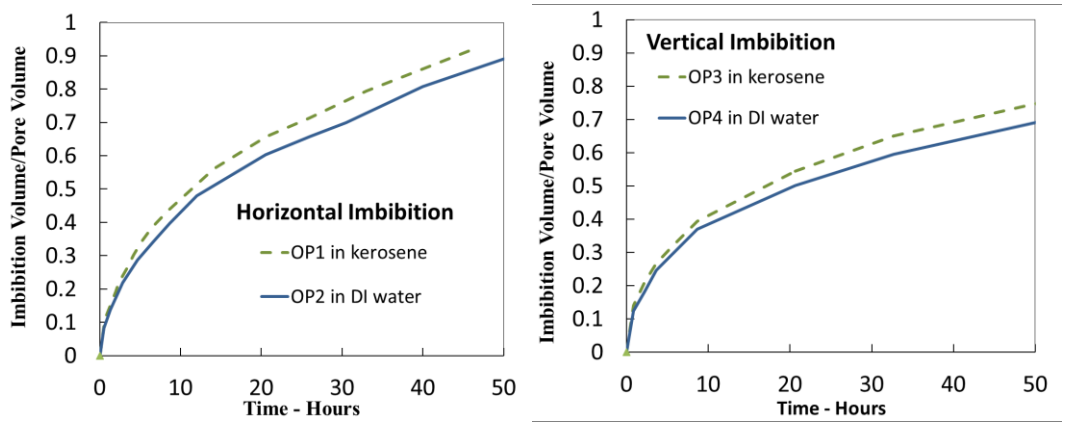

(c) (d)

Figure 9.11 Normalized volume of oil (Kerosene) and DI water into crushed HR samples.

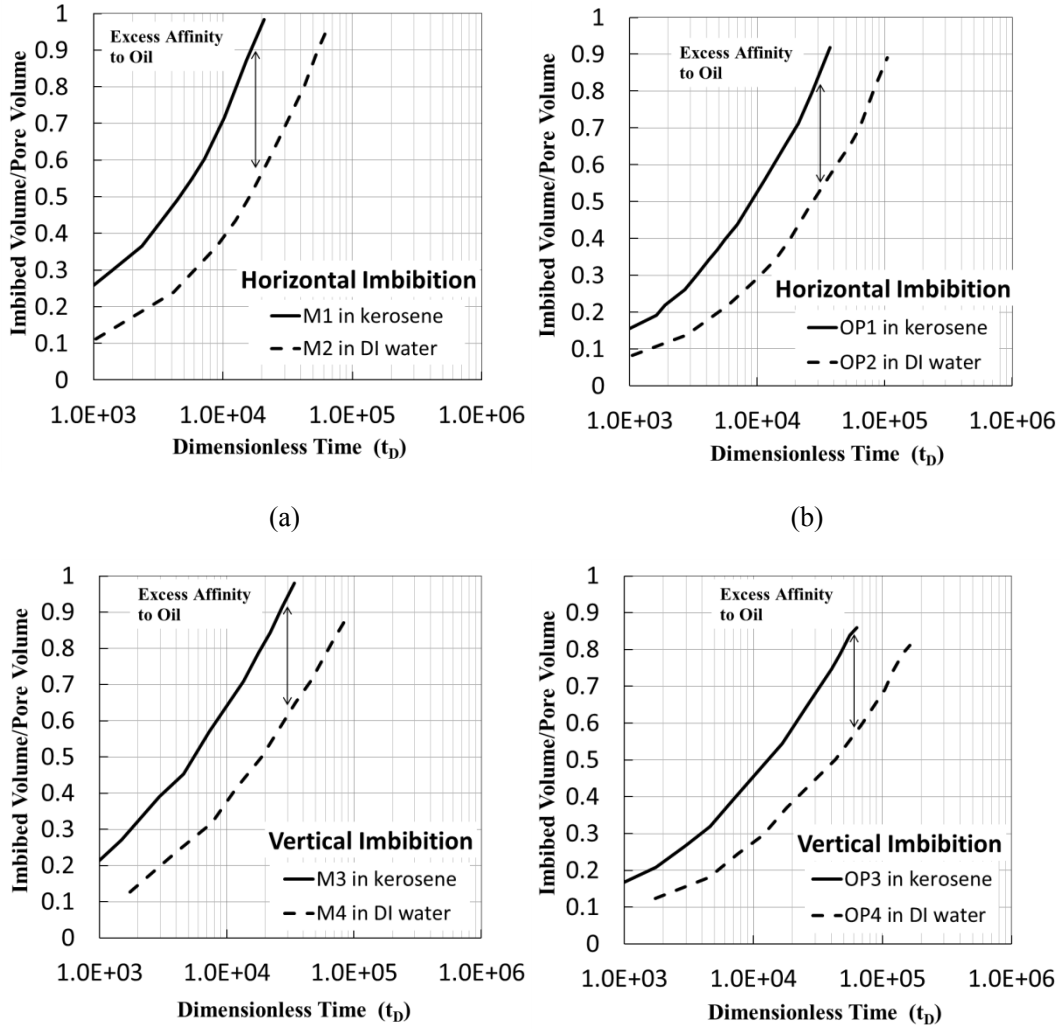

(a) (b)

(c) (d)

Figure 9.12 Normalized imbibed oil volume versus dimensionless time for horizontal (left) and vertical (right) imbibition experiment on M (a, b) and OP (c, d) crushed samples.

9.6.2 Investigation the Strong Oil Uptake of the MT Samples

Here we hypothesize that strong oil-wetness of the Montney samples is partly due to the presence of degraded pyrobitumen in the Montney samples (Wood 2012). To examine this hypothesis, we first investigate the existence of correlation between the oil-wetness and TOC of the MT samples. The separation between the equilibrium imbibed volume of water and oil can be interpreted as an indication of rock wettability. Let us define the following wettability indices for water and oil using the imbibition data:

$$\text{Wetting Affinity Index of Brine } (WI_w) = \frac{I_w}{I_w + I_o} \tag{9.3}$$

$$\text{Wetting Affinity Index of Oil } (WI_o) = 1 - \frac{I_w}{I_w + I_o} \tag{9.4}$$

Here, I_w and I_o are the normalized volume of brine and oil imbibed into the samples. In simple, I_w (or I_o) is calculated by dividing the total imbibed volume of brine (or oil) by the sample total pore volume. The calculated wettability indices for the six binary plugs are listed in Table 9.6.

Table 9.6 Wettability index of oil and brine for the six binary plugs

Label	Wettability index of oil (WI_o)	Wettability index of brine (WI_w)
MT1	0.58	0.42
MT2	0.71	0.29
MT3	0.71	0.29
MT4	0.59	0.41
MT5	0.74	0.26
MT6	0.64	0.36

Figure 9.13 (a) and (b) plot the normalized imbibed volume of oil and water versus TOC content of the six MT samples, respectively. In general, increasing TOC decreases the imbibed volume of both oil and water. This can be explained by the

reduction of effective permeability due to the plugging of the pore network by pyrobitumen, which will be discussed shortly. Figure 9.13 (c) and (d) plot the wettability index of oil (WI_o) and water (WI_w) versus TOC of the six MT samples, respectively. In general, increasing the TOC increases the oil wettability. However, sample MT4 does not follow this trend, and this may be partly due to its high illite concentration.

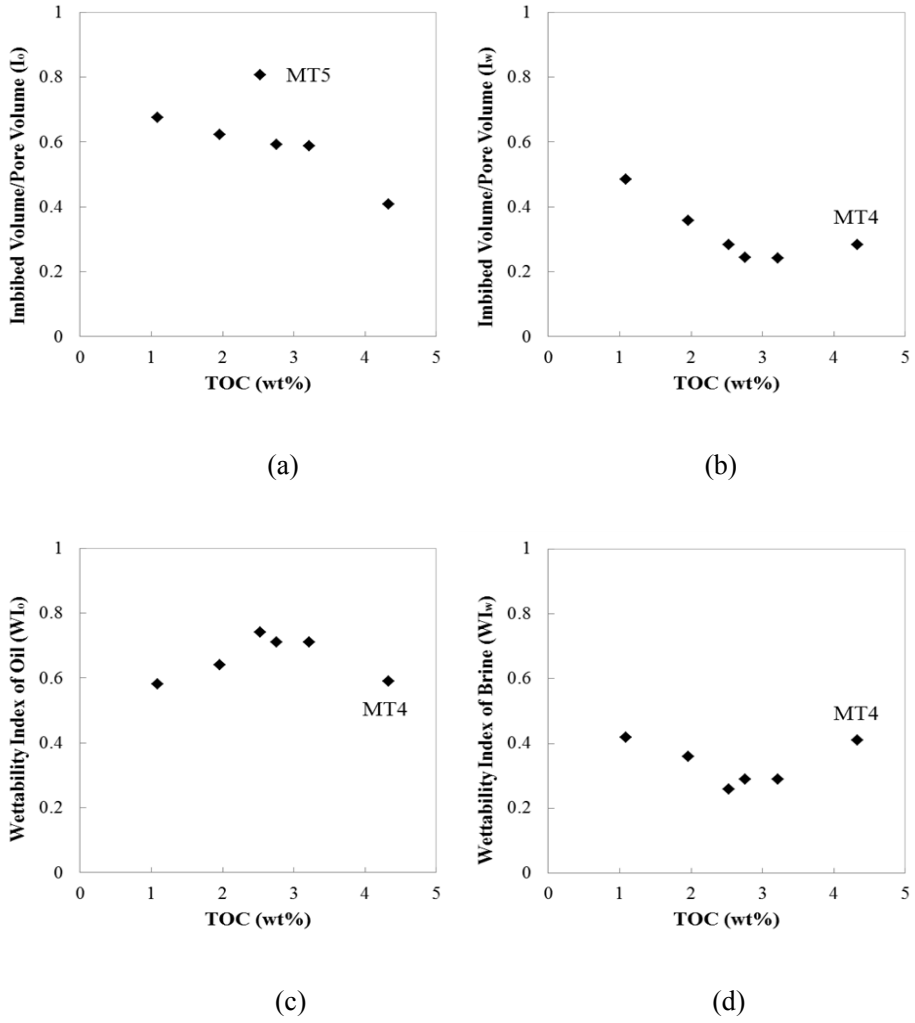

Figure 9.13 TOC content versus (a) normalized imbibed volume of oil, (b) normalized imbibed volume of water, (c) wettability index of oil and (d) wettability index of water.

9.6.3 Observation of Thin Section and SEM Images

Here we examine the presence of pyrobitumen by interpreting the thin section and scanning electron microscopy (SEM) images of the Montney samples, shown in Figures 9.14 and 9.15, respectively.

High magnification view of the thin sections shown in Figure 9.14 shows the lack of visible or open porosity. The images show that the rock matrix is mainly composed of dolomite crystals with some floating quartz (white) and feldspar (yellow) grains. The opaque materials can be a combination of clay, organic, pyrite and pyrobitumen. Further testing (i.e. focus ion beam imaging and reflected light imaging) is required to visualize the porosity and also to confirm the presence of pyrobitumen.

Figure 9.15 (a) indicates the presence of pyrobitumen coating dolomite crystals (center) and detrital clay (lower right). However, reflected light imaging (i.e. organic petrology) is required to confirm the distribution of pyrobitumen. Figure 9.15 (c) view shows the poor porosity due to tightly interlocking crystals and suspected pyrobitumen plugging. Intercrystalline pores (e.g. bottom right) and suspected pyrobitumen coating (center) may also be observed in Figure 9.15 (e). Similarly Figure 9.15 (b), (d) and (f) confirm the likelihood of pyrobitumen coating in the Montney samples.

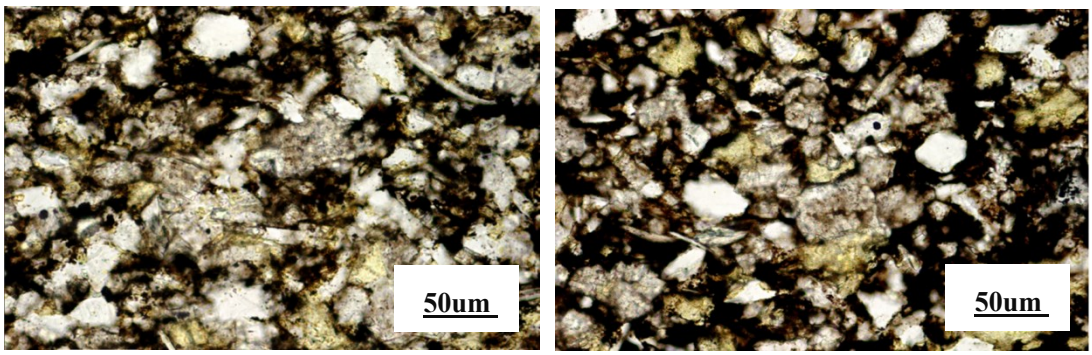

(a) (b)

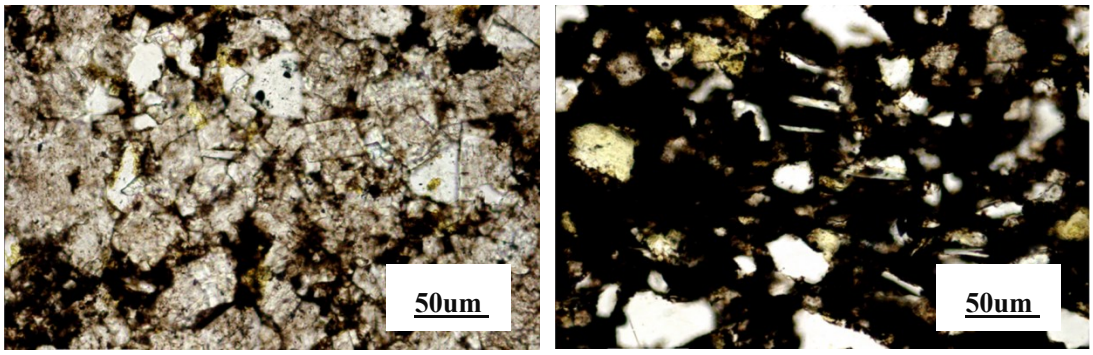

(c) (d)

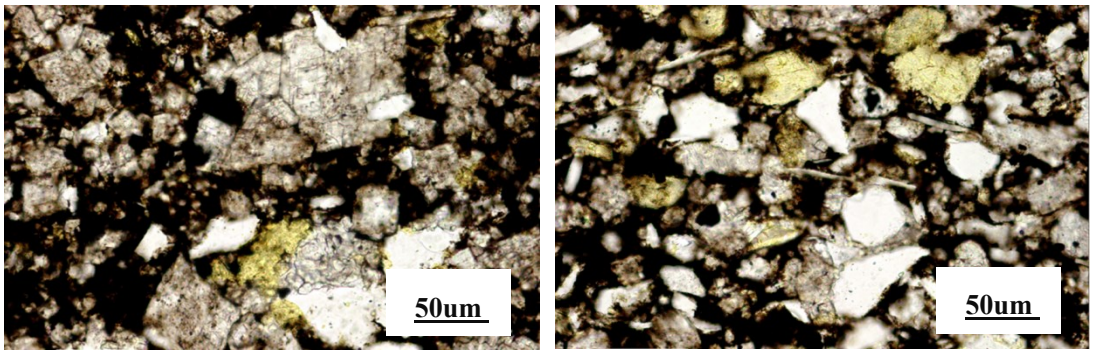

(e) (f)

Figure 9.14 The high magnification (50um) thin section of (a) MT1, (b) MT2, (c) MT3, (d) MT4, (e) MT5 and (f) MT6.

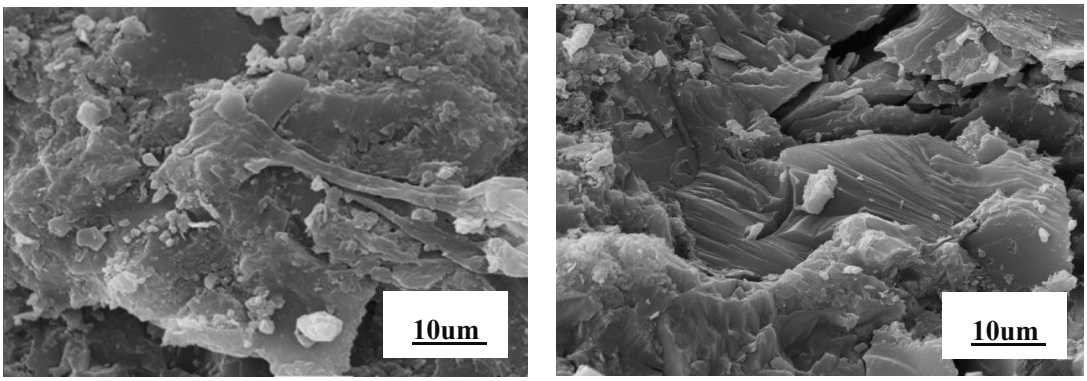

(a) (b)

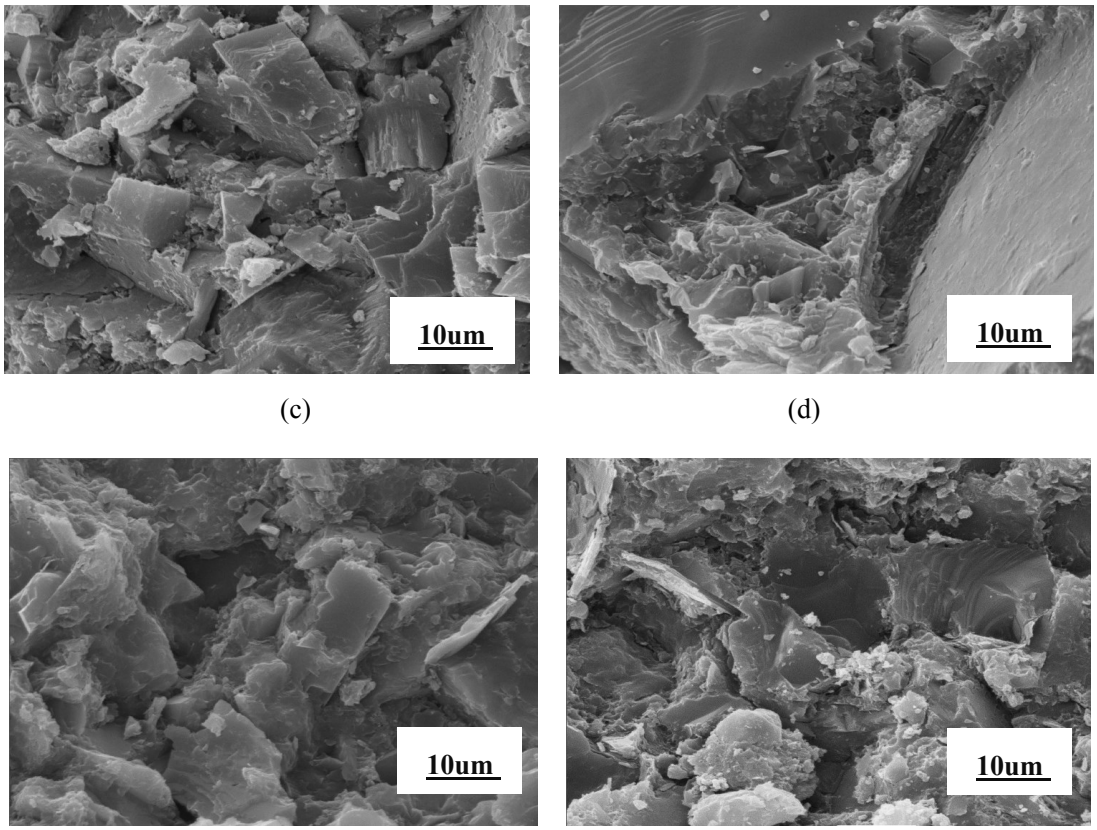

(c) (d)

(e) (f)

Figure 9.15 The high magnification (10um) SEM imaging of (a) MT1, (b) MT2, (c) MT3, (d) MT4, (e) MT5 and (f) MT6.

9.7 Summary

The results of this study indicate that the rock fabric plays a crucial role on the imbibition potential and wettability of unconventional tight rocks. Measurement of contact angle is not sufficient for characterizing the wettability of tight/shale rocks, and in some cases may lead to misleading results. Based on the contact angle results, both MT and HR samples are strongly oil-wet. However, oil hardly imbibes into the HR samples, while it easily imbibes into the MT samples. Insignificant oil uptake of the HR samples suggests that the connected pore network of the rock is strongly hydrophilic, mainly due to the presence of clay minerals and salt crystals coating the grains. However, complete spreading of oil on the fresh break of the HR samples, and strong imbibition of oil into the crushed samples suggest that the majority of rock

mass, in contrast to the connected pore network, is strongly oil-wet. On the other hand, the strong oil uptake of the MT samples suggests that the majority of the pores are strongly oil-wet. In contrast to water, oil can easily imbibe into the pore networks coated by degraded pyrobitumen.

CHAPTER 10

WATER LOSS VERSUS SOAKING TIME: SPONTANEOUS IMBIBITION IN TIGHT ROCKS

This chapter aims at understanding the relationship between water loss and rock petrophysical properties. It also investigates the correlation between water loss and soaking time (well shut-in time). Extensive spontaneous imbibition experiments are conducted on downhole samples from the shale members of the Horn River (HR) Basin and from the Montney (MT) tight gas formation. These samples are characterized by measuring porosity, TOC and mineralogy analysis. Further, a simple methodology is used to scale up the laboratory data for field-scale predictions, and to predict water imbibition volume during the shut-in period after hydraulic fracturing.

10.1 Introduction of Water Loss in Field Scale

Tight oil and gas reservoirs, considered unconventional resources, are emerging as an important source of energy supply in the United States and Canada (Frantz et al., 2005). These unconventional resources with ultralow matrix permeability are capable of producing oil and gas at economic rates when completed by hydraulically fractured horizontal wells (Ning et al., 1993). During hydraulic fracturing, a great amount of fracturing fluid is injected into the target formation to create multiple fractures and increase the contact surface between wellbore and reservoir (Holditch et al., 2005; Palisch et al., 2010). Slick water is commonly used as the primary fracturing fluid with low proppant concentration (Fredd et al., 2001). Water fracturing treatment is cost effective and can create a complex fracture system (Warpinski et al., 2005; Cipolla et al., 2009). Furthermore, water fracturing treatment decreases formation damage and eases the cleanup (Schein, 2005; Palisch et al., 2008).

One of the concerns with water fracturing treatment is that most of the water injected during the hydraulic fracturing is retained in the shale reservoir. In practice, only a small fraction of the injected fluid is recovered during the clean-up phase, although completion of horizontal wells with a multistage hydraulic fracturing treatment requires an enormous amount of water for stimulating the target formation (Fan et al., 2010; King, 2012). The reasons for inefficient water recovery are still poorly understood.

Some researchers believe that low water recovery is due to 1) water retention in secondary fractures (Fan et al., 2010), and 2) unstable displacement and gravity segregation in fractures (Parmar et al., 2012, 2013). Experiments conducted on low-permeability cores suggest that water loss during hydraulic fracturing treatment can be partially explained by spontaneous imbibition of fracturing fluid into the shale matrix (Parmar et al., 2013; Dehghanpour et al. 2012; 2013; Roychaudhuri et al., 2011; Makhanov et al., 2012; 2013). The retained water in the reservoir can leak into the rock matrix due to capillary effect and cause reservoir damage (Holditch, 1979; Mahadevan et al., 2009; Bennion et al., 2005; Shaoul et al., 2001). Wang et al. investigated the impact of each damage mechanism and concluded that lower fracturing water recovery does not always result in lower gas production (Wang et al., 2012). Furthermore, previous simulation studies (Settari et al., 2002; Cheng et al., 2012) show that effective imbibition and extended soaking time, not only has negligible effects on long term well productivity, but also can improve early time gas production.

10.2 Problem Statement

A total of 18 hydraulically fractured horizontal wells were completed in Muskwa, Otter Park and Evie formations. The fracturing fluid used for the treatment is the same for all wells and mainly consists of fresh water. During the flowback operation, the cumulative water and gas production data were measured frequently. Figure 10.1

shows the flowback efficiency of these wells at the end of flowback operations. The vertical axis show flowback efficiency, which is the percentage of injected water recovered at the surface. The horizontal axis displays the various well completed in Muskwa, Otter Park and Evie formations. The flowback efficiency of these wells is in the range of 3% to 32% which means a considerable amount of water is retained in the reservoir.

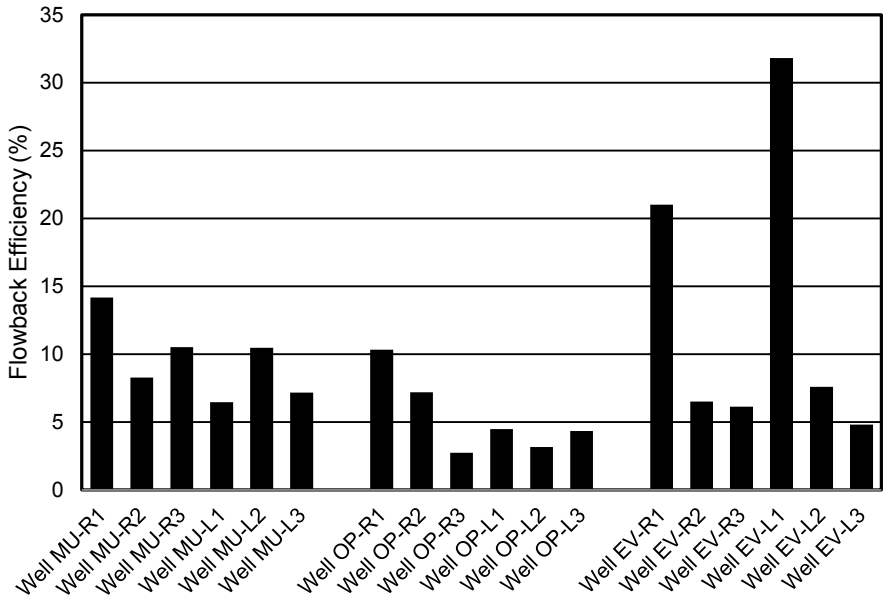

Figure 10.1 Flowback efficiency of 18 hydraulically fractured horizontal wells completed in Muskwa, Otter Park and Evie formations.

10.3 Experiment Study

In previous chapters (Chapter 4 and Chapter 7) we discussed physical reaction of Horn River (HR) shales and Montney (MT) rock samples with water. Here, we compare imbibition rate of water and brine in HR and MT samples. We measured the spontaneous imbibition of deionized (DI) water and brine of various concentrations (1) in the shale samples from Fort Simpson (FS), Muskwa (M), and Otter Park (OP) members of the Horn River (HR) Basin and (2) in the tight sand samples of the Montney (MT) formation.

10.3.1 Materials Used

Experimental materials include core samples and test fluids used for the imbibition experiments.

10.3.1.1 Core Samples Properties

A total of 20 shale samples were selected from two wells completed in the Horn River (HR) Basin and 6 tight sand samples were selected from one well completed in the Montney (MT) formation. The shale samples are still classified into five sections of Fort Simpson (FS), Upper Muskwa (UM), Lower Muskwa (LM), Upper Otter Park (UOP) and Lower Otter Park (LOP). The average depth, gamma ray, core porosity and total organic carbon (TOC) content of all samples are listed in Tables 10.1and 10.2. The average concentration of different minerals determined by X-ray diffraction (XRD) is also given in Tables 10.3 and 10.4.

Table 10.1 Average depth, gamma ray, porosity and TOC of the five HR shale sections.

Label	Depth (m)	GR (API)	Porosity (%)	TOC (%)
FS	1755	138	6.5	1.73
UM	1771	188	8.4	2.25
LM	1792	243	7.1	3.91
UOP	2632	131	8.7	3.01
LOP	2640	162	8.7	3.01

Table 10.2 Average depth, gamma ray, porosity and TOC of the MT samples

Label	Depth (m)	GR (API)	Porosity (%)	TOC (%)
MT1	3723.5	135	5.1	1.09
MT2	3736.5	100	5.5	3.22
MT3	3741.8	90	3.9	2.76
MT4	3743.8	110	4.5	4.33
MT5	3761.9	90	5.8	2.53
MT6	3769.2	119	4.6	1.96

Table 10.3 Average mineral concentration (wt. %) of the five HR shale sections determined by X-Ray diffraction

Label	Dolomite (wt. %)	Quartz (wt. %)	Chlorite (wt. %)	Calcite (wt. %)	Illite (wt. %)	Plagioclase (wt. %)	Pyrite (wt. %)	Matrix Density
FS	2.7	29.03	6.51	0.5	55.46	4.1	1.7	2.747
UM	5.21	36.74	4.4	0	48.35	3.6	1.7	2.744
LM	1.9	45	0	0.9	43	5.2	4	2.79
UOP	2.6	60.8	0	4.4	25.7	3.7	2.8	2.748
LOP	2.2	43.54	0	12.89	33.77	4.4	3.2	2.772

Table 10.4 Average mineral concentration (wt. %) of the MT samples determined by X-Ray diffraction

Label	Dolomite (wt. %)	Quartz (wt. %)	Calcite (wt. %)	K-feldspar (wt. %)	Plagioclase (wt. %)	Pyrite (wt. %)	Illite (wt. %)	Matrix Density
MT1	38	23	8.4	11.4	7.5	1.4	10.3	2.35
MT2	52	21.1	0	11.8	3.8	1.2	10.1	2.32
MT3	81.42	5.99	6.49	3.3	2.8	0	0	2.31
MT4	24.82	27.93	3.1	19.42	7.12	2.2	15.41	2.4
MT5	25.4	19.6	10.3	26.5	3.6	1	13.6	2.06
MT6	29.4	17.9	9.4	23.3	11.5	0.6	7.9	2.33

10.3.1.2 Imbibing Fluids Properties

Deionized water (DI) and KCl solutions with various concentrations were used for the spontaneous imbibition tests. Density, viscosity and surface tension of the fluids are listed in Table 10.5.

Table 10.5 Properties of different fluids used for imbibition experiments at 25^{o}C

Fluid	Density (g/cm^3)	Viscosity (cp)	Surface tension (dyn/cm)
DI water	1	0.9	72
2wt. % KCl	1.02	0.89	72.7
4wt. % KCl	1.04	0.89	73.3
6wt. % KCl	1.06	0.89	73.9

10.3.2 Experiment Procedure

A total of 26 spontaneous imbibition experiments were conducted on Horn River (HR) and Montney (MT) samples. The samples are completely immersed in the water and all the sample faces are open for water imbibition. The imbibed mass is measured using a weight balance. Figure 10.2 schematically shows the experimental set-up for these experiments.

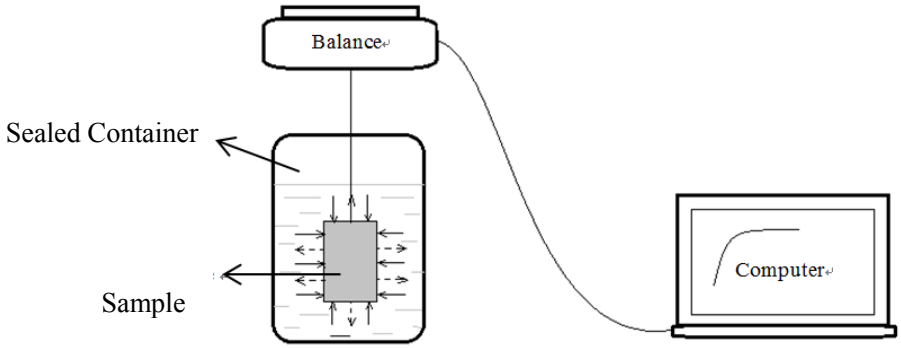

Figure 10.2 Schematic imbibition set-up.

The general test procedure used for the HR and MT samples:

1. Heat the sample at 100°C in the oven for 24 h to ensure moisture evaporation.
2. Measure the dried sample mass and bulk volume.
3. Place the sample in the imbibition cell and measure the weight gain during the imbibition.

10.4 Experiment Results and Discussions

This part presents and discusses the results of spontaneous imbibition experiments of the HR and MT samples.

10.4.1 Experimental Results of HR Samples

Figure 10.3 shows that the water uptake of Fort Simpson and Muskwa samples results in microfracture induction. However, water intake does not significantly change the Otter Park samples, although some microfractures are induced (shown as Figure 6.3). This observation is in agreement with previous imbibition studies on gas shale samples (Dehghanpour et al., 2013; Makhanov et al., 2012; Makhanov, 2013; Ghanbari et al., 2013). Physical alteration degree greatly depends on clay content. Fort Simpson samples have the highest clay content followed by Muskwa and Otter Park. The electrically charged clay layers can adsorb polar water molecules. Water adsorption on clay surfaces produces a net flow of water that induces expansive stresses (Chenevert, 1970; Steiger, 1982). These expansive stresses can lead to expansion of unconfined shale samples. XRD results (Table 10.3) show that illite is the dominant clay mineral in the HR shale samples and swelling clays such as montmorillonite are negligible. However, physical alteration of illitic shales has also been observed in previous studies (Chenevert, 1970). Furthermore, capillary effect is also recognized as an additional cause of shale swelling (Schmitt et al., 1994). Water uptake of shale samples may lead to pressurization of the air, which remains trapped inside the rock. The pore walls have to equilibrate these capillary forces which lead to the expansion of the unconfined samples.

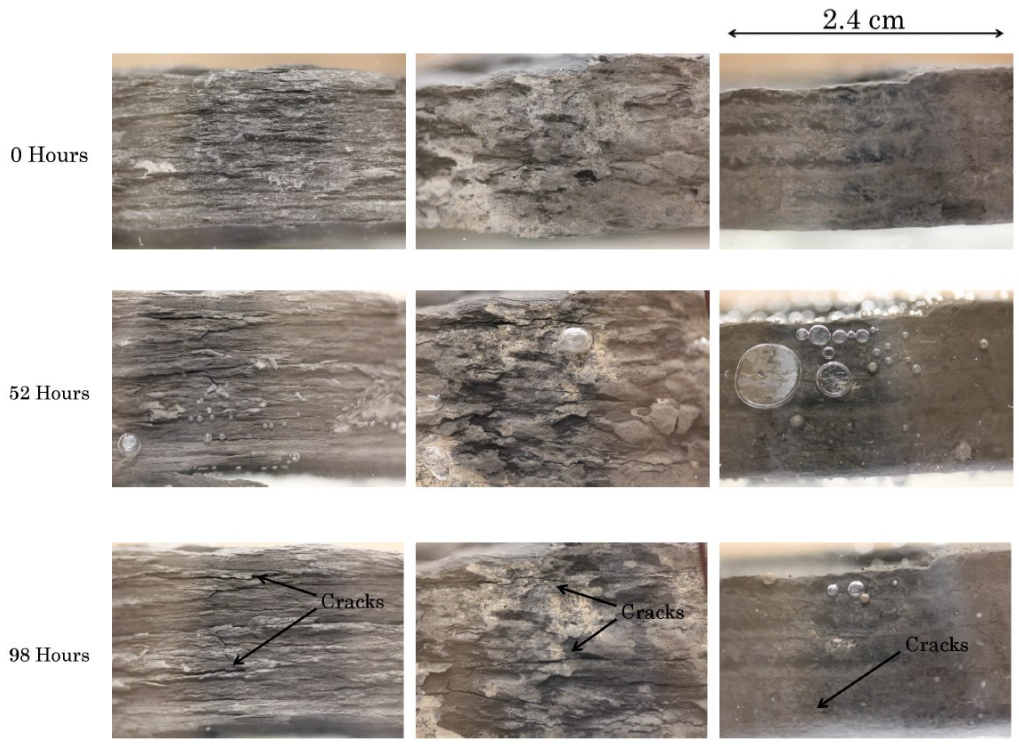

Figure 10.4 Pictures of Fort Simpson (a) Muskwa (b) and Otter Park (c) shale samples before and after exposure to the water (Ghanbari et al., 2013).

10.4.2 Experimental Results of MT Samples

Figure 10.4 shows MT samples after the imbibition experiments. Contrary to the HR shale samples, the MT samples do not show any physical alteration after the imbibition experiments. Furthermore, Table 10.4 shows that illite concentration of the MT samples is much less than that of the HR samples. Therefore, the physical alteration observed in the HR samples can be explained by their relatively high concentration of illite.

Figure 10.4 Pictures of Montney tight sand samples before (a) and after (b) exposure to the 2wt. % KCl solution

10.4.3 Determination of Fracturing Fluid Uptake

The fracture-matrix interface and rock clay mineral types are the critical parameters for quantification of fluid imbibition in the field (Roychaudhury et al. 2011).

Figure 10.5 shows normalized imbibition profiles of DI water and KCl solutions into the shale samples. Water uptake of Fort Simpson and Upper Muskwa samples could not be measured accurately after a certain time due to the extensive physical alteration and sample disintegration. The results also show that KCl salt with concentration below 6wt. % does not have a significant effect on the imbibition rates. However, the recent experiments show that increasing the salt concentration to the values higher than 10wt. % reduces the water uptake and physical alteration (Xu and Dehghanpour, 2014).

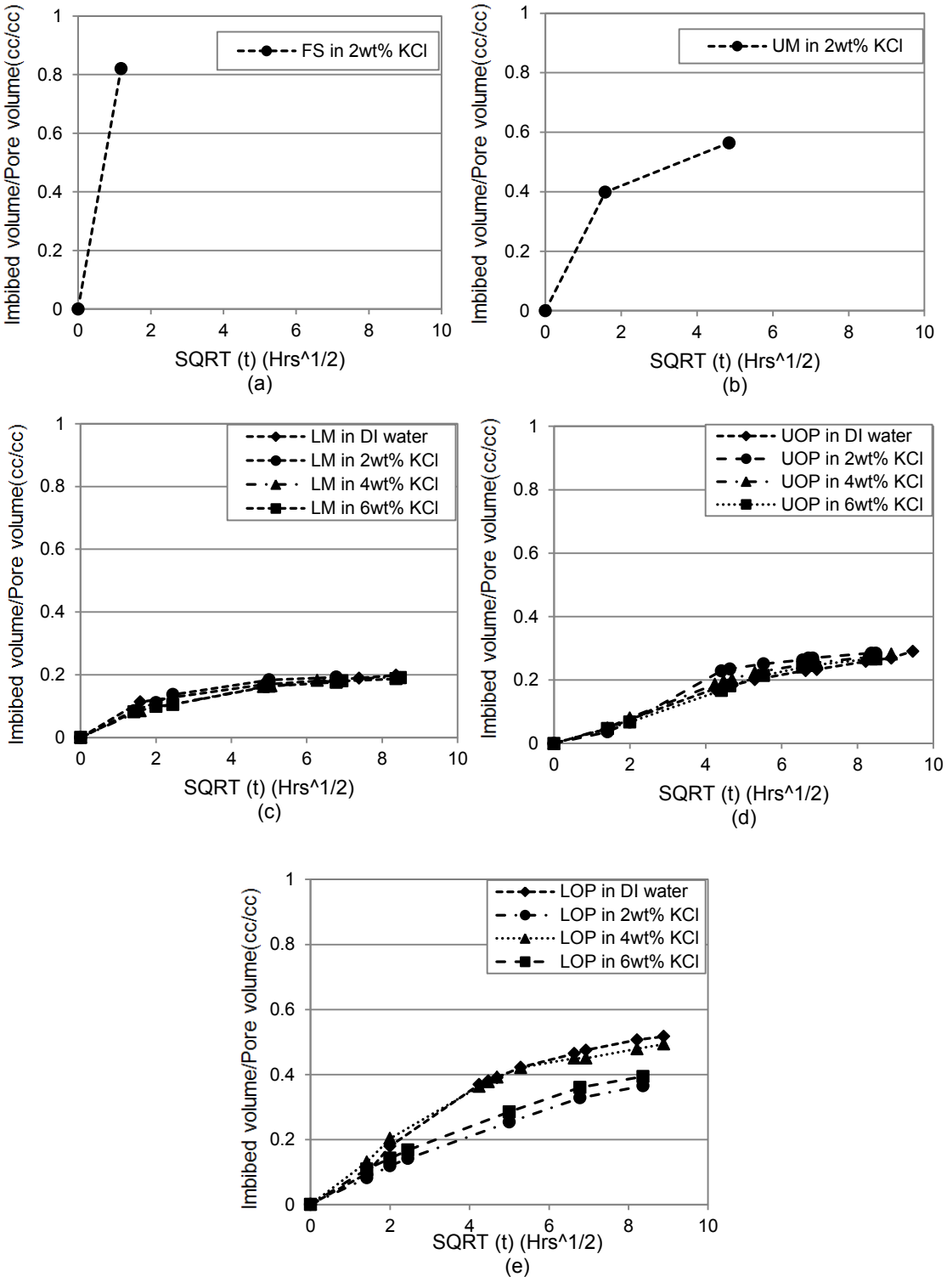

Figure 10.5 Brine normalized imbibed mass versus square root of time in (a) FS, (b) UM, (c) LM (d) UOP and (e) LOP. The clay rich FS and UM samples disintegrated after first hours and therefore their plots are incomplete.

Figure 10.6 shows the total volume of 2wt. % KCl solution imbibed into the FS, UM, LM, UOP and LOP samples versus illite content. In general, increasing the illite concentration increases the imbibed volume. Therefore, it can be interpreted that the adsorption forces in addition to capillary forces significantly contribute to water imbibition. Furthermore, microfracture induction increases the permeability of shale samples and may accelerate imbibition rate. Moreover, samples with higher clay content are more laminated, and it has been shown that the imbibition rate along the lamination is much higher than that perpendicular to the lamination (Makhanov et al., 2013; 2014). Figure 10.6 plots the normalized total imbibed volume versus TOC of the HR shale samples. Increasing the TOC of shale samples decreases the imbibed volume. A similar observation was also noted by Roychaudhuri et al. (Roychaudhuri et al., 2011).

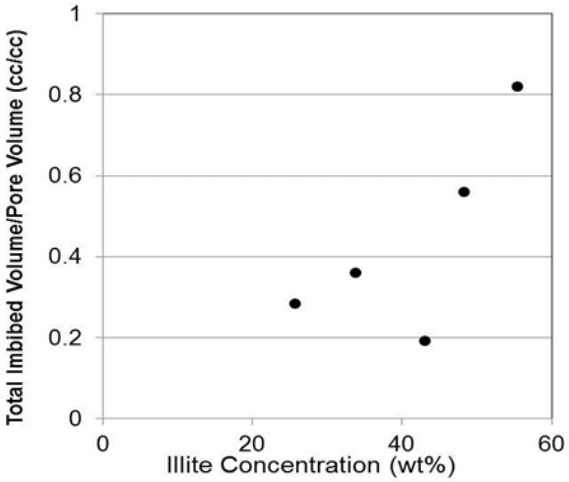

Figure 10.6 Normalized imbibed volume of 2wt. % KCl solution versus illite concentration for the HR samples.

Figure 10.7 compares the normalized imbibition profiles of 2wt. % KCl brine in the MT samples. The volume of brine imbibed in MT1 is much higher than that in other samples. Figure 10.8 plots the normalized total imbibed volume versus TOC of the six MT samples. In general, increasing the TOC content decreases the water uptake. This can be explained by the effect of TOC on sample wettability as we discussed

previously. Samples with higher values of TOC are expected to be more hydrophobic with a less affinity to imbibe brine, spontaneously. However, sample MT 4 with the highest TOC does not follow the decreasing trend in brine uptake. This can be explained by high illite concentration of this sample.

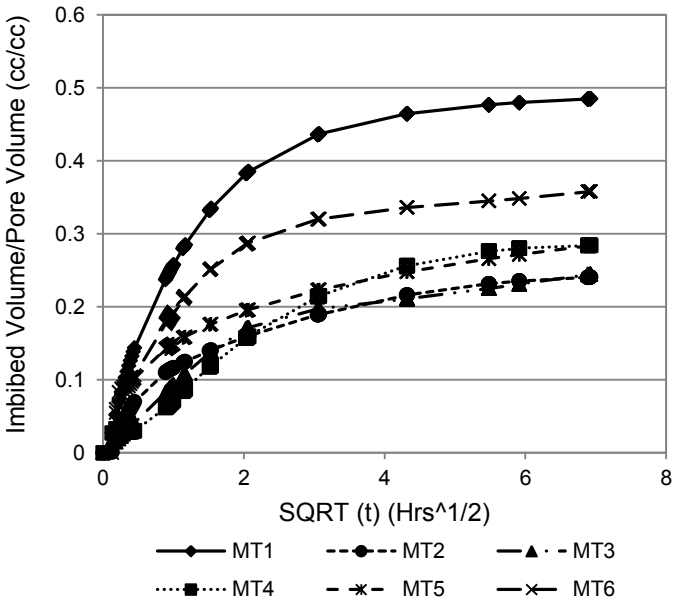

Figure 10.5. Normalized imbibed volume of 2wt. % KCl solution into tight sand samples from Montney formations versus square root of time

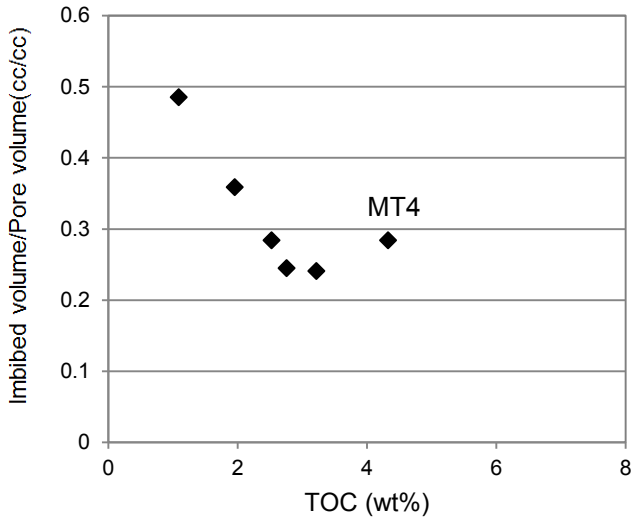

Figure 10.6 Normalized imbibed volume of 2wt. % KCl solution versus TOC for MT samples.

In contrast to the shale samples, Figure 10.9 shows that the MT samples do not present a meaningful correlation with the illite concentration. In other words, changing the illite content does not influence the imbibition rate in the MT samples.

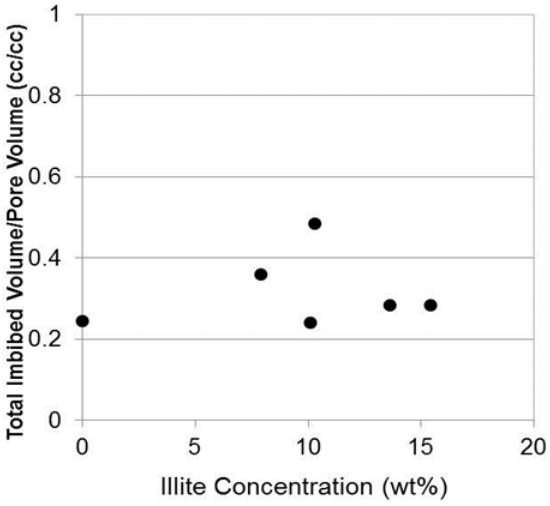

Figure 10.9 Normalized imbibed volume of 2wt. % KCl solution versus illite concentration for the MT samples.

10.5 Scaling the Experimental Data

The objective here is to compare the imbibition behavior of water in the HR and MT samples. Again, as we discussed in Chapter 5 the imbibition behavior in general depends on (1) rock properties such as porosity, permeability and pore structure, (2) fluid properties such as viscosity, surface tension and density; and (3) physical parameters such as size, shape and boundary conditions of the samples. Various expressions have been proposed for the dimensionless time that can be used for scaling the imbibition data (Zhang et al. 1996; Ma et al. 1997). The most frequently used dimensionless time (t_D) for scaling spontaneous imbibition data is:

$$t_D = t\sqrt{k/\emptyset}\frac{\sigma}{\mu}\frac{1}{L_c^2} \qquad (10.1)$$

Where, μ is fluid viscosity, σ is fluid interfacial tension, k is permeability, $\emptyset$ is porosity and L_c is the characteristic length which depends on sample shape and boundary conditions. All faces of the samples were open for imbibition in our

experiments (AFO boundary condition), and the characteristic length in this case is given by:

$$L_c = DL/\sqrt[2]{(D^2 + 2L^2)} \qquad (10.2)$$

Where, D and L are diameter and length of the samples, respectively.

Figures 10.10 (a) and 10.10 (b) show the normalized brine and DI water volume imbibed in the HR and MT samples versus the corresponding dimensionless time, respectively. Besides, Figure 10.10 also shows that the imbibition data of some samples are much above the general trend. Based on the theories of the spontaneous imbibition, all the data should be around one global curve unless there is a difference in the wettability of the samples because contact angle is not included in dimensionless time (equation 10.1). Thus, one explanation for the observed scatter is the difference in wettability of these samples. For example high imbibition values of sample MT1 can be explained by its low TOC value that may suggest its stronger hydrophilic nature. Furthermore, the observed scatter for the HR samples can be explained by (1) the difference in clay concentration and (2) increase in sample permeability as a result of microfracture induction (Dehghanpour et al., 2013).

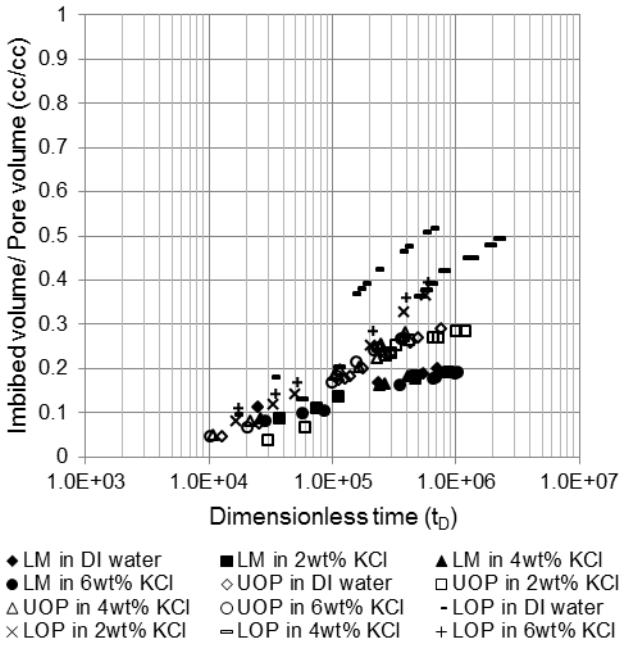

(a)

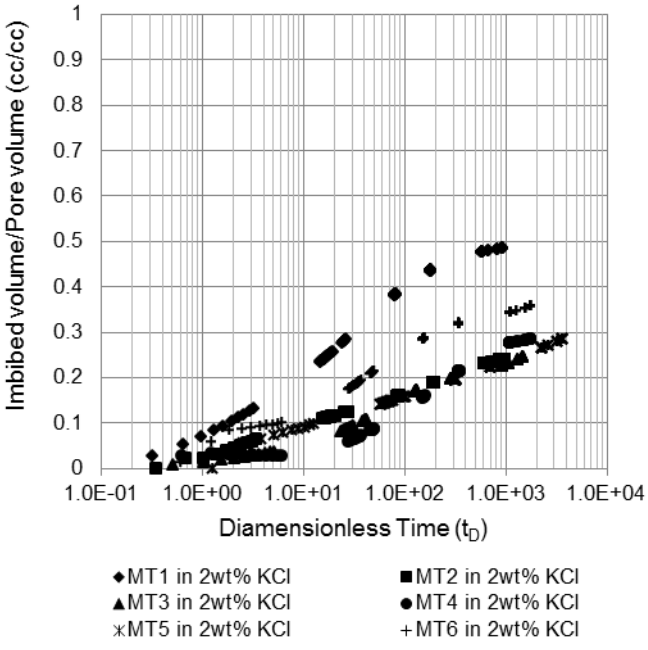

(b)

Figure 10.10. Normalized imbibed volume versus dimensionless time for shale samples (left) and tight sand samples (right).

10.6 Estimation of Water Loss in Field Scale

Based on the data from the laboratory imbibition experiments, the amount of fracturing fluid imbibed into the formation can be estimated during the soaking time. The soaking time is a period between the end of fracturing fluid injection and the beginning of the flowback operation.

To use the imbibition data for estimating the imbibed volume of fracturing water during the soaking time, one can use the simple procedure based on Mattax and Kyte (1962) theory (Reis and Cil, 1993), which is based on the concept of dimensionless time as we mentioned previously. The dimensionless time at the laboratory conditions should be equal to that at the field conditions:

$$t_d = \left[t\sqrt{\frac{k}{\emptyset}}\frac{\sigma}{\mu_w {L_c}^2}\right]_{lab} = \left[t\sqrt{\frac{k}{\emptyset}}\frac{\sigma}{\mu_w {L_c}^2}\right]_{field} \tag{10.3}$$

For any point on the normalized imbibition plot, the corresponding time or imbibed volume at the field conditions can be estimated using this relationship (Eq. 10.3). In other words,

$$t_{lab} = t_{field}\sqrt{\frac{(\frac{k}{\emptyset})_{field}}{(\frac{k}{\emptyset})_{lab}}}\frac{\sigma_{field}}{\sigma_{lab}}\frac{\mu_{lab}}{\mu_{field}}\left[\frac{(L_c)_{lab}}{(L_c)_{field}}\right]^2 \tag{10.4}$$

If we assume that the porosity, permeability, interfacial tension, and viscosity in the laboratory conditions are close to that in the field conditions, the above relationship (Eq.10.4) could be simplified to

$$t_{lab} = t_{field}\left[\frac{(L_c)_{lab}}{(L_c)_{field}}\right]^2 \tag{10.5}$$

Let us assume that the stimulated reservoir can be considered as a dual porosity model with cubic matrix blocks with the characteristic length of $(L_c)_{field}$. This simple relationship (Eq. 10.5) and the measured imbibition data suggest that spontaneous imbibition in the field-scale is a viable mechanism only if $(L_c)_{field}$ is small enough. A rough calculation suggests that if $(L_c)_{field}$ is in the order of meter, one hour in the laboratory corresponds to roughly three days in the field.

10.7 Summary

(1) Water uptake of clay rich shale samples can result in microfracture induction. The degree of physical alteration is correlated to the clay content of the shale samples.

(2) Water uptake of shale samples greatly depends on clay content. Increasing the clay content generally increases water uptake because a significant amount of water can be adsorbed by the clay platelets.

(3) Water uptake of Montney samples is generally correlated to the total organic content (TOC). In general, increasing TOC content decreases the water uptake.

(4) Low flowback efficiency and fracturing fluid loss can be partially explained by the spontaneous water imbibition during soaking period.

CHAPTER 11

CONCLUSIONS AND RECOMMENDATIONS

World production of unconventional liquid fuels, which totaled only 3.9 million barrels per day in 2008, increased to 13.1 million barrels per day and will account for 12 percent of total world liquid fuels supply in 2035 (Rajnauth 2012). The largest components of future unconventional production are 4.8 million barrels per day of Canadian oil sand, 2.2 and 1.7 million per day of US and Brazilian biofuels respectively, and 1.4 million per day of Venezuelan extra-heavy oil (Rajnauth 2012). Adding production of tight gas and coal-bed methane, the US unconventional gas production is expected to increase from 10.9 trillion cube feet in 2008 to 19.8 trillion cube feet in 2035 (Lyon et al. 2012). Moreover, according to the Annual Energy Outlook 2011 by the Energy Information Administration (EIA), the shale gas production will grow from 22.6% in 2010 to 46.5% in 20 years later (Wobbekind et al. 2011).

Since unconventional resources will lead the improvement and progress of the whole world energy, master the advanced technologies to successfully exploit these resources would be one primary task. Due to their complex inherent structure and extremely low permeability, rock samples petrophysical parameters still can hardly be measured accurately only by existing field technologies.

This thesis research is on the basis of spontaneous imbibition experiments for reservoir rocks in the laboratory conditions to simulate reservoir inherent phenomenon during and after hydraulic fracturing in the actual field system. Systematic and comparative study was conducted on Horn River shale and Montney tight gas samples. Factors that would affect imbibition phenomena in our experiments were examined by various fluids and compared among the formation members.

11.1 Conclusions

By investigating spontaneous imbibition data and extensive analysis for these data, key prtrophysical and petrographic properties of our study samples were gained and prepared for field engineering. The major points have been summarized and discussed as follows:

1) Brine intake alters some of the HR shale samples, and the alteration degree depends on sample mineralogy and to some extent on KCl concentration.

2) Brine intake of all HR shale samples studied here is considerably higher than their oil intake.

3) Brine intake of gas shales can induce microfractures, which enhance the sample permeability and, in turn, the imbibition rate.

4) Brine intake is not consistently correlated to KCl salt at concentration lower than 6 wt. %.

5) Brine and oil data of HR shales form two separate clusters on the plot of normalized imbibed mass versus dimensionless time.

6) All of the Montney samples imbibe spontaneously both oil and water. However, the oil uptake is significantly higher than water uptake, which is consistent with the observation that the equilibrium contact angle of oil is almost zero while that of water ranges between 35 and 50 degree.

7) In general, oil wetness of the Montney samples increases by increasing TOC and clay concentration.

8) The measured ratio between the rate of oil and water imbibition is in general higher than the calculated ratio using Young-Laplace equation.

9) The well-connected pore network of the MT samples is primarily hydrophobic and is very likely to be coated by pyrobitumen (or degraded bitumen). On the other hand, the well-connected pore network of the HR samples is strongly

hydrophilic mainly due to the presence of clay minerals and salt crystals coating the rock grains.

10) Spontaneous water imbibition is a viable mechanism for estimating water loss during the soaking period only if the length scale of matrix rock in field is small enough (in the order of meter).

11.2 Recommendations

Although most of the objectives set were achieved, there is still scope for further research and are recommended here:

1) All the test fluids are artificial brine and laboratory oil. Besides, all the experiments are conducted at room temperature and atmospheric pressure. In order to duplicate actual imbibition conditions in reservoirs, experiments sets should be conducted in heated and pressurized tubes with actual fracturing fluids.

2) The HR shale samples used for this study were not preserved and there was a possibility of moisture adsorption by these shale samples. It is recommended to use preserved cores so that obtained results would represented actual downhole processes.

3) Scaling and modeling of spontaneous imbibition in HR shale and MT tight rocks need further investigations. Due to the ultra-tight characteristics and the complex inherent pore structure of these samples, scaling and consequently modeling can be affected by natural or induced microfractures, anisotropy, etc. Therefore, the existing scaling groups, developed for clean reservoir rocks such as sandstones and carbonates, should be modified for application in organic shales. Besides, Handy model assumes the imbibition process is piston-like process which may not occur in real tight and heterogeneous reservoir rocks. Therefore, imbibition model that can be used in field scale for various tight rocks needs to be developed.

4) The methodology which used to scale up the laboratory data for field-scale predication needs to be further studied. The premise of this applied methodology is we assume the simulated reservoir can be considered as a duel porosity model with cubic matrix blocks. A modified methodology that is not restricted to ideal laboratory use should be developed.

REFERENCES

Amott, E., 1959. Observations Relating to the Wettability of Porous Rock. Society of Petroleum Engineers, (216), 156-162.

Amin, E., Christopher, J., Larry, W. L.. Gas Storage Facility Design under Uncertainty. SPE Project, Facilities & Construction, (5):3, 155-165.

Agrawal, S., Sharma, M. M., 2013. Impact of Liquid Loading in Hydraulic Fractures on Well Productivity. Paper SPE 1638837-MS presented at SPE Hydraulic Fracturing Technology Conference, The Woodlands, Texas, USA, 4-6 February.

Arogundada, O., Sohrabi, M., 2012. A Review of Recent Development and Challenges in Shale Gas Recivery. Paper SPE 160869-MS presented at SPE Saudi Arabia Section Technical Symposium and Exhibition, Alkhbar, Saudi Arabia, 8-11 April.

Asadi, M., Woodroof, R. A., Himes, R. E., 2008. Comparative Study of Flowback Analysis Using Polymer Concentration and Fracturing-Fluid Tracer Methods: A Field Study. SPE Production & Opterations. (23):2, 147-157.

Anderson, W., 1986. Wettability Literature Survey- Part 2: Wettability Measurement. Journal of Petroleum Technology, (38):11, 1246-1262.

Alotaibi., M. B., Ramez, A., Hisham, 2010. Wettability Challenges in Carbonate Reservoirs. Paper SPE 129972-MS presented at SPE Improved Oil Recovery Symposium, Tulsa, Oklahoma, USA, 24-28 April.

Brown, R. J. S., Fatt, I., 1956. Measurements of Fractal Wettability of Oil Fields' Rocks By the Nuclear Magnetic Relaxation Method. Society of Petroleum Engineers.

Boek, E. S., Coveney, P. V., Skipper, N. T., 1995. Monte Carlo Molecular Studies of Hydrated Li-, Na-, and K- Smectites: Understanding the Role of Potassium as a Clay Swelling Inhibitor. Journal of the American Chemical Society. (50):117, 12608-12617.

Brezovsk, R., Cui, A., 2013. Laboratory permeability Measurements of Unconventional Reservoirs: Useless of Full of Information? A Montney Example from the Western Canadian Sedimentary

Basin. Paper SPE 167047-MS presented at SPE Unconventional Resources Conference and Exhibition-Asia Pacific, Brisbane, Australia, 11-13 November.

Browning, J., Ikonnikova, S., Gulen, G., Tinker, S., 2013. Barnett Shale Production Outlook. Journal of Petroleum Technology, (5):3, 89-104.

Burke, L., H., Nevison, G., W., Peters, W., E., 2011. Improved Unconventional Gas Recovery with Energized Fracturing Fluids: Montney Example. Paper SPE 149344-MS presented at Columbus, Ohio, USA, 17-19 August.

Bennion, D.B. and Thomas, F.B. 2005. Formation Damage Issues Impacting the Productivity of Low Permeability, Low initial Water Saturation Gas Producing Formations. Journal of Energy Resources Technology. 127 (3): 240–247.

Bai, B., Elgmati, M., Zhang, H., Weia, M., 2013. Rock Characterization of Fayetteville Shale Gas Plays. Fuel. (105), 645-652.

Barree, R. D., Gilbert, J. V., Conway, M., 2009. Stress and Rock Property Profiling for Unconventional Reservoir Stimulation. Paper SPE 118703-MS presented at SPE Hydraulic Fracturing Technology Conference, The Woodland, Texas, USA, 19-21 January.

Clarkson, C., Wood, J., Burgis, S., Aquino, S., Freeman, M., 2012. Nanopore-Structure Analysis and Permeability for a Tight Gas Siltstone Reservoir by Use of Low-Pressure Adsorption and Mercury-Intrusion Techniques. SPE Reservoir Evaluation & Engineering. (15):6, 648-661.

Cheng, Y., 2010. Impact of Water Dynamics in Fractures on the Performance of Hydraulically Fractured Wells in Gas-Shale Reservoirs. Paper SPE 127863-MS presented at SPE International Symposium and Exhibition on Formation Demage Control, Louisiana, USA, 10-12 February.

Chenevert, M.E., 1970. Shale Alteration by Water Adsorption, Journal of Petroleum Technology, (22):9, 1141-1148.

Cui, A., Wust, R., Nassichuk, B., Glover, K., Brezovski, C., 2013. A Nearly Complete Characterization of permeability to Hydrocarbon Gas and Liquid for Unconventional Reservoir: A Challenge to conventional Thinking. Paper SPE 168730-MS presented at Unconventional Resource Technology Conference, Denver, Colorado, USA, 12-14August

Cai, J. C., Yu, B. M., 2011. A Discussion of the Effect of Tortuosity on the Capillary Imbibition in Porous Media. Transport in Porous Media, (89): 2, 251-263.

Culver, B., Augsten, R., Coffin, S., Hur, Y., Abel, J. S., Westlake, A., 2012. Interpretation of Multi-Analysyis Localizations of Microseismic Data: An Alberta Montney Shale Example. Paper SEG 2012-1597 presented at 2012 SEG Annual Meeting, Las vegas, Nevada, USA, 4-9 November.

Cai, J. C., Hu, X. Y., Standnes, D. C., You, L. J., 2012. An Analytical Model for Spontaneous Imbibition in Fractal Porous Media Including Gravity. Colloids and Surfaces A: Physicochemical and Engineering Aspects, (414):20, 228-233.

Davies, G. R., Moslow, T. F., Sherwin, M. D., 1997. The Lower Triassic Montney Formation, West-central Alberta. Bulletin of Canadian Petroleum Geology, (45):4, 474-505.

Donaldson, E. C., Thomas, R. D., Lorenz, P. B., 1969. Wettability Determination and its Effect on Recovery Efferency. Society of Petroleum Engineers, (9):1, 13-20.

Dehghanpour, H., Zubair, H. A., Chhabra, A., Ullah, A., 2012. Liquid Intake of Organic Shale. Energy & Fuels, (26): 9, 5750-5758.

Dehghanpour, H., Lan, Q., Saeed, Y., Fei, H & Qi, Z. 2013. Spontaneous imbibition of brine and oil in gas shale: Effect of water adsorption and resulting micro fractures. Energy & Fuels, (27): 6, 3039-3094.

Frantz, J. H., Jochen, J. V., 2005, Shale Gas, Schlumberger White Paper.

Fan, L., Thompson, J.W., Robinson, J.R., 2010. Understanding Gas Production Mechanism and Effectiveness of Well Stimulation in the Haynesville Shale Through Reservoir Simulation. Paper SPE 136696 presented at Canadian Unconventional Resources and International Petroleum Conference, Calgary, Alberta, Canada, 19-21 October.

Fripiat, J. J., Letellier, M., Levitz, P., Thomas, J. M., 1984. Interaction of Water with Clay Surface. Mathematical Physical & Engineering Sciences. (311):1517, 287- 299.

Fisher, M. K., Heinze, J. R., Harris, C. D., Davidson, B. M., Wright, C. A., Dunn, K. P., 2004. Optimizing Horizontal Completion Techniques in the Barnett Shale Using Microseismic Fracture Mapping, paper SPE 90051-MS presented at SPE Annual Technical Conference and Exhibition, Houston, Texas, USA, 26-29 September.

Fan, L., Thompson, W. J., Robinson, J. R., 2010. Understanding Gas Production Mechanism and Effectiveness of Well Stimulation in the Haynesville Shale through Reservoir Simulation. Paper

136696-MS presented at Canadian Unconventional Resource and International Petroleum Conference, Calgary, Alberta, Canada, 19-21 October.

Gale, J. F. W., Reed, R. M. & Holder, J., 2007. Natural fractures in the Barnett Shale and their importance for hydraulic fracture treatments, AAPG Bulletin, (91):4, 603-622.

Ghanbari, E., Abbasi, M., Dehghanpour, H., Bearinger, D., 2013. Flowback Volumetric and Chemical Analysis for Evaluating Load Recovery and Its Impact on Early-Time Production, paper SPE-167165 presented at Unconventional Resource Conference, Calgary, Canada, 5-7 November.

Gerald, R. C.. Hydraulic Fracturing-New Developments, Petroleum Society of Canada, (15):4.

Glass, D., 1997. Lexicon of Canadian Stratigraphy, Western Canada, (4), 801, Calgary, Alberta: CSPG.

Holditch, S.A., 1979. Factors Affecting water Blocking and Gas Flow From Hydraulically Fractured Gas Wells. Journal of Petroleum Technology, 31 (12): 1515-1524, SPE 7561-PA.

Haskett, W. J., Brown, P. J., 2005. Evaluation of Unconventional Resource Plays. Paper SPE 96879-MS presented at SPE Annual Technical Conference and Exhibition, Dallas, Texas, 9-12 October.

Henderson, C. M., Zonneveld, J. P., 1998. Sequence Biostratigraphic Framework for the Montney Formation and Tectnic Origin of the Mid-Montney Sequence Boundary, Peace River Basin, Northwestern Alberta. CSPG Special Publications, 267-268.

Hensen, E. J. M., Smit, B. J., 2002. Why Clay Swell. The Journal of Physical Chemistry. (49):106, 12664-12667.

Handy, L. L., 1960. Determination of Effective Capillary Pressure for Porous Media from Imbibition Data. Petroleum Transactions, AIME, (219), 75-80.

Hlidek, B., T., Meyer, R., K., Yule, K., Hughes, B., Wittenberg, J., 2012. A Case for Oil-Based Fracturing Fluids in Canadian Montney Unconventional Gas Development. Paper SPE 159952-MS presented at San Antonio, Texas, USA, 8-10 October.

Hamon, G., 2000. Field-wide Variations of Wettability. Paper SPE 63144-MS presented at SPE Annual Technical Conference and Exhibition, Dallas, Texas, USA, 1-4 October.

Jones, S. C., Roszelle, W. O., 1978. Graphical Techniques for Determining Relative Permeability From Displacement Experiments. Journal of Petroleum Technology, (30):5, 807-817.

Juris, V., Hearn, C. L., Dareing, D. W., Rhoades, V.W., 1971. Effect of Rock Stress on Gas Production from Low-Permeability Reservoirs. Journal of Petroleum Technology; (23):9, 1161-1167.

Johnson, E. G., Johnson, L. A., 2012. Hydraulic Fracture Water Usage in Northeast British Columbia: Locations, Volumes and Trends. British Columbia Ministry of Energy and Mines, 41-63.

King, G. E., 2012. Hydraulic Fracturing 101: What Every Representative, Environmentalist, Regulator, Reporter, Investor, University Researcher, Neighbor and Engineer Should know About Estimating Frac Risk and Improving Frac Performance in Unconventional Gas and Oil Wells, paper SPE 152596-MS presented at SPE Hydraulic Fracturing Technology Conference, The Woodlands, Texas, USA, 6-8 February.

Khlaifat, A. L., Arastoopour, H., Qutob, H. 2011. Non-Darcy Flow in Tight Gas Reservoir of Travis Peak Formation. Paper SPE 142048-MS presented in SPE Middle East Unconventional Gas Conference and Exhibition, Muscat, Oman, 31 January-2 February.

Khan, S., Ansari, S. A., Han, H. X., Khosravi, N., 2011. Importance of Shale Anisotropy in Estimating In-Suit Stresses and Wellbore Stability Analysis in Horn River Basin. Paper SPE 149433-MS presented at Canadian Unconventional Resource Conference, Alberta, Canada, 15-17 November.

Khansari, A. N., 2009. Evaluation of Well Productivity Loss Due to Formation Damage Caused by Spontaneous Imbibition in Underbalance Drilling. Paper 122268-MS presented at IADC/SPE Managed Pressure Drilling and Underbalanced Operations Conference and Exihibition, San Antonio, Texas, 12-13 February.

Keneti, S. A. R., Wong, R. C. K., 2011. Investigation of Bimodularity in the Montney Shale Using the Brazilian Test. Paper ARMA-11-278 presented at 45th U.S. Rock Mechanics/Geomechanics Symposium, San Francisco, California, 26-29 June.

Klein, M. M., Kenealey, G. B., Makowecki, B., 2012. Comparison of Hydraulic Fracture Fluids in Multi-stage Fracture Stimulated Horizontal Wells in the Pembina Cardium Formation. Paper SPE 162916-MS presented at SPE Hydrocarbon Economics and Evaluation Symposium, Calgary, Alberta, Canada, 24-25 September.

Keneti, A., Wong, R. C. K., 2010. Investigation of Anisotropic Behavior of Montney Shale Under Indirect Tensile Strength Test. SPE 138104-MS presented at SPE Canadian Unconventional Resources and International Petroleum Conference, Calgary, Alberta, Canada, 19-21 October.

Lan, Q., Ghanbari, E., Dehghanpour, H., Hawkes, R., 2014. Water Loss versus Soaking Time: Spontaneous Imbibition in Tight Rocks. Paper SPE 167713-MS presented at SPE/EAGE European Unconventional Resource Conference and Exhibition, Vienna, Austria, 25-27 February.

Li, K., Horne, R. N., 2006. Generalized Scaling Approach for Spontaneous Imbibition: An Analytical Model. Journal of Petroleum Technology, (9):3, 251-258.

Lyon, Emery, L., 2012-2013. Northeast Natural Energy. 57(4): 971-986.

Medeiros, F., Kurtoglu, B., Ozkan, E., Kazemi, H., 2007. Analysis of Production Data from Hydraulically Fractured Horizontal wells in Tight, Heterogeneous Formations, Paper SPE 110848-MS presented at SPE Annual Technical Conference and Exhibition, Anaheim, California, USA, 11-14 November.

Makhanov, K., Dehghanpour, H., Kuru, E., 2012. An Experimental Study of Spontaneous Imbibition in Horn River Shales, paper SPE 162650-MS presented at SPE Canadian Unconventional Resources Conference, Calgary, Alberta, Canada, 30 October-1 November.

Mahadevan, J., Le, D., Hoang, H., 2009. Impact of Capillary Suction on Fracture Face Skin Evolution in Water Blocked Wells. Paper SPE presented at SPE Hydraulic Fracturing Technology Conference, The Woodlands, Texas.

Makhanov K., 2013. An Experimental Study of Spontaneous Imbibition in Horn River Shales. MSc. Thesis, University of Alberta.

Ma, S., Morrow, N. R., Zhang, X. J., 1997. Generalized scaling of spontaneous imbibition data for strongly water-wet systems, Journal of Petroleum Science and Engineering. (18):3-4, 165-178.

Micheal, J. M., Xiao, Z. J., Leopoldo, S., 2013. Production Forecasting of Hydraulically Conventional Low-Permeability and Unconventional Reservoirs Linking the More Detailed Fracture and Reservoir Parameters. Paper SPE 163833-MS presented at SPE Hydraulic Fracturing Technology Conference, The Woodlands, Texas, USA, 4-6 February.

Moore, S., Cripps, C., 2010. Bacterial Survival in Fractured Shale Gas Wells of the Horn River Basin. Paper SPE 137010-MS presented at Calgary, Alberta, Canada, 19-21 October.

Ma, S., Zhang, X., Morrow, N., Zhou, X., 1999. Characterization of Wettability From Spontaneous Imbibition Measurements. Journal of Canadian Petroleum Technology, (38):13.

Mohammadlou, M., Mork, M. B., 2012. Complexity of Wettability Analysis in Heterogeneous Carbonate Rocks, A Case Study. Paper SPE 154402-MS presented at SPE Europec/EAGE Annual Conference, Copenhagen, Denmark, 4-7 June.

Morrow, N., R., 1990. Wettability and its effect on oil recovery. SPE Reservoir Engineering, (12):42, 1476-1484.

Morrow, N. R., Ma, S., Zhou, X., Zhang, X., 1994. Characterization of Wettability From Spontaneous Imbibition Measurements. Paper PETSOC-94-47 presented at Annual Technical Meeting, Calgary, Alberta, Canada, June 12 – 15.

Mohanty, K., Kathel, P., 2013. EOR in Tight Oil Reservoirs through Wettability Alteration. Paper SPE 16628 presented at SPE Annual Technical Conference and Exhibition, New Orleans, Louisiana, USA, 30 September-2 October.

Mirzaei-Paiaman, A., Masihi, M., Standnes, D. C., 2013. Index for Characterizing Wettability of Reservoir Rocks Based on Spontaneous Imbibition Recovery Data. Energy & Fuels, 27, 4662-2676.

Ning, X., Fan, J., Holditch, S. A., Lee, W. J., 1993. The Measurement of Matrix and Fracture Properties in Naturally Fractured Cores, Paper SPE 25898-MS presented at Low Permeability Reservoirs Symposium, Denver, Colorado, USA, 26-28 April.

Newsham, K. E., Rushing, J. A., 2002. Laboratory and Field Observations of an Apparent Sub-Capillary-Equibrium Water Saturation Distribution in a Tight Gas Sand Reservoir. Paper SPE 75710 presented at the SPE Gas Technology Symposium, Calgary, Alberta, Canada, 30 April- 2 May.

Nieto, J., Bercha, R., Chan, J., 2009. Shale Gas Petrophysics – Montney and Muskwa, Are They Barnett Look-Alikes? Paper SPWLA-2009-84918 presented at SPWLA 50th Annual Logging Symposium, the woodlands, Texas, 21-24 June.

Odusina, E., Sondergeld, C., Rai, C., 2011. NMR Study of Shale Wettability. Paper SPE 147371-MS presented at Canadian Unconventional Resources Conference, Alberta, Canada, 15-17 November.

Olafuyi, O. A., Cinar, r., Knackstedt, M., Pinczewski, W. F., 2007. Spontaneous Imbibition in Small Cores. Paper SPE 109724-MS presented at Asia Pacific Oil and Gas Conference and Exhibition, Jakarta, Indonesia, 30 October-1 November.

Parmar, J. S., Dehghanpour, H., Kuru, E., 2012. Unstable Displacement: A missing Factor in Fracturing Fluid Recovery, paper SPE 162649-MS presented at SPE Canadian Unconventional Resources Conference, Calgary, Alberta, Canada, 30 October- 1 November.

Parmar, J. S., Dehghanpour, H., Kuru, E., 2013. Drainage against Gravity: Factors Impacting the Load Recovery in Fractures, paper SPE 164530-MS presented at SPE Unconventional Resources Conference, The Woodlands, TX, USA, 10-12 April.

Pond, J., Zerbe, T., Oldand, K. W., 2010. Horn River Frac Water: Past, Present, and Future. Paper SPE 138222-MS presented at Canadian Unconventional Resource and International Petroleum Conference, Calgary, Alberta, Canada, 19-21 October.

Reis, J. C., Cil, M., 1993. A model for oil expulsion by counter-current water imbibition in rocks: one-dimensional geometry. Journal of Petroleum Science and Engineering, 10, 97-107.

Roychaudhuri, B., Tsotsis, T., and Jessen, K., 2011. An Experimental and Numerical Investigation of Spontaneous Imbibition in Gas Shales Paper SPE presented at SPE Annual Technical Conference and Exhibition, Denver, Colorado, USA, 30 October-2 November.

Rahm, D., 2011. Regulating Hydraulic Fracturing in Shale Gas Plays: The Case of Texas. Energy Policy, (5):39, 2974-2981.

Reynolds, M. M., Munn, D. L., 2010. Development Updata for an Emerging Shale Gas Giant Field – Horn River Basin, British Columbia, Canada. Paper SPE 130103-MS presented at SPE Unconventional Gas Conference, Pittsburgh, Pennsylvania, 23-25 February.

Rokosh, C. D., Anderson, S. D. A., Beaton, A. P., Berhane, M., Pawlowicz, J., 2010. Geochemical and Geological Characterization of the Duvernay and Muskwa Formation in Alberta. Paper SPE 137799-MS presented at Calgary, Alberta, Canada, 19-21 October.

Romanson, R., Riviere, N., Taylor, B., Wilson, M., Loran, C., Cockbill, J., 2010. Montney Fracturing-Fluid Considerations: Case History. Paper SPE 137039-MS presented at Canadian Unconventional Resources and International Petroleum Conference, Calgary, Alberta, Canada, 19-21 October.

Rajnauth, J. J., 2012. Is it Time to focus on Unconventional Resources? Paper SPE 158654-MS presented at SPETT 2012 Energy Conference and Exhibition, Port-of-Spain, Trinidad, 11-13 June.

Roychaudhuri, B., Tesotesis, T. T., Jessen, K., 2011. An Experimental and Numerical Investigational of Spontaneous Imbibition in Gas Shale. Paper SPE 147652-MS presented at SPE Annual Technical Conference and Exhibition, Denver, Colorado, USA, 30 October-2 November.

Rao, D. N., Girard, M. G., 1994. A New Technique for Reservoir Wettability Characterization. Paper SPE 94-48 presented at Annual Technical Meeting, Calgary, Alberta, Canada, 12-15 Jun.

Rao, D. N., 1997. Is There a Correlation Between Wettability From Corefloods and Contact Angles? Paper SPE 37234-MS presented at International Symposium on Oilfield Chemistry, Houston, Texas, USA, 18-21 February.

Settari, A., Sullivan, R.B., and Bachman, R.C. 2002. The Modeling of the Effect of Water Blockage and Geomechanics in Waterfrac. Paper SPE 77600 presented at the SPE Annual Technical Conference and Exhibition, San Antonio, Texas, USA, 29 September–2 October.

Steiger, R.P., Fundamentals and Use of Potassium/Polymer Drilling Fluids to Minimize Drilling and Completion Problems Associated With Hydratable Clays, J. Pet. Technol. 1982, 34, 1661.

Schmid, K. S., Geiger, S., 2012. Universal scaling of spontaneous imbibition for water-wet systems. Water Resource Research, (48):3.

Soeder, D. J., 2011. Preliminary Analysis of the Weathering Potential of Marcellus Shale Drill Cuttings. Geological Society of American Northeast Section. (43):1, 50-58.

Stewart, M. R., Kosich, B., Warren, B. K., Urquhart, J. C., McDonald, M. J., 2000. Use of Silicate Mud to Control Borehole Stability and Overpressured Gas Formations in Northeastern British Columbia. Paper SPE 59751-MS presented at SPE/CERI Gas Technology Symposium, Calgary, Alberta, Canada, 3-5 April.

Shaoul, J., Zelm, V., De Peter, H., 2011. Damage Mechanisms in Unconventional Gas Well Stimulation-A New Look at an Old Problem. Paper SPE 142479-MS presented at SPE Middle East Unconventional Gas Conference and Exhibition, Muscat, Oman, 31 January-2 February.

Shah, S. N., 1993. Rheological Characterization of Hydraulic Fracturing Slurries. Journal of Petroleum Technology, (8):2,123-130.

Schembre, J. M., Akin, S., Castanier, L. M., Kovscek, A. R., 1998 Spontaneous Water Imbibition into Diatomite. Paper SPE 46211-MS presented at SPE Western Regional Meeting, Bakersfield, California, 10-13 May.

Sherwood, J. D., 1994. A Model for the Flow of Water and Lons into Swelling Shale, (7):10, 2480-2486.

Sulucarnain, I., Sondergeld, C., Rai, C., 2012. An NMR Study of Shale Wettability and Effective Surface Relaxivity. Paper SPE 162236-MS presented at SPE Canadian Unconventional Resources Conference, Calgary, Alberta, Canada，30 October-1 November.

Torsaeter, O., 1988. A Comparative Study of Wettability Test Methods Based on Experimental Results from North Sea Reservoir Rocks. Paper SPE 18281-MS presented at SPE Annual Technical Conference and Exhibition, Houston, Texas, 2-5 October.

Tonn, R., 1996. Seismic Reservoir Characterization of Montney Sand in the Peace River Arch Area, Canada. Paper SEG-1996-0299 presented at 1996 SEG Annual Meeting, Denver, Colorado, 10-15 November.

Tang, G., Morrow, N., 1997. Influence of Composition and Fines Migration on Crude Oil/Brine/Rock Interactions and Oil Recovery. Journal of Petroleum Science and Engineering. (24): 2, 98-111.

Takahashi, S., Kovscek, A. R., 2010. Spontaneous countercurrent Imbibition and Forced Displacement Characteristics of Low-permeability, Siliceous Shale Rocks. Journal of Petroleum Science and Engineering, (71): 1-2, 47-55.

Tadayoni, M., 2012. New Approach for the prediction of Klinkenberg Permeability in Situ for Low Permeability Sandstone in Tight Gas Reservoir. Paper SPE 152451-MS presented at SPE Middle East Unconventional Gas Conference and Exhibition, Abu Dhabi, UAE, 23-25 January.

Volk, L., 1995. Modeling of Wellbore Stability. Paper SPE 19240 presented atOff-shore Europe ’89 Symposium, Aberdeen, September 5-9.

Wang, Y. L., Holditch, S. A., McVay, D. A., 2008. Simulation of Gel Damage on Fracture-Fluid Cleanup and Long-Term Recovery in Tight-Gas Reservoir, paper SPE 117444-MS presented at SPE Eastern Regional/AAPG Eastern Section Joint Meeting, Pittsburgh, Pennsylvania, USA, 11-15 October.

Wilson, B., Lui, D., Kim, J., Kenyon, M., McCaffrey, M., 2011. Comparative Study of Multistage Cemented Liner and Openhole System Completion Technologies in the Montney Resource Play. Paper SPE 149437-MS presented at Canadian Unconventional Resource Conference, Alberta, Canada, 15-17 November.

Wood, J. M., 2013. Water Distribution in the Montney Tight Gas Play of the Western Canadian Sedimentary Basin: Significance for Resource Evaluation. SPE Res Evaluation & Engineering, (16):3, 290-302.

Wang, D., Bulter, R., Liu, H., Ahmed, S., 2011. Flow-Rate Behavior and Imbibition in Shale. Journal of Petroleum Technology, (14):4, 485-492.

Wobbekind, R., Lewandowski, B., Christensen, E., 2011. Assessment of Oil and Gas Industry: Economic and Fiscal Impacts in Colorado in 2010.

Zhang, J. Y., Nguyen, Q. P., Flaaten, A. K., Pope, G. A., 2008. Mechanisms of Enhanced Natural Imbibition with Novel Chemicals. Paper SPE 113453-MS presented at SPE/DOE Symposium on Improved Oil Recovery, Tulsa, Oklahoma, USA, 20-23 April.

Zhang, X. Y., Morrow, N. R., Ma, S. X., 1996. Experimental Verification of a Modified Scaling Group for Spontaneous Imbibition. SPE Reservoir Evaluation & Engineering, (11):4, 280-285.

Zhou, X.M., Morrow, N. R., Ma, S. X., 2000. Interrelationship of Wettability, Initial Water Saturation, Aging Time, and Oil Recovery by Spontaneous Imbibition and Waterflooding. Society of Petroleum Engineers, (5):2, 199-207.

Zhao, H., Li, K., 2009. A Fractal Model of Production by Spontaneous Water Imbibition. Paper SPE 119525 presented at Latin American and Caribbean Petroleum Engineering Conference, Catagena de Indias, Colombia, 31 May- 3 June.

Zhang, X.; Morrow, N. R.; Shouxiang Ma, S., 1996. Experimental Verification of a Modified Scaling Group for Spontaneous Imbibition, SPE Reservoir Engineering, (11):4, 280-285.